# EFFECTIVE LAGRANGIAN MODELS FOR GAUGE THEORIES OF FUNDAMENTAL INTERACTIONS

Francesco Sannino <sup>1</sup>

Dept. of Physics, Yale University, New Haven, CT 06520-8120

### Abstract

In this thesis we show that the effective Lagrangian models, encoding the relevant symmetries of the underlying fundamental gauge theory for strong interactions (QCD), provide a reasonable understanding of the interactions among light mesons at intermediate energies as well as of the properties of Heavy baryons. In the first part of the thesis we show that it is possible to build a chiral and crossing symmetric model for light meson interactions at intermediate energies, which we have called the Chiral Resonance Model (ChRM). Using the previous scheme we can understand  $\pi\pi$ -scattering up to the 1 GeV region by considering the resonance exchange together with the contact term contributions. We also observe that to fully describe low energy  $\pi\pi$ -scattering in the Chiral Resonance framework a broad scalar  $\sigma(550)$  particle is needed. In the second part of the thesis we investigate the heavy baryon spectra in the bound state picture. In this picture the heavy baryon is treated as a heavy spin multiplet of mesons  $(Q\bar{q})$  bound in the background field of the nucleon (qqq), which in turn arises as a soliton configuration of light meson fields. We show that a relativistic model with light vectors gives a very satisfactory account of the  $\Sigma_c^* - \Sigma_c$  hyperfine splitting in contrast to the model without light vectors. In the last chapter we also present a generalization of the bound state model. Indeed by binding heavy spin excited multiplets to the background Skyrmion field we can describe the spectrum of excited heavy baryons of arbitrary spin.

<sup>1</sup>sannino@zen.physics.yale.edu

 $Patet\ omnibus\ veritas,\ nondum\ est\ occupata.$ 

Multum ex illa etiam futuris relictum est.

Vale.

Lucius Annaeus Seneca, "Ad Lucilium Epistulae Morales".

Truth lies open for all; it has not yet been monopolized.

And there is plenty of it left even for posterity to discover.

Farewell.

Lucius Annaeus Seneca, "Letters addressed to Lucilius".

La verità è accessibile a tutti, non è dominio riservato di nessuno, e il campo che essa lascia ai posteri è ancora vasto.

Addio.

Lucius Annaeus Seneca, "Lettere a Lucilio".

# To Lucia and my parents

# Contents

In	trod	uction	xiv
A	ckno	wledgments	xvii
Ι	Cł	niral Resonance Model	1
1	Intr	roduction to the Chiral Resonance Model	3
	1.1	Brief review of QCD, Chiral Symmetry and $1/N_c$	3
	1.2	Chiral Resonance Model	7
	1.3	Regularization of the Model	10
	1.4	Chiral Lagrangian	12
2	A f	undamental process: $\pi\pi$ scattering	16
	2.1	Introduction to $\pi\pi$ scattering	16
	2.2	Current Algebra and $\rho$ vector—meson exchange	18
	2.3	Is the $\sigma(550)$ alive ?	24
	2.4	Comment on higher derivative contact terms	33
3	Exp	ploring the 1 GeV region	35
	3.1	What is happening in the 1 GeV region	35

		3.1.1 The Ramsauer-Townsend Effect	38
	3.2	Next group of Resonances	39
		3.2.1 The Tensor $f_2(1270)$	41
		3.2.2 The vector meson $\rho(1450)$ and the $f_0(1300)$ scalar	43
		3.2.3 $f_2(1270) + f_0(1300) + \rho(1450) \dots \dots \dots \dots \dots \dots$	43
	3.3	Inelastic effects	48
	3.4	Phase Shifts	49
	3.5	The inelastic channel $\pi\pi \to K\bar{K}$	52
	3.6	The lonely $\sigma$	59
	3.7	Conclusions for the Chiral Resonance Model	61
II	Н	Leavy Systems	65
4	Hea	avy Baryons in the Bound State Approach	67
	4.1	Brief Introduction to the Heavy Physics	67
	4.2	Bound State Approach to the Heavy Baryon system	69
		4.2.1 Effective Lagrangian for the Heavy-Light system	70
	4.3	Mechanics of Baryon States	71
	4.4	Collective Quantization	74
5	Hea	avy Baryon Hyperfine Splitting	77
	5.1	Introduction	77
		5.1.1 Relativistic Lagrangian for the Heavy Mesons	81
	5.2	An apparent puzzle	82
		5.2.1 Expansion of Lagrangian	85
	5.3	Hyperfine splitting from the Hidden Terms	86
	5.4	Perturbative Approach and the Vector contribution	91

c C		1
	neralization of the Bound State Model	1
6.1	Introduction	]
6.2	The Enigma of the Excited Missing States	1
6.3	The Planetary Conjecture	1
6.4	Model for the Missing First Excited States	1
6.5	Extension to the Higher Orbital Excitations	]
6.6	Conclusions for the Generalized Heavy Baryon Model	]
$\mathbf{App}$	endices	1
Appo A Pa	endices rt I Appendix	1
<b>A</b> ppo <b>A P</b> a A.1	endices rt I Appendix Scattering kinematics	1
Appo A Pa	endices  rt I Appendix  Scattering kinematics	1
<b>A</b> ppo <b>A P</b> a A.1	endices  rt I Appendix  Scattering kinematics	1
<b>A</b> ppo <b>A Pa</b> A.1	endices  rt I Appendix  Scattering kinematics	1
<b>A</b> ppo <b>A P</b> a A.1 A.2	endices  rt I Appendix  Scattering kinematics	1
<b>A</b> ppo <b>A P</b> a A.1 A.2	endices  rt I Appendix  Scattering kinematics	1

# List of Figures

1.1	(a) schematically represents the 4-point Green function. (b) represents		
	the 3-point Green function. In (a) and (b) the external lines represent		
	a quark $loop$ , while $(ullet)$ are the insertions of the non exotic meson fields.	7	
2.1	Schematic representation of a scattering process	17	
2.2	The solid line is the current algebra result for $R_0^0$ . The dotted and		
	dot-dashed lines are the Roy curves for $R_0^0$	19	
2.3	The solid line is the current algebra result for $R_0^0$ . The dot-dashed line		
	is the $\rho + \pi$ for $R_0^0$	21	
2.4	The solid line represents the imaginary term $I_1^1$ . The dot-dashed line		
	is $R_1^1$	23	
2.5	The solid line is the $\pi + \rho$ contribution for the real part of $I = 2, \ l =$		
	0. The dot-dashed line is the $\pi + \rho$ contribution for the real part of		
	$I = 0, l = 2. \dots $	25	
2.6	Enlarged version of Fig. 2.3. The solid line which shows the current		
	algebra + $\rho$ result for $R_0^0$ is much closer to the unitarity bound of 0.5		
	than the dashed line which shows the current algebra result alone.   .	26	
2.7	Contribution to $R_0^0$ due to the $\sigma(550)$ particle	28	

2.8	imental points, in this and succeeding figures, are extracted from the phase shifts using Eq. (A.6) and actually correspond to $R_0^0/\eta_0^0$ . ( $\square$ ) are extracted from the data of Ref. [28] while ( $\triangle$ ) are extracted from the	
	data of Ref. [29]. The predicted $R_0^0$ is small around the 1 $GeV$ region.	29
2.9	A blowup of the low energy region. The solid line is the <i>current algebra</i> $+ \rho$ contribution to $R_0^0$ . The dashed line includes the $\sigma$ particle and has the effect of turning the curve down to avoid unitarity violation while beauting it at lower energies.	20
0.10	while boosting it at lower energies	30
2.10	The solid line is the current algebra $+\rho$ contribution for $R_0^2$ . The dashed line is the current algebra $+\rho + \sigma$ contribution for $R_0^2$ . The dot-dashed line is the current algebra solution for $R_0^2$ .	20
	line is the <i>current algebra</i> contribution for $R_0^2$	32
2.11	Four-derivative contact term contribution for $R_0^0$ . The solid line corresponds to $a = +1.0$ . The dotted line corresponds to $a = +0.7$ . The	
	dot-dashed line corresponds to $a = 0.5$ . $a$ is represented in units of	
	$10^{-3}$	34
3.1	(a): The solid line is the current algebra + $\rho$ + $\sigma$ + $f_0(980)$ result for $R_0^0$ obtained by assuming column 1 in Table 3.2 for the $\sigma$ and $f_0(980)$ parameters $(Br(f_0(980) \to 2\pi) = 100\%)$ . (b): The solid line is the current algebra + $\rho$ + $\sigma$ + $f_0(980)$ result for $R_0^0$ obtained by assuming	27
	column 2 in Table 3.2 $(Br(f_0(980) \to 2\pi) = 78.1\%)$	37
3.2	Contributions for $R_0^0$ . Solid line: $f_2(t+u)$ . Dashed line: $f_2(s)$ . Dotted line: $f_0(1300)$ . Dot-dashed line: $\rho(1450)$	44
3.3	Sum of the contributions in Fig. 3.2	45

3.4	Contribution from the <i>next group</i> of resonances; the solid line is ob-	
	tained with the reverse sign of the $f_0(1300)$ piece; the dashed line is as	
	in Fig. 3.3.	46
3.5	Prediction for $R_0^0$ with the <i>next group</i> of resonances. (a) assumes (col-	
	umn 5 in Table 3.2) $(BR(f_0(980) \rightarrow 2\pi) = 100\%)$ while (b) assumes	
	(column 6) $(BR(f_0(980) \to 2\pi) = 78.1\%)$	47
3.6	An experimental determination of $\eta_0^0 = \sqrt{1 - 4 T_{12,0}^0 ^2}$ [45]	48
3.7	Predictions with phenomenological treatment of inelasticity ( $\eta_0^0 = 0.8$ )	
	above $K\overline{K}$ threshold. (a): without next group. (b): with next group.	49
3.8	Estimated phase shift using the predicted real part and unitarity rela-	
	tion	51
3.9	Contributions to $\pi\pi \to K\overline{K}$ $(R_{12;0}^0)$ . The solid line shows the current	
	algebra result, the dashed line represents the inclusion of $K^*(892)$ , the	
	dotted line includes the $\sigma(550)$ too	53
3.10	Effect of $f_0(980)$ on $\pi\pi \to K\overline{K}$ . The solid curve corresponds to a	
	negative $\gamma_{f_0K\overline{K}}$ and the dashed one to a positive sign	55
3.11	Effects on $\pi\pi \to K\overline{K}$ due to the <i>next group</i> of resonances for the two	
	different sign choices in Fig. 3.10.	57
3.12	$ R_{12;0}^0 $ together with one experimental determination [45] of $ T_{12;0}^0 $ =	
	$\sqrt{(R_{12;0}^0)^2 + (I_{12;0}^0)^2}$ . Signs for $\gamma_{f_0 K\overline{K}}$ as in Fig. 3.10	58
3.13	The solid line is the <i>current algebra</i> + $\sigma$ + $f_0(980)$ result for $R_0^0$	60
3.14	Effective resonance $-2\pi$ coupling due to the pions' rescattering effects.	
	The latter has been shown schematically in a generic pertubative scheme.	
	For simplicity we only considered the rescattering due to a four pion	
	contact term $(\bullet)$	62

5.1	$\chi$ vs. $M$ computed by numerical integration. Solid line $M^* = M$ ,	
	$d'=d;$ dotted line $M^*\neq M, d'=d,$ dashed line $M^*=M, d'\neq d.$	84
5.2	The $d$ dependence of $\chi$ for $M=M^*=30\mathrm{GeV}$ and $d=d'$ . Solid	
	line is the exact numerical calculation. Dashed line is the large ${\cal M}$	
	perturbation formula given in Eq. (5.19)	89
6.1	Schematic planetary picture for large $N_c$ excited heavy baryons in the	
	bound state approach	115
6.2	Schematic picture of the "two body" approximation for the $N_c=3$	
	excited heavy baryons	116

# List of Tables

Note that the $\sigma$ was not present in the 1994 PDG and is not being	
described exactly as a Breit-Wigner shape; we listed the fitted param-	
eters shown in column 1 of Table 3.2 where $G'$ is the analog of the	
Breit-Wigner width	36
Fitted parameters for different cases of interest	40
Typical results for the present model (including light vectors) com-	
pared with model with light pseudoscalars only ("Skyrme" column)	
and compared with experiment. No "manifest" heavy spin violation	
effects other than $M^* \neq M$ have been included. The column "present	
model + CM" simply takes into account recoil corrections by replacing	
the heavy meson mass by the reduced mass. $\Lambda_c'$ denotes a negative	
parity, spin 1/2 state. The quantity $\alpha$ in Eqs (5.4) was taken to be	
zero. All masses in MeV	80
Parameters for heavy baryons and mass differences with respect to $\Lambda_c$ .	
Primes indicate negative parity baryons, $i.e.$ S—wave bound states. All	
energies are in MeV	100
	described exactly as a $Breit\text{-}Wigner$ shape; we listed the fitted parameters shown in column 1 of Table 3.2 where $G'$ is the analog of the $Breit\text{-}Wigner$ width

5.3	Parameters for heavy baryons and mass differences with respect to $\Lambda_b$ .	
	Primes indicate negative parity baryons, $i.e.$ S—wave bound states. All	
	energies are in MeV. The empirical value for the relative position of	
	the nucleon is $4701 \pm 50 \text{MeV}$ [37]	101
5.4	Parameters for heavy baryons and mass differences with respect to	
	$\Lambda_c$ . Primes indicate negative parity states, <i>i.e.</i> S–wave bound states.	
	All energies are in MeV. In this calculation the reduced masses (5.44)	
	enter the bound state equations from which the binding energies are	
	extracted. The physical meson masses 1865MeV and 5279MeV are	
	used when computing the mass differences to the nucleon and the $\Lambda_b$	
	from these binding energies. Radially excited states are omitted be-	
	cause they are only very loosely bound, if at all. The empirical data	
	are taken from the PDG [37], see also [92]	103
5.5	Same as Table 5.4 for even parity baryons in the kaon sector	104
6.1	Examples of the heavy baryon multiplets predicted by the CQM. $$ . $$	111
6.2	Contributions to energies of new predicted $\ell=1$ states. Here, $\lambda=1$	
	$\frac{1}{4}F'(0)\left[\left(d_{\rm S} + \frac{5}{3}d_{\rm T}\right) - \sqrt{\left(d_{\rm S} - \frac{5}{3}d_{\rm T}\right)^2 + \frac{32}{3} f_{\rm ST} ^2}\right]$ is the presumed neg-	
	ative binding potential in the $k'=1$ channel. Furthermore $\chi=\chi(1)$	
	in Eq. (6.30); it satisfies $-\frac{1}{4} \le \chi \le \frac{1}{2}$	125
6.3	Notation for the heavy meson multiplets. $j_l$ is the angular momentum	
	of the "light cloud" surrounding the heavy quark while $J^P$ is the spin	
	parity of each heavy meson in the multiplet	128
6.4	Pattern of states for Eqs. (6.41) and (6.42). Note that $j_l = n + \frac{1}{2}$ is	
	the light cloud spin of the heavy meson. The columns marked $\#$ stand	
	for the number of channels which are expected to be bound, for that	
	particular $k'$ , according to the CQM	131

6.5	Contributions to energies of the new predicted states made from ${\cal H}-$				
	type heavy mesons. Note that $n$ is a positive integer. The $n=0$ case				
	is given in Table 6.2. The $\lambda_+$ entries in the $V$ column are more tightly				
	bound than the $\lambda$ entries. $\left  {m K}' + {m J}^{ m sol}  ight $ is the light part of the heavy				
	baryon angular momentum for $r=0$ (See Eq. (6.32).)	134			
6.6	Contributions to energies of the new predicted states made from $H-$				
	type heavy mesons. Other details as for Table 6.5.	136			

### INTRODUCTION

The non abelian gauge theory which describes, in the perturbative regime, the strong interactions is Quantum Chromodynamics (QCD). Quarks and gluons are the fundamental degrees of freedom of the theory. A key feature of the theory (due to quantum corrections) is asymptotic freedom, i.e. the strong coupling constant increases as the energy scale of interest decreases. The perturbative approach becomes unreliable below a characteristic scale of the theory ( $\Lambda$ ). Quarks and gluons confine themselves into colorless particles called hadrons (pions, protons,..). The latter are the true physical states of the theory.

We need to investigate alternative ways to describe strong interactions, and in general any asymptotically free theory, in the non perturbative regime. This is the fundamental motivation of the present thesis. Although the underlying gauge theory cannot be easily treated in the non perturbative regime we can still use its global symmetries as a guide to build Effective Lagrangian Models. These models will be written directly in terms of the colorless physical states of the theory, i.e. hadrons. Two relevant, approximate symmetries are of extreme theoretical as well as phenomenological interest: Chiral Symmetry and Heavy Spin Symmetry. Chiral Symmetry is the approximate symmetry associated with the light quarks u, d and s, when their masses  $m_q$  are considered to be negligible compared to the invariant scale of the theory  $\Lambda$ . Heavy Spin Symmetry on the other hand is associated with the heavy quarks b, c, and t, whose masses  $M_Q$  are large with respect to  $\Lambda$ . These symmetries greatly reduce the number of unknown parameters and provide a systematic expansion

of the effective Lagrangians in  $m_q$  and 1/M. Another useful guide for the construction of effective Lagrangians will be the expansion for large number of colors  $N_c$  of QCD. In this thesis we will show that the effective Lagrangian models, encoding the relevant symmetries of the underlying fundamental gauge theory, provide a reasonable understanding of the interactions among light mesons at intermediate energies as well as of the properties of Heavy baryons.

In part I of the thesis we will focus our attention on the physics related to the three light quark flavors u, d and s. In part II we will consider the physics associated with the heavy quarks.

In the first part of the thesis we will show that it is possible to build a reasonable chiral and crossing symmetric model for light meson interactions at intermediate energies, which we have called the Chiral Resonance Model (ChRM). Using the previous scheme we will demonstrate that we can understand  $\pi\pi$ -scattering up to the 1 GeV region by considering the resonance exchange together with the contact term contributions and by employing a suitable regularization procedure. We will also observe that to fully describe low energy  $\pi\pi$ -scattering in the Chiral Resonance framework a broad scalar  $\sigma(550)$  particle is needed. At the time when the research work was done this state was not present in the Particle data Group review (PDG). In the latest PDG this state is finally present. Although the parameters associated with the  $\sigma$  are still not well known the quoted range of parameters (mass and width) is consistent with the one determined using the Chiral Resonance Model. We will also see that the resonance  $f_0(980)$  has to be introduced with a mechanism à la Ramsauer-Townsend. It seems likely that any crossing symmetric approximation will

have a similar form. We will regard the ChRM as a leading order  $1/N_c$  mean field approximation for Quantum Chromodynamics.

In the second part of the thesis we will investigate the heavy baryon spectra in the bound state picture. In this picture the heavy baryon is treated as a heavy spin multiplet of mesons  $(Q\bar{q})$  bound in the background field of the nucleon (qqq), which in turn arises as a soliton configuration of light meson fields. A nice feature of this approach is that it permits, in principle, an exact expansion of the heavy baryon properties in simultaneous powers of 1/M and  $1/N_c$ , where M is the heavy quark mass. We will show that a relativistic model with light vectors gives a very satisfactory account of the  $\Sigma_c^* - \Sigma_c$  hyperfine splitting in contrast to the model without light vectors. We will also show that the source of hyperfine splitting is hidden in non manifest heavy spin breaking terms. In the last chapter we will present a generalization of the bound state model. Indeed by binding heavy spin excited multiplets to the background Skyrmion field we will see that we can describe the spectrum of excited heavy baryons of arbitrary spin.

## Acknowledgments

I am deeply grateful to my mentor, Prof. Joseph Schechter for his excellent academic guidance, invaluable advice, and for strongly supporting and encouraging me during my research work. I greatly benefited from the long afternoon discussions about the enchanting world of physics.

I am very happy to thank Dr. Masayasu Harada and Dr. Herbert Weigel, for being very valuable collaborators, for their suggestions and for helpful discussions. I would like to thank Asif Qamar for his collaboration.

I am indebted to Deirdre Black for careful reading of the thesis.

I would like to express my gratitude to the Theoretical High Energy group at Syracuse University for being always very supportive and for providing a very fertile research environment.

I would like to thank the Dipartimento di Fisica Teorica of Napoli University (Italy) for always supporting me and for allowing me to do my research work at Syracuse University, the Italian National Institution for Nuclear Physics (INFN) and the Italian Doctoral Program for partial financial support.

# Part I

Chiral Resonance Model

# Chapter 1

# Introduction to the Chiral Resonance Model

# 1.1 Brief review of QCD, Chiral Symmetry and $1/N_c$

The non abelian theory which describes, in the perturbative regime, the strong interactions is Quantum Chromdynamics (QCD). Quarks and gluons are the associated degrees of freedom [1, 2]. SU(3) is the non abelian gauge group of QCD. We will denote by  $q_c^{\alpha}$  the fermionic matter fields associated with quarks.  $\alpha = u, d, s, ...$  is the flavor index, while c = 1, 2, 3 is the color index. The gauge bosons (gluons) belong to the adjoint representation of the gauge group ( $G_{\mu}^{a}$ , a = 1, ..., 8). The classical QCD Lagrangian density (i.e. which does not include quantum corrections) is

$$L_{color} = -\frac{1}{4}G_a^{\mu\nu}G_{\mu\nu}^a + \sum_{\alpha} \bar{q}_c^{\alpha} \left(i \not\!\!\!D^{cd} - m^{\alpha}\delta^{cd}\right) q_d^{\alpha} , \qquad (1.1)$$

### 4 CHAPTER 1. INTRODUCTION TO THE CHIRAL RESONANCE MODEL

where the color indices are summed via the Einstein convention. The field strength tensor is

$$G_{\mu\nu}^a = \partial_\mu G_\nu^a - \partial_\nu G_\mu^a - g_s f^{abc} G_{b\mu} G_{c\nu} , \qquad (1.2)$$

where  $g_s$  is the coupling constant and  $f^{abc}$  are the group structure constants. The covariant derivative acting on a single quark is

$$D_{\mu}q = (\partial_{\mu} + ig_s G_{\mu}^a T^a)q , \qquad (1.3)$$

where  $T^a$  are the SU(3) generators. A key feature of the theory, due to quantum corrections, is asymptotic freedom, i.e. the strong coupling constant  $g_s$ , decreases as the renormalization scale ( $\mu$ ) increases [3–5]. Indeed at first order in perturbation theory quantum corrections provide

$$\alpha_s(\mu) = \frac{6\pi}{(33 - 2N_f) \ln\left(\frac{\mu}{\Lambda}\right)} + \cdots , \qquad (1.4)$$

where  $N_f$  is the number of flavors whose masses are less than  $\mu$  and  $\Lambda$  is a renormalization invariant scale while,  $g_s^2 = 4\pi\alpha_s$ . It is clear that the perturbative approach is not reliable when  $\mu \to \Lambda$ . Hence Eq. (1.4) itself cannot be trusted in this regime. However, a commonly accepted working hypothesis is that the strong coupling constant keeps increasing at low energies, leading to the phenomenon of quark and gluon confinement. In Eq. (1.4)  $\alpha_s$  is a function of  $\Lambda$ . So the latter can actually be substituted for the dimension free quantity  $\alpha_s$  in any result deduced using QCD. This phenomenon is called dimensional trasmutation.

We need to investigate alternative ways to describe strong interactions, and in general any asymptotically free theory, in the non perturbative regime. This is the fundamental motivation of the present thesis.

It is, however, possible to deduce more information from QCD, by studying it for some limiting values of its parameters. The parameters which we can tune are  $\alpha_s$ 

(i.e.  $\Lambda$ ), the flavor number, the quark masses and the color number <sup>1</sup>.

For the purposes of the research work presented in part I we will consider only the lightest three flavors u, d and s ( $N_f = 3$ ). In part II we will consider heavy quark physics. The QCD Lagrangian density in the limit of zero mass for the light quarks gains the classical symmetry  $U_L(3) \otimes U_R(3)$ . The quark fields will transform as (for convenience we omit the color indices)

$$q_L^{\alpha} \to g_{L\beta}^{\ \alpha} q_L^{\beta} , \quad q_R^{\alpha} \to g_{R\beta}^{\ \alpha} q_R^{\beta} ,$$
 (1.5)

where  $g_{L,R} \in U_{L,R}(3)$  acts, respectively, on the *Left* and *Right* components of the Dirac spinors.

The classical symmetry  $U_L(3) \otimes U_R(3)$  is *explicitly* broken via quantum corrections, i.e.

$$U_L(3) \otimes U_R(3) \longrightarrow U_V(1) \otimes SU_L(3) \otimes SU_R(3)$$
, (1.6)

This phenomenon is called the chiral anomaly.  $U_V(1)$  is associated with baryon number conservation. Invariance under the non abelian symmetry group  $SU_L(3) \otimes SU_R(3)$  predicts that all the physical states must be classified according to irreducible representations of the group. Nature does not realize such a physical spectrum and it is assumed that the symmetry is spontaneously broken via

$$SU_L(3) \otimes SU_R(3) \stackrel{SSB}{\longrightarrow} SU_V(3)$$
 (1.7)

The Nambu-Goldstone theorem states that the lost symmetry must be compensated by the presence of massless bosons (Goldstone bosons). In QCD such Goldstone bosons, associated with the spontaneously broken chiral symmetry, can be identified

<sup>&</sup>lt;sup>1</sup>Among these parameters (for completness) we must mention the  $\Theta$  – vacuum parameter, associated with the strong CP (Charge times Parity) violation. The experimental determination of the neutron dipole moment provides a very stringent upper bound, i.e.  $\Theta \leq 2 \times 10^{-10}$ . Hence, in the following discussion we will not consider it.

with the octet of pseudoscalar mesons  $\pi, K, \bar{K}, \eta$ . All of the other particles can be classified according to the irreducible representations of the diagonal subgroup  $SU_V(3)$ .

Now we will consider the large  $N_c$  limit of Quantum Chromodynamics [6]. The expansion in  $1/N_c$  will allow us to deduce much new information whose key feature is its validity in the non perturbative as well as perturbative regime of QCD. In this paragraph we will review only some of the  $1/N_c$  predictions, the reader will find more results in [6]. In particular here we will consider only the key features relevant for part I of the thesis.

For  $N_c \to \infty$ , keeping constant the following product  $\alpha_s N_c$  one can prove the following meson properties.

a At the leading order in  $1/N_c$  the two point Green's functions built out of local quark bilinear operators ( $J = \bar{q}q$ ,  $\bar{q}\gamma_{\mu}q$ , etc.) are saturated by the exchange of an infinite number of non exotic meson resonances, i.e. of the  $\bar{q}q$  type.

$$\langle J(k)J(-k)\rangle = \sum_{n=1}^{\infty} \frac{a_n^2}{k^2 - m_n^2} .$$
 (1.8)

 $m_n$  is  $n^{\text{th}}$  meson mass, and  $a_n = <0|J|n>$  is the J matrix element which creates the  $n^{\text{th}}$  meson from the vacuum.

- b The meson-meson scattering amplitude described by a 4-point Green's function, schematically represented in Fig.1.1(a), is  $O(1/N_c)$ . So we can deduce that the interactions among the mesons are subleading in the  $1/N_c$  expansion.
- c Non exotic mesons are stable. The 3-point Green function associated with the decay amplitude is represented in Fig.1.1(b) and is  $O(1/\sqrt{N_c})$ . Hence the decay itself is  $O(1/N_c)$ .

The chiral limit together with the  $1/N_c$  expansion are the two ingredients motivating the chiral resonance model which we will describe in the following paragraph.

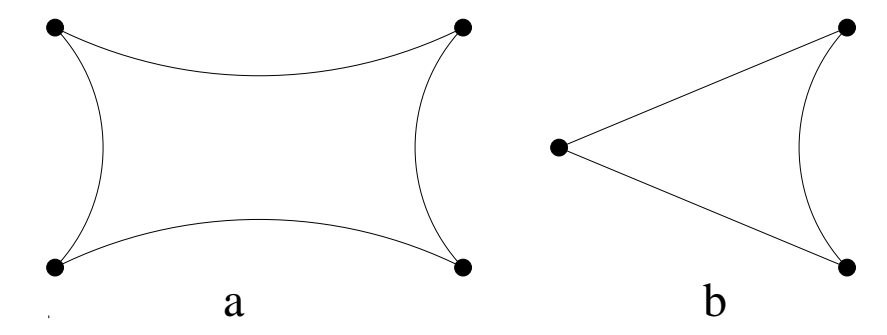


Figure 1.1: (a) schematically represents the 4-point Green function. (b) represents the 3-point Green function. In (a) and (b) the external lines represent a quark loop, while ( $\bullet$ ) are the insertions of the non exotic meson fields.

# 1.2 Chiral Resonance Model

Asymptotic freedom strongly reduces the predictive power of QCD, in particular for the description of strong interactions among mesons at low energies. Chiral perturbation theory  $(\chi PT)$  [7] allowes a systematic investigation of the strong interactions of the octect of Goldstone bosons  $(\pi, K, \overline{K}, \eta)$ .  $\chi PT$ , essentially, relies on the expansion in energies of the scattering amplitudes, and it improves the Born terms of the Chiral Lagrangian by including quantum corrections via *loops* and necessary counterterms. The energy expansion converges very fast for energies less than 400-500~MeV. It is a very hard task to extend the  $\chi PT$  scheme at higher energies, since the physical singularities associated with the resonances which exist in this region cannot be easily reproduced by a truncated (in energy) power expansion.

In order to describe the interactions among light mesons up to an energy (in the center of mass) of 1-1.5 GeV is clear that one is forced to include the effects of these resonances in this region.

The question is: How to include such resonances? As noted in the previous

paragraph the meson-meson scattering amplitudes in the leading order in  $1/N_c$  can be obtained by summing up all possible tree diagrams obtained via an effective Lagrangian density, which contains an *infinite* number of bosonic resonances per each possible spin. An *infinite* number of contact terms is also allowed [6].

The  $1/N_c$  analysis is very interesting, since it supports the Lagrangian effective models as reasonable models, but at the moment is so general as to appear useless. We will see that this is not the case.

Using the  $1/N_c$  analysis as a guide we will try to build a *new* effective model [8–10] to describe the meson scattering up to about 1 GeV.

A scattering amplitude built using an effective Lagrangian, automatically satisfies crossing symmetry. On the other hand just calculating the tree approximation to an effective Lagrangian will not guarantee that unitarity is satisfied. This is the handle we will use to try to investigate additional structure. Unitarity has of course the consequence that the amplitude must have some suitable imaginary term which in the usual field theory is provided by loop diagrams. However the leading  $1/N_c$  approximation will give a purely real amplitude away from the singularities at the direct s-channel poles. We may consider the imaginary part of the leading  $1/N_c$  amplitude to consist just of the sum of delta functions at each such singularity. Clearly, the real part has a much more interesting structure and we will mainly confine our attention to it.

Unitarity has the further consequence that the real parts of the partial wave amplitudes must satisfy certain well known bounds. The crucial question is how these bounds are satisfied since, as will see, individual contributions tend to violate them badly. At first one might expect that all of the infinite number of resonances are really needed to obtain cancellations. However the success of chiral dynamics at very low energies where none of the resonances have been taken into account suggests that

this might not be the case. It is clear that we need to postulate a new principle which has been introduced in Ref. [8] and we will call it *local cancellation*. Local cancellation cannot be easily derived from QCD, but if true it would greatly simplify the task of extending the phenomenological description of scattering processes to higher energies.

According to this simple principle the inclusion of the resonances, up to the energy one wants to describe, in the direct channel as well as in the cross channels, will allow us to saturate the unitarity bounds and also will allow us to describe the phenomenology involved. Now one can easily understand the relevant role played by crossing symmetry, already pointed out in Veneziano's famous paper [11]. Indeed, as we will see in the next chapter, local cancellations among the different contributions from the resonances will, non trivially, enforce unitarity. In  $\pi\pi$  scattering, we will see that the introduction of the cross term due to  $\rho$  meson exchange in a chirally invariant manner, in the Isospin = 0 and zero orbital angular momentum case, substantially delays the onset of the severe unitarity violation which would be present in the simplest chiral Lagrangian of pions.

The onset of the unitarity bound via the *local cancellation* principle will also require the existence of the scalar particle  $\sigma(550)$  [8–10] in order to successfully describe  $\pi\pi$ -scattering up to about 1.2 GeV.

In order to start this investigation it seems reasonable to keep in the Lagrangian only local operators with the lowest number of derivatives. Operators with a higher number of derivatives destabilize the theory at high energy and will make it more difficult to accomplish the required *local cancellation*. Further restrictions will be obtained by imposing chiral symmetry.

In the last paragraph of the present chapter we will show how to include the scalar, vectorial and tensorial resonances in order to preserve chiral symmetry.

We will now summarize the chiral resonance model according to the following

- a The effective Lagrangian will contain only terms with the lowest number of derivatives. These local operators will be chirally symmetric.
- b The model will be suitable for the real part of the physical amplitude. Such an amplitude must obey *crossing* symmetry.
- c We will include in the scheme only the resonances whose masses lie in the energy range of interest. Away from the poles in the direct channel unitarity is expected to be provided by the *local cancellation* principle.
- d A suitable regularization method must be employed to avoid divergences at each direct channel pole for the physical amplitude.

In the next paragraph we will explain how to regularize the s-channel poles. The other points will be investigated in the next two chapters. In particular we will study the  $\pi\pi \to \pi\pi$  and  $\pi\pi \to K\bar{K}$  scattering amplitudes. These two channels are a classically important check for any model whose goal is to describe meson interactions at intermediate energies.

# 1.3 Regularization of the Model

In the large  $N_c$  picture the leading amplitude (of order  $1/N_c$ ) is a sum of polynomial contact terms and tree-type resonance exchanges. Furthermore the resonances should be of the simple  $q\overline{q}$  type; glueball and multi-quark meson resonances are suppressed. In our phenomenological model there is no way of knowing *a priori* whether a given experimental state is actually of the  $q\overline{q}$  type. For definiteness we will keep all relevant resonances even though the status of a low lying scalar resonances like the  $f_0(980)$ 

has been considered especially controversial [32]. If such resonances turn out in the future to be not of type  $q\bar{q}$ , their tree contributions would be of higher order than  $1/N_c$ . In this event the amplitude would still of course satisfy crossing symmetry.

The most problematic feature involved in comparing the leading  $1/N_c$  amplitude with experiment is that it does not satisfy unitarity. In fact, resonance poles like

$$\frac{1}{M^2 - s} \tag{1.9}$$

will yield a purely real amplitude, except at the singularity, where they will diverge and drastically violate the unitarity bound. Thus in order to compare the  $1/N_c$  amplitude with experiment we must regularize the denominators in some way. The usual method, as employed in Ref. [8], is to regularize the propagator so that the resulting partial wave amplitude has the locally unitary form

$$\frac{M\Gamma}{M^2 - s - iM\Gamma} \ . \tag{1.10}$$

This is only valid for a narrow resonance in a region where the *background* is negligible. Note that the  $-iM\Gamma$  is strictly speaking a higher order in  $1/N_c$  effect.

For a very broad resonance there is no guarantee that such a form is correct. Actually, in Ref. [8] it was found necessary to include a rather broad low lying scalar resonance (denoted  $\sigma(550)$ ) to avoid violating the unitarity bound. A suitable form turned out to be of the type

$$\frac{MG}{M^2 - s - iMG'} , \qquad (1.11)$$

where G is not equal to the parameter G' which was introduced to regularize the propagator. Here G is the quantity related to the squared coupling constant.

Even if the resonance is narrow, the effect of the background may be rather important. Demanding local unitarity in this case yields a partial wave amplitude of the well known form [13]:

$$\frac{e^{2i\delta}M\Gamma}{M^2 - s - iM\Gamma} + e^{i\delta}\sin\delta , \qquad (1.12)$$

where  $\delta$  is a background phase (assumed to be slowly varying). We will see in the next chapters that such a regularization method is needed to fully understand the  $\pi\pi \to \pi\pi$  and  $\pi\pi \to K\bar{K}$  scattering in the  $f_0(980)$  region. We will adopt a point of view in which this form is regarded as a kind of regularization of our model. Of course, non zero  $\delta$  represents a rescattering effect which is of higher order in  $1/N_c$ . The quantity  $e^{2i\delta}$ , taking  $\delta = constant$ , can be incorporated, for example, into the squared coupling constant connecting the resonance to two pions. In this way, crossing symmetry can be preserved. From its origin, it is clear that the complex residue does not signify the existence of a *ghost* particle. The non-pole background term in Eq. (1.12) and hence  $\delta$  is to be predicted by the other pieces in the effective Lagrangian.

Another point which must be addressed in comparing the leading  $1/N_c$  amplitude with experiment is that it is purely real away from the singularities. The regularizations mentioned above do introduce some imaginary pieces but these are clearly very model dependent. Thus it seems reasonable to compare the real part of our predicted amplitude with the real part of the experimental amplitude. Note that the difficulties mentioned above arise only for the direct channel poles; the crossed channel poles and contact terms will give purely real finite contributions.

It should be noted that if we predict the real part of the amplitude, the imaginary part can always be recovered by assuming elastic unitarity.

# 1.4 Chiral Lagrangian

In the low energy physics of hadrons it is important to correctly introduce the spontaneous chiral symmetry breaking structure. In our approach we will introduce it via non linear realizations. It is known that this method reproduces the low energy theorems obtained via current algebra. We start here with the definition of the  $3 \times 10^{-5}$ 

3 matrix U,

$$U = \xi^2 , \qquad \xi = e^{i\phi/F_{\pi}} , \qquad (1.13)$$

where  $F_{\pi}$  is a pion decay constant. U is parameterized by the pseudoscalar matrix  $\phi$ , which is identified with the pseudoscalar meson octect. Under the chiral group  $U(3)_{\rm L} \times U(3)_{\rm R}$ , U transforms linearly.

$$U \to g_{\rm L} U g_{\rm R}^{\dagger} ,$$
 (1.14)

where  $g_{L,R} \in U(3)_{L,R}$ . Under the chiral transformation Eq. (1.14),  $\xi$  transforms non-linearly:

$$\xi \to g_{\mathcal{L}} \xi K^{\dagger}(\phi, g_{\mathcal{L}}, g_{\mathcal{R}}) = K(\phi, g_{\mathcal{L}}, g_{\mathcal{R}}) \xi g_{\mathcal{R}}^{\dagger} . \tag{1.15}$$

The previous equation implicitly defines the matrix  $K(\phi, g_L, g_R)$ . The vector meson nonet  $\rho_{\mu}$  is introduced as a gauge field [15] which transforms as

$$\rho_{\mu} \to K \rho_{\mu} K^{\dagger} - \frac{i}{\widetilde{q}} K \partial_{\mu} K^{\dagger} ,$$
(1.16)

where  $\tilde{g}$  is a gauge coupling constant. (For an alternative approach see, for a review, Ref. [16].) It is convenient to define

$$p_{\mu} = \frac{i}{2} \left( \xi \partial_{\mu} \xi^{\dagger} - \xi^{\dagger} \partial_{\mu} \xi \right) ,$$

$$v_{\mu} = \frac{i}{2} \left( \xi \partial_{\mu} \xi^{\dagger} + \xi^{\dagger} \partial_{\mu} \xi \right) ,$$

$$(1.17)$$

which transform as

$$p_{\mu} \rightarrow K p_{\mu} K^{\dagger} ,$$
  
 $v_{\mu} \rightarrow K v_{\mu} K^{\dagger} + i K \partial_{\mu} K^{\dagger} ,$  (1.18)

and are the chiral group Maurer - Cartan one form. Using the above quantities we construct the chiral Lagrangian including both pseudoscalar and vector mesons:

$$\mathcal{L} = +\frac{1}{2}m_v^2 \text{Tr} \left[ (\tilde{g}\rho_\mu + v_\mu)^2 \right] + \frac{F_\pi^2}{2} \text{Tr} \left[ p_\mu p^\mu \right] - \frac{1}{4} \text{Tr} \left[ F_{\mu\nu}(\rho) F^{\mu\nu}(\rho) \right], \tag{1.19}$$

where  $F_{\mu\nu} = \partial_{\mu}\rho_{\nu} - \partial_{\nu}\rho_{\mu} + i\tilde{g}[\rho_{\mu}, \rho_{\nu}]$  is a gauge field strength of vector mesons.  $\tilde{g}$  is connected to the vector meson coupling to two pions  $g_{\rho\pi\pi}$  via

$$g_{\rho\pi\pi} = \frac{m_{\rho}^2}{\tilde{g}F_{\pi}^2} \ . \tag{1.20}$$

In the real world chiral symmetry is explicitly broken by the quark mass term  $-\widehat{mq}\mathcal{M}q$ , where  $\widehat{m} \equiv (m_u + m_d)/2$ , and  $\mathcal{M}$  is the dimensionless matrix:

$$\mathcal{M} = \begin{pmatrix} 1+y & & \\ & 1-y & \\ & & x \end{pmatrix} . \tag{1.21}$$

Here x and y are the quark mass ratios:

$$x = \frac{m_s}{\widehat{m}} , \qquad y = \frac{1}{2} \left( \frac{m_d - m_u}{\widehat{m}} \right) .$$
 (1.22)

These quark masses lead to mass terms for pseudoscalar mesons. Moreover, in considering the processes related to the kaon, (in this thesis we will consider  $\pi\pi \to K\overline{K}$  scattering amplitude) we need to take account of the large mass gap between the s quark mass and the u and d quark masses. These effects are included as SU(3) symmetry breaking terms in the above Lagrangian, which are summarized, for example, in Refs. [17,18]. Here we write the lowest order pseudoscalar mass term only:

$$\mathcal{L}_{\phi-\text{mass}} = \delta' \text{Tr} \left[ \mathcal{M} U^{\dagger} + \mathcal{M}^{\dagger} U \right] , \qquad (1.23)$$

where  $\delta'$  is an arbitrary constant.

We next introduce higher resonances into our Lagrangian. Firstly, we write the interaction between the scalar nonet field S and pseudoscalar mesons. Under the chiral transformation, this S transforms as  $S \to KSK^{\dagger}$ . A possible form which includes the minimum number of derivatives is proportional to

$$\operatorname{Tr}\left[Sp_{\mu}p^{\mu}\right] . \tag{1.24}$$

The coupling of a physical isosinglet field to two pions is then described by

$$\mathcal{L}_{\sigma} = +\frac{\gamma_0}{\sqrt{2}} \, \sigma \, \partial_{\mu} \vec{\pi} \cdot \partial^{\mu} \vec{\pi} \, . \tag{1.25}$$

Here we should note that chiral symmetry requires derivative-type interactions between scalar fields and pseudoscalar mesons. Secondly, we represent the tensor nonet field by  $T_{\mu\nu}$  (satisfying  $T_{\mu\nu} = T_{\nu\mu}$ , and  $T^{\mu}_{\mu} = 0$ ), which transforms as

$$T_{\mu\nu} \to K T_{\mu\nu} K^{\dagger}$$
 (1.26)

The interaction term is given by

$$\mathcal{L}_T = -\gamma_2 F_\pi^2 \text{Tr} \left[ T_{\mu\nu} p^\mu p^\nu \right] . \tag{1.27}$$

The heavier vector resonances such as  $\rho(1450)$  can be introduced in the same way as  $\rho$  in Eq. (1.19).

In general, for a complete description of the mesonic processes one should include the effects due to chiral anomalies. Since in this part of the thesis we will not deal with such processes we refer the reader to the following references [17–19].

# Chapter 2

# A fundamental process: $\pi\pi$ scattering

# 2.1 Introduction to $\pi\pi$ scattering

Historically, the analysis of  $\pi\pi$  scattering has been considered an important test of our understanding of strong interaction physics (QCD, now) at low energies. It is commonly accepted that the key feature is the approximate spontaneous breaking of chiral symmetry. Of course, the kinematical requirements of unitarity and crossing symmetry should be respected. The chiral perturbation scheme ( $\chi$ PT) [7], which improves the tree Lagrangian approach by including loop corrections and counterterms, can provide a description of the scattering up to the energy region slightly above threshold (400-500~MeV). Hence  $\chi$ PT is very useful for describing kaon decays into  $2\pi$  and  $3\pi$  (for an application see Ref. [20]). In Ref. [21] the derivative expansion has been used to estimate some of the parameters associated with CP violation for the  $3\pi$  decays of neutral kaons. In order to describe the scattering up to energies beyond this region (say to around 1 GeV) it is clear that the effects of particles lying in this region

must be included. The Chiral Resonance Model (ChRM) provides a simple prescription for including these resonances. We will see that by applying the ChRM recipe we will be able to understand the scattering processes schematically represented in Fig.2.1. The kinematics, the unregularized invariant scattering amplitudes and the

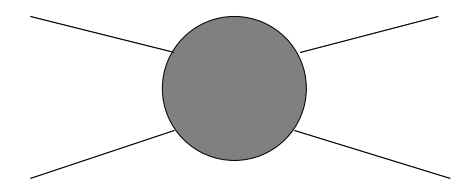


Figure 2.1: Schematic representation of a scattering process.

generic scattering matrix S are presented in Appendix A.

In the previous chapter we stated that the ChRM predicts the real part of the scattering amplitude. The imaginary term can be recovered via the unitarity relations. Specializing Eq. (A.6) in Appendix A to the  $\pi\pi$  channel we have, for the imaginary piece  $I_l^I$  of the I, l partial wave amplitude

$$I_l^I = \frac{1}{2} \left[ 1 \pm \sqrt{\eta_l^{I^2} - 4R_l^{I^2}} \right] ,$$
 (2.1)

where  $\eta_l^I$  is the elasticity parameter. I and l are the isospin and the orbital angular momentum. Obviously, this formula is only meaningful if the real part obeys the bound

$$|R_l^I| \le \frac{\eta_l^I}{2} \ . \tag{2.2}$$

The main difficulty one has to overcome in obtaining a unitary amplitude by the present method is the satisfaction of this bound Eq. (2.2).

We want to remark that making the regularizations of direct channel poles such as in Eqs. (1.10) and (1.12) which provide unitarity in the immediate region of a narrow resonance, is not at all tantamount to unitarizing the model by hand.

In this chapter we will present the first evidence of local cancellation, obtained among the current algebra and the vector meson  $\rho$  contributions. We will then show that we need to introduce a broad scalar resonance (i.e.  $\Gamma \gtrsim M$ ) to fully understand the scattering process at low energies ( $\leq 800 \text{ MeV}$ ). The effect of chirally invariant contact terms with a higher number of derivatives will also be investigated.

# 2.2 Current Algebra and $\rho$ vector-meson exchange

In this section we will study the partial waves for  $\pi\pi$  scattering computed in a chiral Lagrangian model which contains both the pseudoscalar and vector mesons, (i.e., the lowest lying s-wave quark-antiquark bound states). Near threshold  $\eta_l^I=1$ ,  $R_l^I$  is small and we should choose the minus sign in Eq. (2.1) so that

$$I_l^I(s) \approx \left[R_l^I\right]^2. \tag{2.3}$$

In the large  $N_c$  limit the amplitude near threshold is purely real and of the order  $1/N_c$ . This is consistent with Eq. (2.3) which shows that  $I_l^I(s)$  is of order  $1/N_c^2$  and hence comes in at the second order. This agrees with the chiral perturbation theory approach [7] in which  $R_l^I(s)$  comes from the lowest order tree diagram while  $I_l^I$  arises from the next order loop diagram. On the other hand, when we depart from the threshold region the  $1/N_c$  approach treats the contribution of the  $\rho$ -meson at first order while the chiral perturbation theory approach treats it at second and higher orders. A straightforward computation using the pion lagrangian (second term in Eq. (1.19)) together with the explicit chiral breaking term in Eq. (1.23) yields the  $\pi\pi$  scattering amplitude [22] defined in Eq. (A.8):

$$A_{CA}(s,t,u) = 2\frac{s - m_{\pi}^2}{F_{-}^2} \ . \tag{2.4}$$

This equation will be called the *current algebra result*. With (A.9) and (A.11) we obtain  $R_0^0(s) = T_{11;0}^0(s)$  as illustrated in Fig. 2.2. The experimental Roy curves [23] are also shown. Up until about 0.5 GeV the agreement is quite reasonable (and can be fine—tuned with second order chiral perturbation terms) but beyond this point  $R_0^0$  keeps increasing monotonically and badly violates the unitarity bound (2.2). We

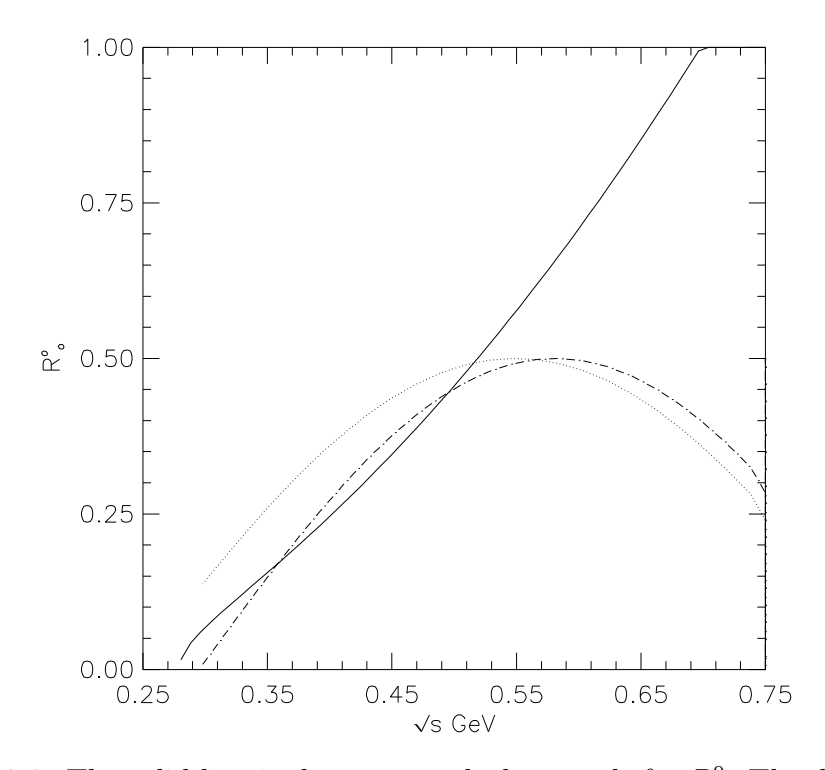


Figure 2.2: The solid line is the current algebra result for  $R_0^0$ . The dotted and dot-dashed lines are the Roy curves for  $R_0^0$ .

will see now that the introduction of the  $\rho$ -meson greatly improves the situation. The chiral Lagrangian for the vector-meson pion system is displayed in Eq. (1.19). The Lagrangian piece in (1.19) yields both a pole-type contribution (from the  $\rho_{\mu}v^{\mu}$  cross term) and a contact term contribution (from the  $v_{\mu}v^{\mu}$  term) to the amplitude at tree

level:

$$A_{\rho}(s,t,u) = -\frac{g_{\rho\pi\pi}^2}{2} \left( \frac{u-s}{m_{\rho}^2 - t} + \frac{t-s}{m_{\rho}^2 - u} \right) + \frac{g_{\rho\pi\pi}^2}{2m_{\rho}^2} \left[ (t-s) + (u-s) \right] . \tag{2.5}$$

where  $m_{\rho} = 0.769~GeV$  and  $g_{\rho\pi\pi} = 8.56$ . We notice that the entire first term in (1.19)

$$\operatorname{Tr}\left[\left(\tilde{g}\rho_{\mu}+v_{\mu}\right)^{2}\right] , \qquad (2.6)$$

is chiral invariant since  $v_{\mu}$  and  $-\tilde{g}\rho_{\mu}$  transform identically. However the  $\text{Tr}(\rho_{\mu}v^{\mu})$  and  $\text{Tr}(v_{\mu}v^{\mu})$  pieces are not separately chiral invariant. This shows that the addition of the  $\rho$ -meson in a chiral invariant manner necessarily introduces a contact term in addition to the minimal pole term. Adding up the two terms in Eq. (2.5) and the term in Eq. (2.4) yields finally

$$A_{CA+\rho}(s,t,u) = 2\frac{s - m_{\pi}^2}{F_{\pi}^2} - \frac{g_{\rho\pi\pi}^2}{2m_{\rho}^2} \left[ \frac{t(u-s)}{m_{\rho}^2 - t} + \frac{u(t-s)}{m_{\rho}^2 - u} \right] . \tag{2.7}$$

In this form we see that the threshold (current algebra) results are unaffected since the second term drops out at t = u = 0. An alternative approach [24] to obtaining Eq. (2.7) involves introducing a chiral invariant  $\rho\pi\pi$  interaction with two more derivatives. A(s,t,u) has no singularities in the physical region. Reference to Eq. (A.9) shows that the isospin amplitudes  $T_{11}^0$  and  $T_{11}^2$  also have no singularities. However the  $T_{11}^1$  amplitude has the expected singularity at  $s = m_\rho^2$ . This may be cured in a conventional way, while still maintaining crossing symmetry, by the replacements

$$\frac{1}{m_{\rho}^{2} - t, u} \to \frac{1}{m_{\rho}^{2} - t, u - i m_{\rho} \Gamma_{\rho} \theta(t, u - 4m_{\pi}^{2})} . \tag{2.8}$$

A modification of this sort would enter automatically if we were to carry the computation to order  $\frac{1}{N_c^2}$ . However we shall regard (2.8) as a phenomenological regularization of the leading amplitude.

Now let us look at the actual behaviour of the real parts of the partial wave amplitudes.  $R_0^0$ , as obtained from Eq. (2.7), is graphed in Fig. 2.3 for an extensive range of  $\sqrt{s}$ , together with the *current algebra* result.

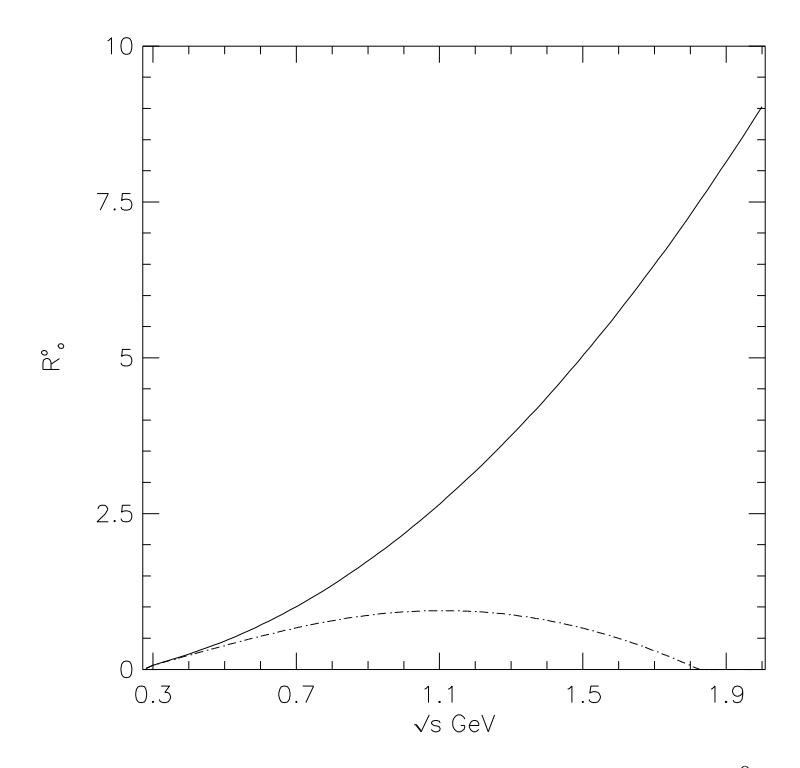


Figure 2.3: The solid line is the current algebra result for  $R_0^0$ . The dot-dashed line is the  $\rho + \pi$  for  $R_0^0$ .

We immediately see that there is a remarkable improvement; the effect of adding  $\rho$  is to bend back the rising  $R_0^0(s)$  so there is no longer a drastic violation of the unitarity bound until after  $\sqrt{s} = 2 \ GeV$ . There is still a relatively small violation which we will discuss later. Note that the modification in Eq. (2.8) plays no role in the improvement since it is only the non-singular t and u channel exchange diagrams which contribute.

It is easy to see that the *delayed* drastic violation of the unitarity bound  $|R_l^I| \leq \frac{1}{2}$  is a property of all partial waves. We have already learned from (2.7) that the amplitude A(s,t,u) starts out rising linearly with s. Now Eq. (2.5) shows (for fixed scattering angle) that for large s the  $\rho$  exchange terms behave as  $s^0$ . The leading large s behavior will therefore come from the sum of the original *current-algebra* term and the new *contact-term*:

$$A_{CA+\rho}(s,t,u) \simeq \frac{2s}{F_{\pi}^2} \left( 1 - 3\frac{k}{4} \right), \quad k \equiv \frac{m_{\rho}^2}{\tilde{g}F_{\pi}^2}$$
 (2.9)

But k is numerically around 2 [25], so A(s,t,u) eventually decreases linearly with s. This turn-around, which is due to the contact term that enforces chiral symmetry, delays the onset of drastic unitarity violation until well after the  $\rho$  mass. It thus seems natural to speculate that, as we go up in energy, the leading tree contributions from the resonances we encounter (including both crossed channel as well as s-channel exchange) conspire to keep the  $R_l^I(s)$  within the unitarity bound This is the first evidence of the local cancellation phenomenon. We notice that the cancellation among resonance and contact term contributions for large s allowed Weinberg in Ref. [26] to deduce some remarkable asymptotic relations about the resonance spectrum and the pion couplings.

In Figure 2.4 we show the partial waves  $R_1^1$  and  $I_1^1$  computed using Eq. (2.7) and Eq. (2.8). Not surprisingly, these display the standard resonant forms. The dominance of the vector–meson  $\rho$  in the I = l = 1 channel is used in  $\chi$ PT to estimate

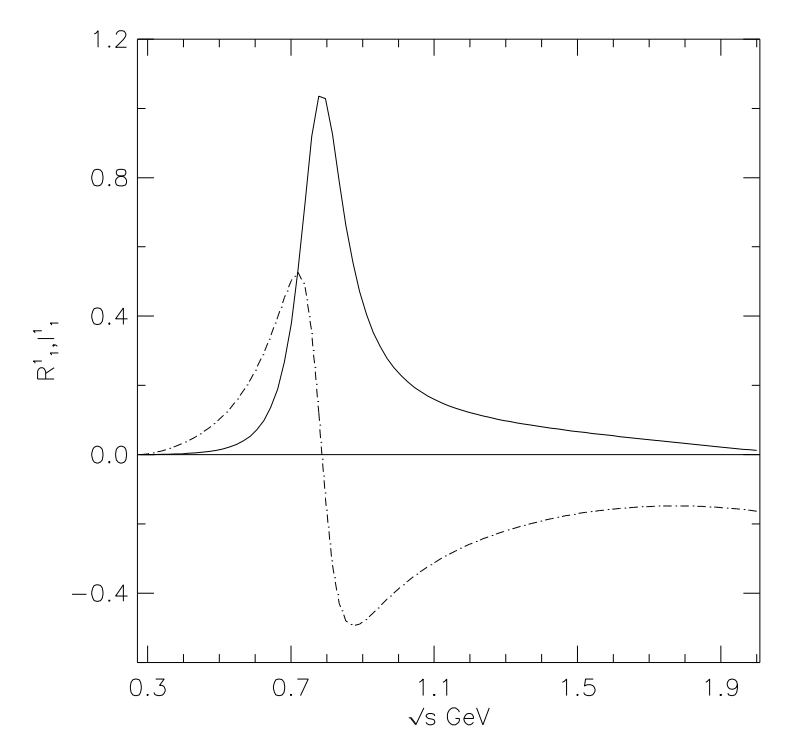


Figure 2.4: The solid line represents the imaginary term  $I_1^1$ . The dot-dashed line is  $R_1^1$ .

some of the counterterm coefficients [27]. For completeness we present the  $R_0^2$  and  $R_2^0$  amplitudes in Fig. 2.5. We notice that these amplitudes obey the unitarity limits up to about 2 GeV.

In this section we have shown that the inclusion of the  $\rho$ -meson dramatically reduces the onset of unitarity violation in the  $R_0^0$  channel (see. Fig. 2.3). We notice that this channel contains the exchange vector meson diagram which provides a decisive contribution. This result is a confirmation, not only, of the exchange symmetry but also of the relevance of the *crossing* symmetry.

The cancellation for large s is due to the contact term  $v^{\mu}v_{\mu}$ . The last term is fundamental in order to introduce the  $\rho$  in a chiral symmetric way. In the following we will mainly study the  $R_0^0$  channel, since this has the worst behaviour for large s.

### 2.3 Is the $\sigma(550)$ alive?

As shown in Figure 2.6, although the introduction of the  $\rho$ -meson dramatically improves unitarity up to about 2 GeV,  $R_0^0$  violates unitarity to a lesser extent starting at around 500 MeV. What is needed to restore unitarity over the full range of interest and to give better agreement with the experimental data for  $\sqrt{s} \lesssim 900 \ MeV$ ?

- i. Below 450 MeV,  $R_0^0(s)$  actually lies a little below the Roy curves (see Fig. 2.2). Hence it would be nice to find a tree level mechanism which yields a small positive addition in this region.
- ii. In the  $600 1300 \ MeV$  range, an increasingly negative contribution is clearly required to keep  $R_0^0$  within the unitarity bound.

In Reference [8] it has been shown that it is possible to satisfy both of these criteria by introducing a broad scalar resonance (like the old  $\sigma$ ) with a mass around 550 MeV.

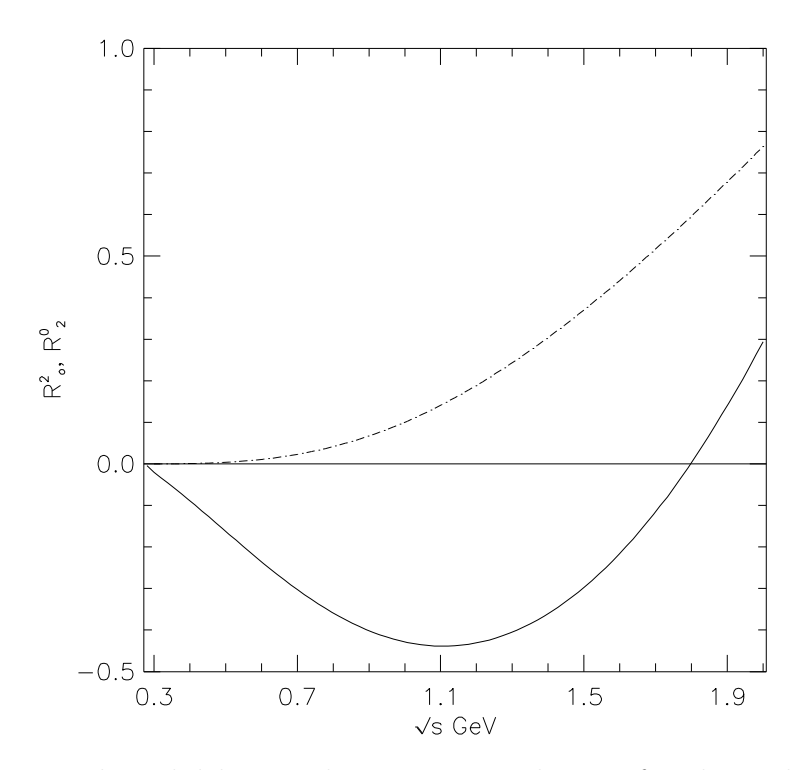


Figure 2.5: The solid line is the  $\pi + \rho$  contribution for the real part of  $I=2,\ l=0.$  The dot-dashed line is the  $\pi + \rho$  contribution for the real part of  $I=0,\ l=2.$ 

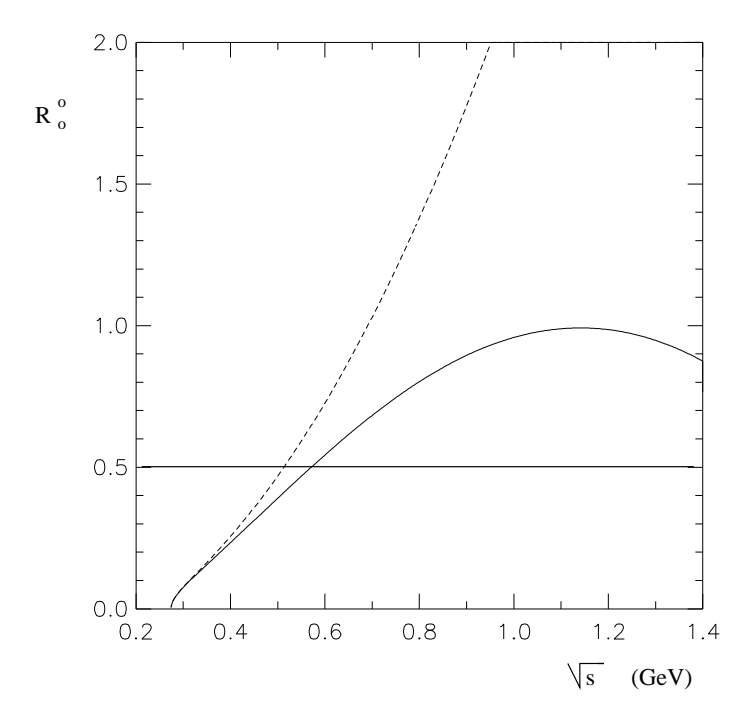


Figure 2.6: Enlarged version of Fig. 2.3. The solid line which shows the current algebra  $+ \rho$  result for  $R_0^0$  is much closer to the unitarity bound of 0.5 than the dashed line which shows the current algebra result alone.

In this model the  $\sigma$  is not realized as a *chiral partner* but is introduced as a matter field with respect to chiral transformations. The  $\sigma$  contribution to the invariant amplitude A(s,t,u) is

$$ReA_{\sigma}(s,t,u) = Re\frac{32\pi}{3H}\frac{G}{M_{\sigma}^{3}}(s-2m_{\pi}^{2})^{2}\frac{(M_{\sigma}^{2}-s)+iM_{\sigma}G'}{(s-M_{\sigma}^{2})^{2}+M_{\sigma}^{2}G'^{2}},$$
 (2.10)

where

$$H = \left(1 - 4\frac{m_{\pi}^2}{M_{\sigma}^2}\right)^{\frac{1}{2}} \left(1 - 2\frac{m_{\pi}^2}{M_{\sigma}^2}\right)^2 \approx 1 , \qquad (2.11)$$

and G is related to the coupling constant  $\gamma_0$  defined in Eq. (1.25) as

$$G = \gamma_0^2 \frac{3HM_\sigma^3}{64\pi} \ . \tag{2.12}$$

Note that the factor  $(s-2m_\pi^2)^2$  is due to the derivative-type coupling required for chiral symmetry in Eq. (1.25). The total amplitude will be crossing symmetric since A(s,t,u) and A(u,t,s) in Eq. (A.8) are obtained by performing the indicated permutations. G' is a parameter which we introduce to regularize the propagator. It can be called a width, but it turns out to be rather large so that, after the  $\rho$  and  $\pi$  contributions are taken into account, the partial wave amplitude  $R_0^0$  does not clearly display the characteristic resonant behavior. In the most general situation one might imagine that G could become complex as in Eq. (1.12) due to higher order in  $1/N_c$  corrections. It should be noted, however, that Eq. (1.12) expresses nothing more than the assumption of unitarity for a narrow resonance and hence should not really be applied to the present broad case.

A reasonable fit was found in Ref. [8] for G purely real, but not equal to G'. By the use of Eq. (2.1), unitarity is in fact locally satisfied. In [10] a best overall fit is obtained with the parameter choices  $M_{\sigma} = 559 \ MeV$ , G/G' = 0.29 and  $G' = 370 \ MeV$ . These have been slightly fine-tuned from the values in Ref. [8] in order to obtain a better fit in the 1 GeV region. The contribution to  $R_0^0$  due only to the presence of the low mass broad scalar  $\sigma(550)$  is displayed in Fig. 2.7.

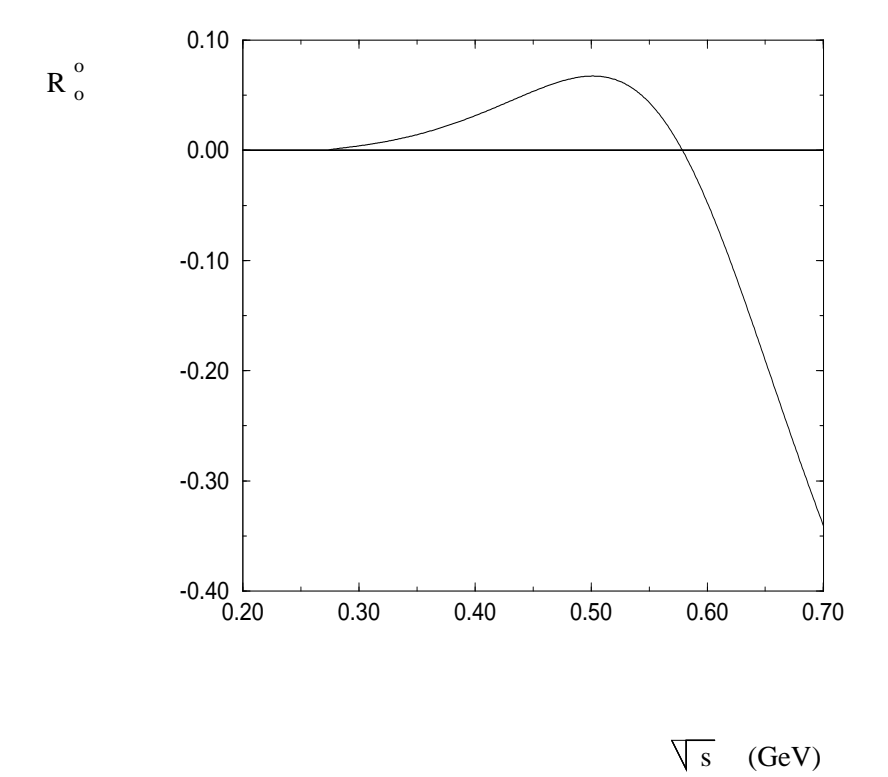


Figure 2.7: Contribution to  $R_0^0$  due to the  $\sigma(550)$  particle.

29

The curve crosses zero at about  $\sqrt{s} = 560$  MeV. The small deviation is due to the effect of the cross diagrams. The result for the real part of  $R_0^0$  due to the inclusion of the  $\sigma$  contribution along with the  $\pi$  and  $\rho$  contributions is shown in Fig. 2.8. It

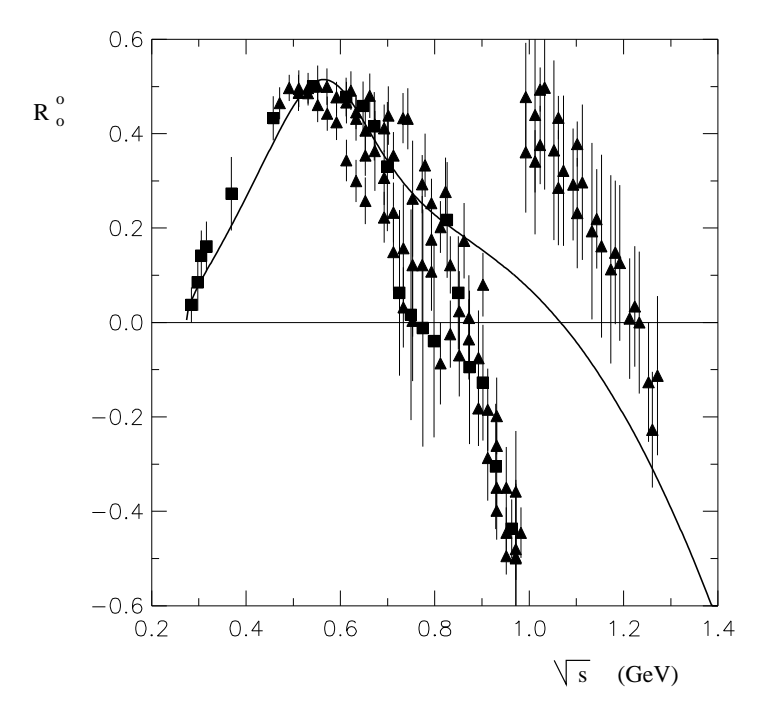


Figure 2.8: The solid line is the current algebra +  $\rho$  +  $\sigma$  result for  $R_0^0$ . The experimental points, in this and succeeding figures, are extracted from the phase shifts using Eq. (A.6) and actually correspond to  $R_0^0/\eta_0^0$ . ( $\Box$ ) are extracted from the data of Ref. [28] while ( $\triangle$ ) are extracted from the data of Ref. [29]. The predicted  $R_0^0$  is small around the 1 GeV region.

is seen that the unitarity bound is satisfied and there is a reasonable agreement with the experimental points [28,29] up to about 800 MeV. Beyond this point the effects of other resonances (mainly the  $f_0(980)$ ) are required. From Eqs. (2.10), (A.9) and (A.11) we see that the contribution of  $\sigma$  to  $R_0^0$  becomes negative when  $s > M_{\sigma}^2$ . This is the mechanism which leads to satisfaction of the unitarity bound (c.f. Fig. 2.6).

For  $s < M_{\sigma}^2$  one gets a positive contribution to  $R_0^0$ . This is helpful to push the predicted curve upwards and closer to the experimental results in this region, as shown in Fig. 2.9. The four-derivative contribution in the chiral perturbation theory

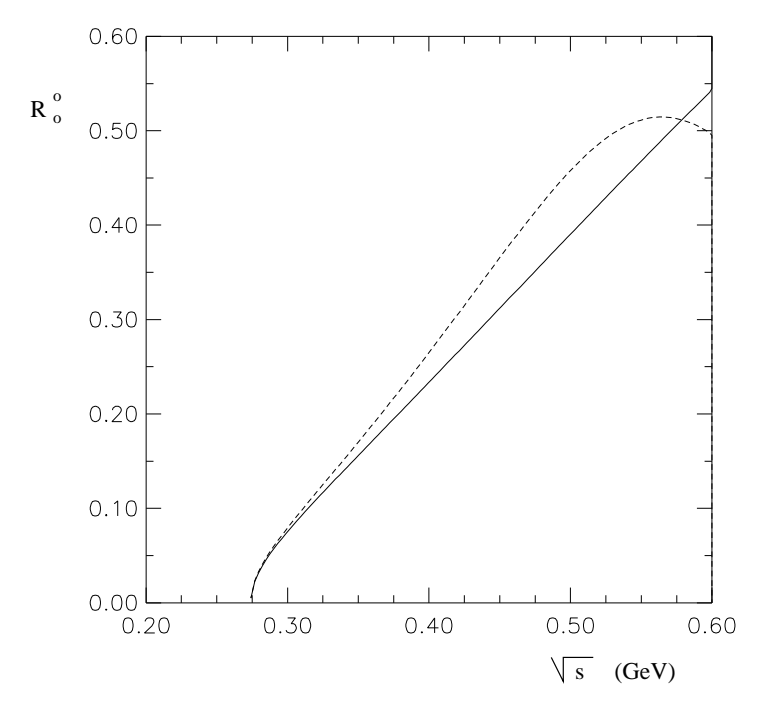


Figure 2.9: A blowup of the low energy region. The solid line is the current algebra +  $\rho$  contribution to  $R_0^0$ . The dashed line includes the  $\sigma$  particle and has the effect of turning the curve down to avoid unitarity violation while boosting it at lower energies.

approach performs the same function, however it does not change sign and hence does not satisfy the unitarity bound above the  $450 \ MeV$  region [30].

It is also interesting to notice that the main effect of the sigma particle comes from its tail in Fig. 2.7. Near the pole region, its effect is hidden by the dominant  $\pi + \rho$  contribution. This provides a possible explanation of why such a state may have escaped definitive identification. It is interesting to remark that a particle with

mass and width very similar to those given above for the  $\sigma$  was predicted [31] as part of a multiquark  $qq\bar{q}q$  nonet on the basis of the MIT bag model. Hence, even though they do not give rise to formally leading  $\pi\pi$  amplitudes in the  $1/N_c$  scheme, the picture has a good deal of plausibility from a polology point of view. It is not hard to imagine that some  $1/N_c$  subleading effects might be important at low energies where the QCD coupling constant is strongest. For completeness in Fig. 2.10 we also show the real part of the I=2 l=0 scattering amplitude  $(R_0^2)$ . for the  $\sigma$  parameters those presented in the first column of Table 3.2. It is clear that there is a fair agreement with the data up until about 1 GeV for the dashed line which represents the current algebra  $+\rho+\sigma$ , while the current algebra prediction alone departs quite soon from the experimental results. The solid line (current algebra  $+\rho$ ) seems to better follow the experimental data up to about 1.2 GeV. However since we have not tried to fit this channel we will merely stress that the results are also consistent with the local cancellation principle. For other authors [26, 32, 35] the  $\sigma$  is a  $q\bar{q}$  state, while in [36] is considered as an interpolating multi pionic state. In the actual model it is not possible to uncover what makes the  $\sigma$ . This state is however essential according to the Chiral Resonance Model.  $M_{\sigma}$ , G and G' are in practice the only unknown parameters in the present model. Here we remark that the  $\sigma$  has been introduced to understand low energy  $\pi\pi$  scattering in the following two papers: Exploring  $\pi\pi$  Scattering in the  $1/N_c$  Picture (Ref. [8]) and Simple description of  $\pi\pi$ scattering to 1 GeV (Ref. [10]). At the time when these papers were written this state was not present in the Particle Data Group (PDG) [37] review. In the latest PDG [38] this state is finally present. Although the parameters associated with the  $\sigma$  are still not well known the quoted range of parameters (mass and width) is consistent with the one determined in the Chiral Resonance framework. As the conclusion to this paragraph we can say that the  $\sigma$  is alive and well.

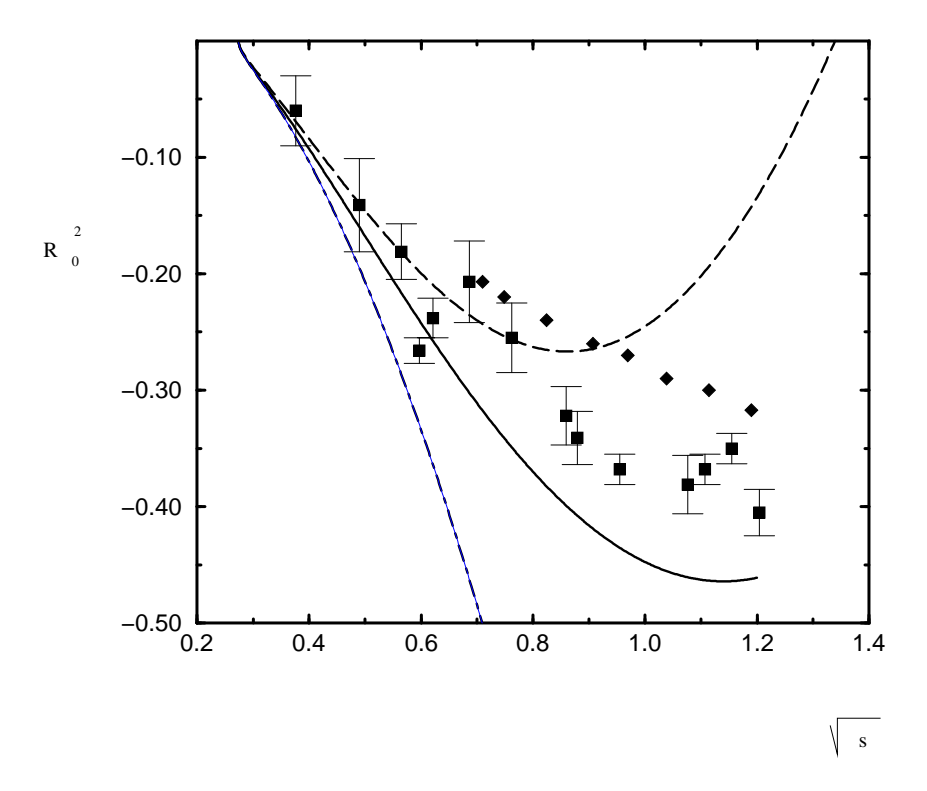


Figure 2.10: The solid line is the current algebra  $+\rho$  contribution for  $R_0^2$ . The dashed line is the current algebra  $+\rho + \sigma$  contribution for  $R_0^2$ . The dot-dashed line is the current algebra contribution for  $R_0^2$ .

## 2.4 Comment on higher derivative contact terms

In the previous paragraph we concluded that the  $\sigma$  is crucial in order to satisfy the unitarity bounds and to fit the low energy data in the  $R_0^0$  channel. But why do we need to introduce a new particle if we still have at our disposal higher derivative contact terms? Here we will analyze this possibility. For simplicity, here we will investigate four-derivative contact terms. There are two four-derivative chiral invariant contact interactions which are single traces in flavor space:

$$L_4 = a \operatorname{Tr} \left[ \partial_{\mu} U \partial_{\nu} U^{\dagger} \partial^{\mu} U \partial^{\nu} U^{\dagger} \right] + b \operatorname{Tr} \left[ \partial_{\mu} U \partial^{\mu} U^{\dagger} \partial_{\nu} U \partial^{\nu} U^{\dagger} \right] , \qquad (2.13)$$

where a and b are real constants. The single traces should be leading in the  $1/N_c$  expansion. Notice that the magnitudes of a and b will differ from those in the chiral perturbation theory approach [7] since the latter essentially also includes the effects of expanding the  $\rho$  exchange amplitude up to order  $s^2$ . The four pion terms which result from Eq. (2.13) are:

$$L_4 = \frac{8}{F_{\pi}^4} \left[ 2a \left( \partial_{\mu} \vec{\pi} \cdot \partial_{\nu} \vec{\pi} \right)^2 + (b - a) \left( \partial_{\mu} \vec{\pi} \cdot \partial^{\mu} \vec{\pi} \right)^2 \right] + \cdots$$
 (2.14)

This leads to the following contribution to the  $\pi\pi$  amplitude:

$$A_4(s,t,u) = \frac{16}{F_{\pi}^4} \left\{ a \left[ (t - 2m_{\pi}^2)^2 + (u - 2m_{\pi}^2)^2 \right] + (b - a)(s - 2m_{\pi}^2)^2 \right\} . \tag{2.15}$$

It is reasonable to require that Eq. (2.15) yields no correction at threshold, i.e. at  $s = 4m_{\pi}^2$ , t = u = 0. This gives the condition b = -a and leaves the single parameter a to play with. In Figure 2.11 we show  $R_0^0$ , as gotten by adding the piece obtained from Eq. (2.15) for several values of a to the contribution of  $\pi + \rho$ . For  $a = +1.0 \times 10^{-3}$  the four-derivative contact term can pull the curve for  $R_0^0$  down to avoid violation of the unitarity bound until around  $\sqrt{s} = 1.0 \, GeV$ . The price to be paid is that  $R_0^0$  decreases very rapidly beyond this point. We consider this to be an undesirable feature since it

would make a possible local cancellation scheme very unstable. Another drawback of the four-derivative contact term scheme is that it lowers  $R_0^0(s)$  just above threshold, taking it further away from the Roy curves. Hence in the following we will stick with the deus ex machina  $\sigma$  particle and will keep only the minimal number of derivatives.

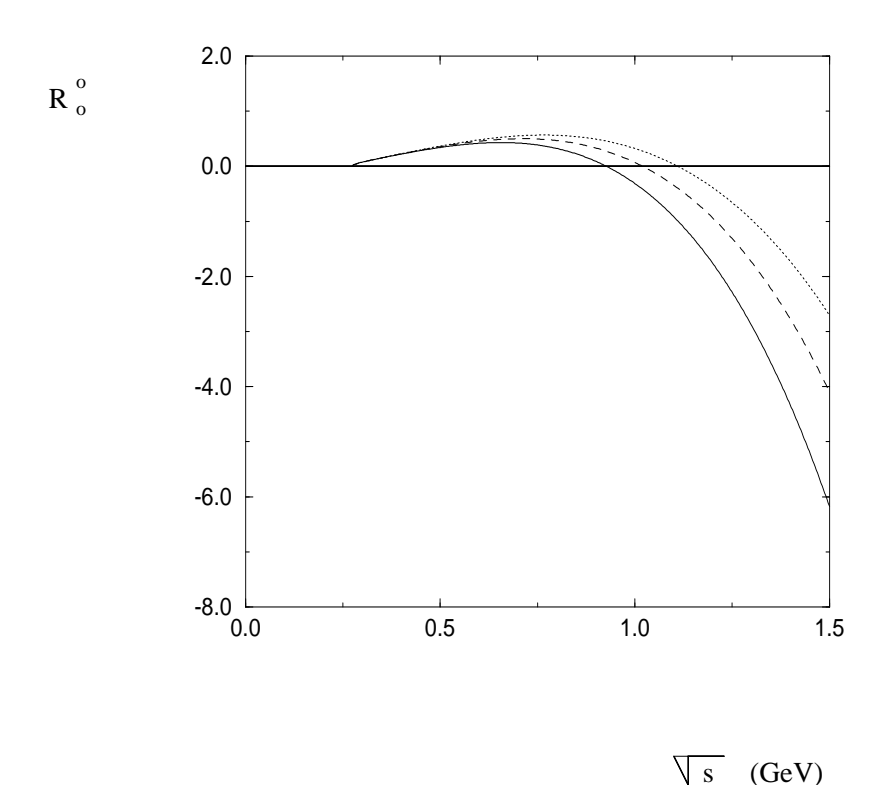


Figure 2.11: Four-derivative contact term contribution for  $R_0^0$ . The solid line corresponds to a = +1.0. The dotted line corresponds to a = +0.7. The dot-dashed line corresponds to a = 0.5. a is represented in units of  $10^{-3}$ .

# Chapter 3

# Exploring the 1 GeV region

## 3.1 What is happening in the 1 GeV region

In the previous chapter we have shown [8] that the Chiral Resonance Model is capable of describing  $\pi\pi$  scattering up to about 800 MeV in the I=l=0 channel (see Fig.2.8). In this chapter we will investigate the 800-1200 MeV energy range [10]. We will study in some detail the  $f_0(980)$  properties and the problems connected with inelastic effects induced by the opening of the  $K\bar{K}$  threshold.

The neutral resonances which can contribute to the I=l=0 channel have the quantum numbers  $J^{PC}=0^{++}$ ,  $1^{--}$  and  $2^{++}$ . In the quark model these states are naturally interpreted as s and p wave  $q\bar{q}$  bound states. We show in Table 3.1 the specific ones which are included, together with their masses and widths, where available from the Particle Data Group (PDG) [37] listings.

Reference to Fig. 2.8 shows that the experimental data for  $R_0^0$  lie considerably below the  $\pi + \rho + \sigma$  contribution between 0.9 and 1.0 GeV and then quickly reverse sign above this point. We will now see that this distinctive shape is almost completely explained by the inclusion of the relatively narrow scalar resonance  $f_0(980)$  in a

	$I^G(J^{PC})$	M(MeV)	$\Gamma_{tot}(MeV)$	$Br(2\pi)\%$
$\sigma(550)$	0+(0++)	559	370	_
$\rho(770)$	1+(1)	769.9	151.2	100
$f_0(980)$	$0^+(0^{++})$	980	40-400	78.1
$f_2(1270)$	$0^+(2^{++})$	1275	185	84.9
$f_0(1300)$	$0^+(0^{++})$	1000-1500	150-400	93.6
$\rho(1450)$	1+(1)	1465	310	seen

Table 3.1: Resonances included in the  $\pi\pi \to \pi\pi$  channel as listed in the PDG. Note that the  $\sigma$  was not present in the 1994 PDG and is not being described exactly as a *Breit-Wigner* shape; we listed the fitted parameters shown in column 1 of Table 3.2 where G' is the analog of the *Breit-Wigner* width.

suitable manner. One can understand what is going on very simply by starting from the real part of Eq. (1.12):

$$M\Gamma \frac{(M^2 - s)\cos(2\delta) - M\Gamma\sin(2\delta)}{(M^2 - s)^2 + M^2\Gamma^2} + \frac{1}{2}\sin(2\delta) . \tag{3.1}$$

This expresses nothing more than the restriction of local unitarity in the case of a narrow resonance in the presence of a background. We have seen that the difficulty of comparing the tree level  $1/N_c$  amplitude to experiment is enhanced in the neighborhood of a direct channel pole. Hence it is probably most reliable to identify the background term  $\frac{1}{2}\sin(2\delta)$  with our prediction for  $R_0^0$ . In the region of interest, Fig. 2.8 shows that  $R_0^0$  is very small so that one expects  $\delta$  to be roughly 90° (assuming a monotonically increasing phase shift). Hence the first pole term is approximately

$$-\frac{(M^2 - s)M\Gamma}{(M^2 - s)^2 + M^2\Gamma^2} , \qquad (3.2)$$

which contains a crucial reversal of sign compared to the real part of Eq. (1.10).

Thus, just below the resonance there is a sudden *negative* contribution which jumps to a positive one above the resonance. This is clearly exactly what is needed to bring experiment and theory into agreement up until about  $1.2 \, GeV$ , as is shown in Fig. 3.1. The actual amplitude used for this calculation properly contains the effects

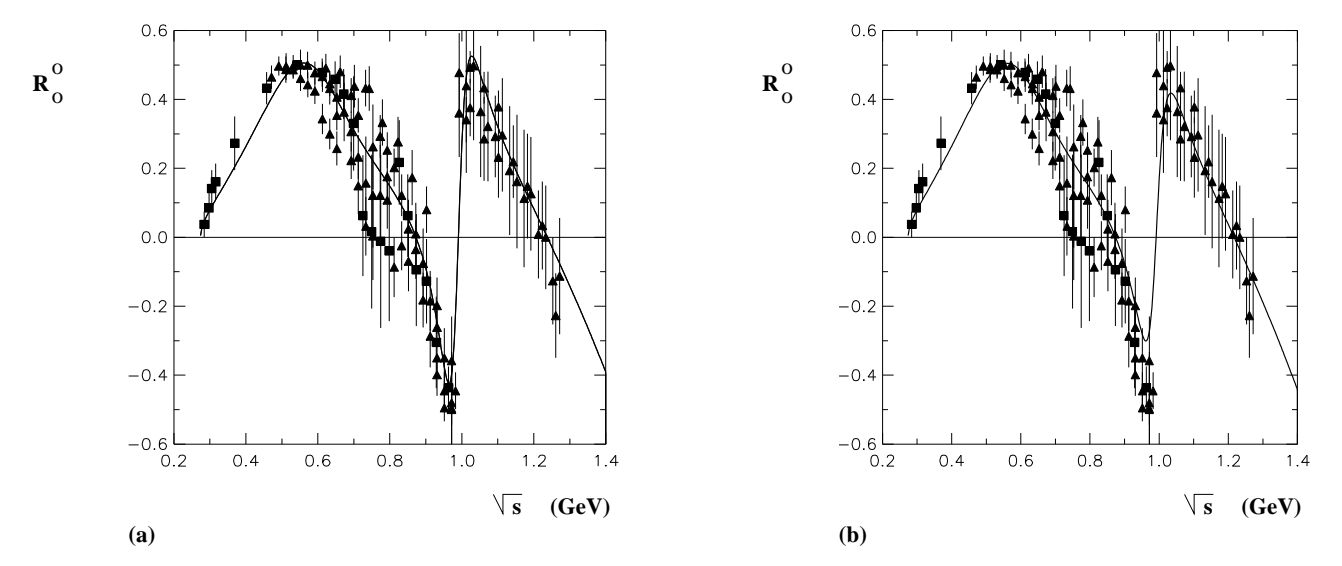


Figure 3.1: (a): The solid line is the current algebra +  $\rho$  +  $\sigma$  +  $f_0(980)$  result for  $R_0^0$  obtained by assuming column 1 in Table 3.2 for the  $\sigma$  and  $f_0(980)$  parameters  $(Br(f_0(980) \to 2\pi) = 100\%)$ . (b): The solid line is the current algebra +  $\rho$  +  $\sigma$  +  $f_0(980)$  result for  $R_0^0$  obtained by assuming column 2 in Table 3.2  $(Br(f_0(980) \to 2\pi) = 78.1\%)$ .

of the pions' derivative coupling to the  $f_0(980)$  as in Eq. (2.10).

The above mechanism, which leads to a sharp dip in the I=J=0 partial wave contribution to the  $\pi\pi$ -scattering cross section, can be identified with the very old Ramsauer-Townsend effect [40] which concerned the scattering of 0.7 eV electrons on rare gas atoms. The dip occurs because the background phase of  $\pi/2$  causes the phase shift to go through  $\pi$  (rather than  $\pi/2$ ) at the resonance position. (Of course, the cross section is proportional to  $\sum_{I,J} (2J+1) \sin^2(\delta_I^J)$ .) This simple mechanism

seems to be all that is required to understand the main feature of  $\pi\pi$  scattering in the 1 GeV region.

#### 3.1.1 The Ramsauer-Townsend Effect

Here we will compare the real part of the I=J=0 partial wave amplitude which results from our crossing symmetric model with experimental data. Firstly we will consider the sum of the contributions of the *current algebra*,  $\rho$ -meson,  $\sigma$  and  $f_0(980)$ pieces. Then we will add pieces corresponding to the next group of resonances, namely the  $f_2(1270)$ , the  $\rho(1450)$  and the  $f_0(1300)$ . In this section we will continue to neglect the  $K\overline{K}$  channel.

The current algebra plus  $\rho$  contribution to the quantity A(s,t,u) is defined in Eq. (2.7). Note that for the I=J=0 channel the expression in Eq. (2.7) will yield a purely real contribution to the partial wave amplitude. The contribution of the low-lying  $\sigma$  meson was given in Eq. (2.10). For the important  $f_0(980)$  piece we have

$$ReA_{f_0(980)}(s,t,u) = Re\left[\frac{\gamma_{f_0\pi\pi}^2 e^{2i\delta}(s-2m_{\pi}^2)^2}{m_{f_0}^2 - s - im_{f_0}\Gamma_{tot}(f_0)\theta(s-4m_{\pi}^2)}\right],$$
 (3.3)

where  $\delta$  is a background phase parameter and the real coupling constant  $\gamma_{f_0\pi\pi}$  is related to the  $f_0(980) \to \pi\pi$  width by

$$\Gamma(f_0(980) \to \pi\pi) = \frac{3}{32\pi} \frac{\gamma_{f_0\pi\pi}^2}{m_{f_0}} \sqrt{1 - \frac{4m_{\pi}^2}{m_{f_0}^2}}$$
 (3.4)

We will not consider  $\delta$  to be a new parameter but shall predict it as being

$$\frac{1}{2}\sin(2\delta) \equiv \tilde{R}_0^0(s = m_{f_0}^2) , \qquad (3.5)$$

where  $\tilde{R}_0^0$  is computed as the sum of the current algebra,  $\rho$ , and sigma pieces. Since the  $K\overline{K}$  channel is being neglected, one might want to set the regularization parameter  $\Gamma_{tot}(f_0)$  in the denominator to  $\Gamma(f_0(980) \to \pi\pi)$ . We shall try both this possibility as well as the experimental one  $\frac{\Gamma(f_0(980) \to \pi\pi)}{\Gamma_{tot}(f_0)} \approx 78.1\%$ .

A best fit of our parameters to the experimental data results in the curves shown in Fig. 3.1 for both choices of branching ratio. Only the three parameters G/G', G' and  $M_{\sigma}$  are essentially free. The others are restricted by experiment. Unfortunately the total width  $\Gamma_{tot}(f_0)$  has a large uncertainty; it is claimed by the PDG to lie in the 40-400~MeV range. Hence this is effectively a new parameter. In addition we have considered the precise value of  $m_{f_0}$  to be a parameter for fitting purposes. The parameter values for each fit are given in Table 3.2 together with the  $\chi^2$  values. It is clear that the fits are good and that the parameters are stable against variation of the branching ratio. The predicted background phase is seen to be close to  $90^{\circ}$  in both cases. Note that the fitted width of the  $f_0(980)$  is near the low end of the experimental range. The low-lying sigma has a mass of around 560~MeV and a width of about 370~MeV. As explained in section 3, we are not using an exactly conventional Breit-Wigner type form for this very broad resonance. The numbers characterizing it do however seem reasonably consistent with other determinations thereof [32, 41, 42].

## 3.2 Next group of Resonances

The *local cancellation* principle together with *crossing* works up to 1 GeV in energy. What about above 1 GeV? Does the inclusion of the resonances present in this range of energy modifies the results obtained at low energy?

In the  $1/N_c$  approximation the  $q\bar{q}$  mesons belong to ideally mixed nonets [6]. Following the  $1/N_c$  prescriptions, at the first order, only excited p—wave and radially excited states in the s—wave must be included.

					With Next Group			No ρ(1450)	
$BR(f_0(980) \to 2\pi)\%$	100	78.1	78.1	78.1	100	78.1	78.1	78.1	100
$\eta_0^0$	1	1	0.8	0.6	1	1	0.8	0.6	1
$M_{f_0(980)} \ (MeV)$	987	989	990	993	991	992	993	998	992
$\Gamma_{tot} \ (MeV)$	64.6	77.1	75.9	76.8	66.7	77.2	78.0	84.0	64.6
$M_{\sigma} \ (MeV)$	559	557	557	556	537	537	535	533	525
$G'\ (MeV)$	370	371	380	395	422	412	426	451	467
G/G'	0.290	0.294	0.294	0.294	0.270	0.277	0.275	0.270	0.263
$\delta$ (deg.)	85.2	86.4	87.6	89.6	89.2	89.7	91.3	94.4	90.4
$\chi^2$	2.0	2.8	2.7	3.1	2.4	3.2	3.2	3.4	2.5

Table 3.2: Fitted parameters for different cases of interest.

The neutral members of the p-wave  $q\bar{q}$  nonets have the quantum numbers  $J^{PC}=0^{++},~1^{++},~1^{+-}$  and  $2^{++}$ . Of course, the neutral members of the radially excited  $s-wave~q\bar{q}$  nonets have  $J^{PC}=0^{-+}$  and  $1^{--}$ . Only members of the  $0^{++},~1^{--}$  and  $2^{++}$  nonets can couple to two pseudoscalars  $^1$ . By G-parity conservation we finally note that it is the I=0 member of the  $0^{++}$  and  $2^{++}$  nonets and the I=1 member of the  $1^{--}$  nonet which can couple to two pions. Are there good experimental candidates for these three particles?

The cleanest case is the lighter I=0 member of the  $2^{++}$  nonet: the  $f_2(1270)$  has, according to the August 1994 Review of Particle Properties (PDG) [37], the right quantum numbers, a mass of  $1275 \pm 5$  MeV, a width of  $185 \pm 20$  MeV, a branching ratio of 85% into two pions, and a branching ratio of only 5% into  $K\overline{K}$ . On the other hand the  $f'_2(1525)$  has a 1% branching ratio into  $\pi\pi$  and a 71% branching ratio into

 $<sup>^{-1}</sup>$ It is possible to write down a two point mixing interaction between  $0^{-+}$  and radially excited  $0^{-+}$  particles etc., but we shall neglect such effects here.

 $K\overline{K}$ . It seems reasonable to approximate the  $2^{++}$  nonet as an ideally mixed one and to regard the  $f_2(1270)$  as its non-strange member.

The  $\rho(1450)$  is the lightest listed [37] particle which is a candidate for a radial excitation of the usual  $\rho(770)$ . It has a less than 1% branching ratio into  $K\overline{K}$  but the  $\pi\pi$  branching ratio, while presumably dominant, is not yet known. In the following analysis, for definitness, we will assume that the  $\rho(1450)$  mainly decays into  $\pi\pi$ . However, we notice that the  $K^*(1410)$ , which presumably belongs to the same  $\rho(1450)$  SU(3) multiplet has a  $K\pi$  branching ratio of only 7%. Hence we might also expect a small coupling to the two pions. We will also consider this effect by also excluding the  $\rho(1450)$  from the analysis. The  $\rho(1700)$  is a little too high for our region of interest.

An understanding of the I=0,  $0^{++}$  channel has been elusive, despite much work. We have already included the low mass scalar  $\sigma(550)$  in order to understand  $\pi\pi$  scattering at low energy. In the 1 GeV region we expect the narrow resonance  $f_0(980)$  to play a key role. The  $f_0(980)$  has a 22% branching ratio into  $K\overline{K}$  even though its central mass is below the  $K\overline{K}$  threshold. The PDG also lists the scalar  $f_0(1300)$  which has about a 93% branching ratio into  $\pi\pi$  and a 7% branching ratio into  $K\overline{K}$ . We shall use the  $f_0(1300)$  here. It is hard to understand why, if the  $f_0(980)$  is the  $\overline{s}s$  member of a conventional  $0^{++}$  nonet, it is lighter than the  $f_0(1300)$ . Most likely, the  $f_0(980)$  is an exotic or a  $K\overline{K}$  molecule [31]. If that is the case, its coupling to two pions ought to be suppressed in the  $1/N_c$  picture.

Now we will give, in turn, the  $\pi\pi$  scattering amplitudes due to the exchange of the  $f_0(1300)$ , the  $f_2(1270)$  and the  $\rho(1450)$ .

#### **3.2.1** The Tensor $f_2(1270)$ .

In the first chapter we already observed that we represent the  $3 \times 3$  matrix of tensor fields by a symmetric traceless matrix  $T_{\mu\nu}$ .  $T_{\mu\nu}$  transforms covariantly under a generic

chiral transformation (Eq. (1.26)). The 2-pion coupling can be deduced from the following chirally preserving term obtained from Eq. (1.27)

$$-\frac{\gamma_2}{\sqrt{2}}(f_2)_{\mu\nu} \left[\partial^{\mu}\vec{\pi}\cdot\partial^{\nu}\vec{\pi}\right] . \tag{3.6}$$

In this case we note that the chiral invariant interaction is just the same as the minimal one we would have written down without using chiral symmetry. The partial width is then

$$\Gamma(f_2(1270) \to \pi\pi) = \frac{\gamma_2^2}{20\pi} \frac{p_\pi^5}{M_{f_2}^2} ,$$
 (3.7)

where  $p_{\pi}$  is the pion momentum in the  $f_2$  rest frame. This leads to  $|\gamma_2| = 13.1 \; GeV^{-1}$ .

To calculate the  $f_2$  exchange diagram we need the spin 2 propagator [44] (see also Eq. (A.16)).

$$\frac{i}{q^2 - m_{f_2}^2} \left[ \frac{1}{2} \left( \theta_{\mu_1 \nu_1} \theta_{\mu_2 \nu_2} + \theta_{\mu_1 \nu_2} \theta_{\mu_2 \nu_1} \right) - \frac{1}{3} \theta_{\mu_1 \mu_2} \theta_{\nu_1 \nu_2} \right] , \qquad (3.8)$$

where

$$\theta_{\mu\nu} = -g_{\mu\nu} + \frac{q_{\mu}q_{\nu}}{m_{f_2}^2} \ . \tag{3.9}$$

A straightforward computation then yields the  $f_2$  contribution to the  $\pi\pi$  scattering amplitude:

$$A_{f_2}(s,t,u) = \frac{\gamma_2^2}{2(m_{f_2}^2 - s)} \left( -\frac{16}{3} m_{\pi}^4 + \frac{10}{3} m_{\pi}^2 s - \frac{1}{3} s^2 + \frac{1}{2} (t^2 + u^2) - \frac{2}{3} \frac{m_{\pi}^2 s^2}{m_{f_2}^2} - \frac{s^3}{6 m_{f_2}^2} + \frac{s^4}{6 m_{f_2}^4} \right).$$
(3.10)

We notice that in the previous expression the behavior at high energy is dominated by the  $s^3$  power. This is due to the fact that the present tensor is a massive particle not protected by any symmetry. This indicates that at higher energy we need to include a larger number of resonant states in order to bring the amplitudes inside the unitarity bounds. From this point of view our model is very close to the string mode [11], where an infinite number of resonances are identified with the string vibrational modes. The singularity in the propagator will be regulated as prescribed in the first chapter.

#### **3.2.2** The vector meson $\rho(1450)$ and the $f_0(1300)$ scalar.

The contribution of the s-wave radially excited  $\rho(1450)$  meson to the scattering amplitude is

$$A_{\rho'}(s,t,u) = -\frac{g_{\rho'\pi\pi}^2}{2m_{\rho'}^2} \left[ \frac{t(u-s)}{m_{\rho'}^2 - t} + \frac{u(t-s)}{m_{\rho'}^2 - u} \right] , \qquad (3.11)$$

where  $g_{\rho'\pi\pi}$  is related to the  $\rho(1450) \to \pi\pi$  partial width by

$$\Gamma(\rho(1450) \to \pi\pi) = \frac{g_{\rho'\pi\pi}^2 p_{\pi}^3}{12\pi m_{\rho'}^2}.$$
 (3.12)

With a branching ratio of 100% into two pions we get  $|g_{\rho'\pi\pi}| \simeq 7.9$ . In order to get the invariant amplitude in Eq. (3.11) there is no need to include the  $\rho(1450)$  as a massive chiral gauge field. [24].

By using Eq. (1.25)) we can easily deduce the chiral coupling to two pions

$$+\frac{\gamma_0}{\sqrt{2}} f_0 \partial_\mu \vec{\pi} \cdot \partial^\mu \vec{\pi} . \tag{3.13}$$

The partial decay width is

$$\Gamma(f_0(1300) \to \pi\pi) = \frac{3\gamma_0^2}{64\pi M_{f_0}} \sqrt{1 - \frac{4m_\pi^2}{M_{f_0}^2}} \times \left(M_{f_0}^2 - 2m_\pi^2\right)^2 .$$
 (3.14)

Since these resonance parameters are not well defined, for definiteness we will assume the PDG central values [37], i.e.  $\Gamma_{tot}(f_0(1300)) = 0.275$  GeV and  $M_{f_0} = 1.3$  GeV. Hence we deduce  $|\gamma_0| \simeq 2.88$  GeV<sup>-1</sup>. The unregularized invariant scattering amplitude is

$$A_{f_0}(s,t,u) = \frac{\gamma_0^2 \left(s - 2m_\pi^2\right)^2}{2 M_{t_0}^2 - s} \ . \tag{3.15}$$

We will regularize this resonance propagator as for the  $f_0(980)$ 

#### **3.2.3** $f_2(1270) + f_0(1300) + \rho(1450)$

Now we are in a position to appraise the contribution to  $R_0^0$  of the next group of resonances. In order to better understand the *local cancellation* mechanism in this energy

range we will not consider the background effect at the moment. The contributions of each resonance are shown in Fig. 3.2 Note that the  $f_0(1300)$  piece is not the largest,

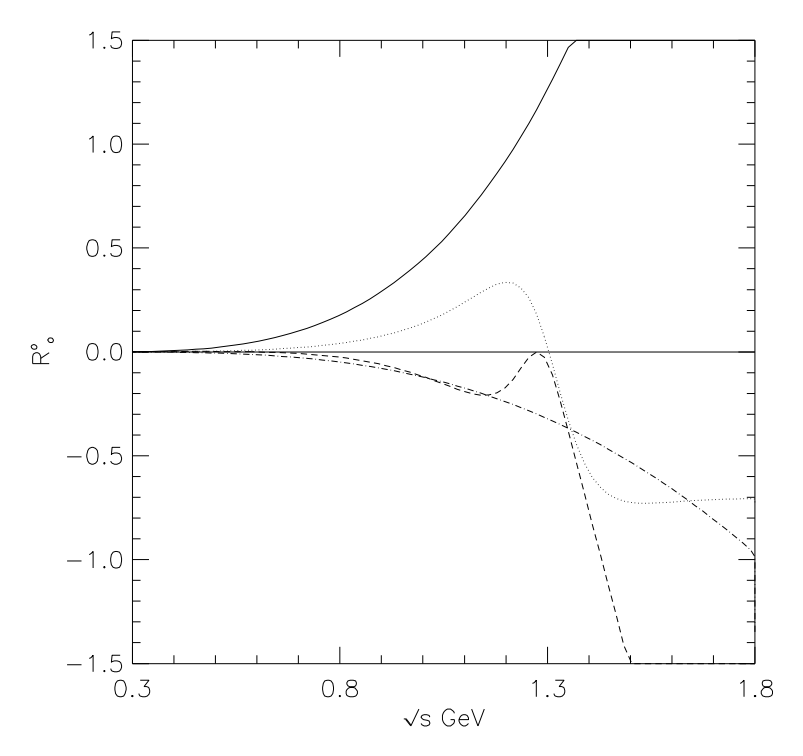


Figure 3.2: Contributions for  $R_0^0$ . Solid line:  $f_2(t+u)$ . Dashed line:  $f_2(s)$ . Dotted line:  $f_0(1300)$ . Dot-dashed line:  $\rho(1450)$ 

as one might at first expect. That honor goes to the  $f_2$  contribution which is shown divided into the s-channel pole piece and the (t+u) pole piece. We observe that the s-channel pole piece, associated with the  $f_2$ , vanishes at  $\sqrt{s} = M_{f_2}$ . This happens because the numerator of the propagator in (A.16) is precisely a spin-2 projection operator at that point. The  $\rho(1450)$  contribution is solely due to the t and u-channel poles. It tends to cancel the t and u-channel pole contributions of the  $f_2(1270)$  but does not quite succeed. The t and u-channel pole contributions of the  $f_0(1300)$  turn out to be negligible. Notice the difference in characteristic shapes between the s and (t+u) exchange curves. Fig. 3.3 shows the sum of all these individual contributions.

There does seem to be cancellation. At the high end,  $R_0^0$  starts to run negative well past the unitarity bound around 1.5 GeV. But it is reasonable to expect resonances in the 1.5 – 2.0 GeV region to modify this. The maximum positive value of  $R_0^0$  is about 1 at  $\sqrt{s} = 1.2 \ GeV$ . This would be a problem if we did not have the low energy contributions (current algebra  $+\rho+\sigma$ ). The background contribution is providentially negative (Fig. 2.8), showing once again the need for the  $\sigma$ . Let us now check that

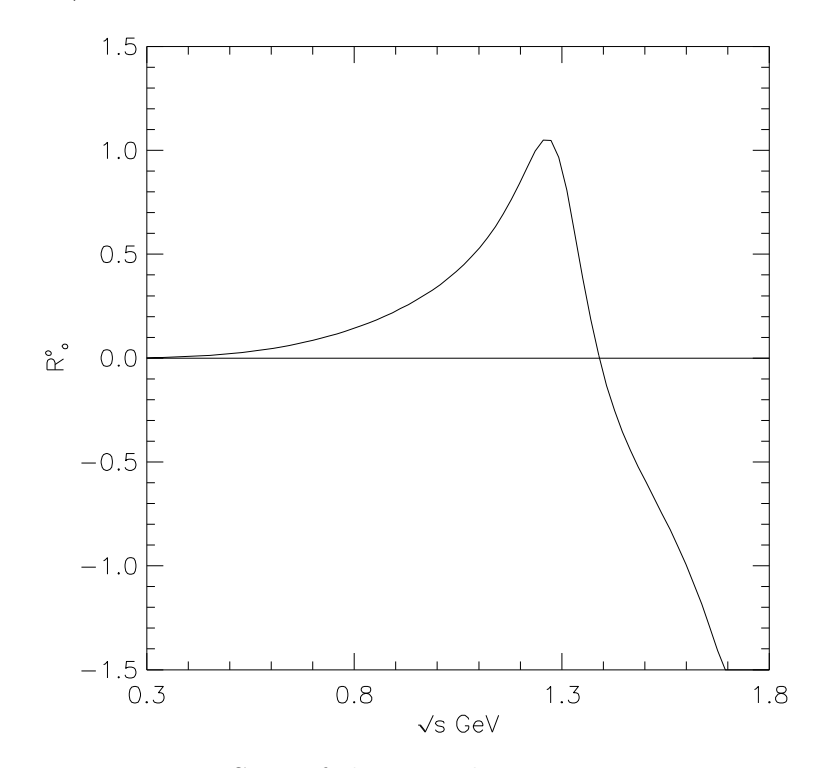


Figure 3.3: Sum of the contributions in Fig. 3.2.

the next group does not essentially modify the low energy results up to 1.2 GeV. The somewhat positive net contribution of these resonances to  $R_0^0$  is compensated for by readjustment of the parameters describing the low lying sigma.

It may be interesting to include the effect of the background phase for the  $f_0(1300)$  as we have just seen that it was very important for a proper understanding of the  $f_0(980)$ . To test this possibility we reversed the sign of the  $f_0(1300)$  contribution and

show the result as the solid curve in Fig. 3.4. This sign reversal is reasonable since our model suggests a background phase of about 270° in the vicinity of the  $f_0(1300)$ . It can be seen that there is now a significantly greater cancellation of the *next group* particles among themselves up to about 1.2 GeV. The resulting total fits are shown

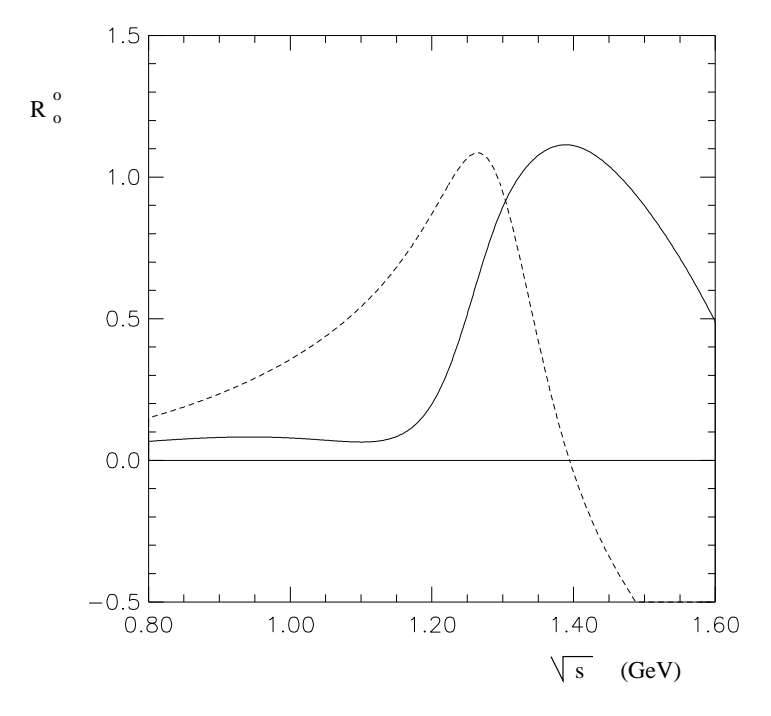


Figure 3.4: Contribution from the *next group* of resonances; the solid line is obtained with the reverse sign of the  $f_0(1300)$  piece; the dashed line is as in Fig. 3.3.

in Fig. 3.5 for assumed  $f_0(980) \to \pi\pi$  branching ratios of both 100% and 78.1% and the parameters associated with the fits are shown in Table 3.2. It is clear that the fitted parameters and results up to about 1.2 GeV are very similar to the cases when the *next group* was absent. Above this region there is now, however, a positive bump in  $R_0^0$  at around 1.3 GeV. This could be pushed further up by choosing a higher mass (within the allowable experimental range) for the  $f_0(1300)$ . Resonances in the

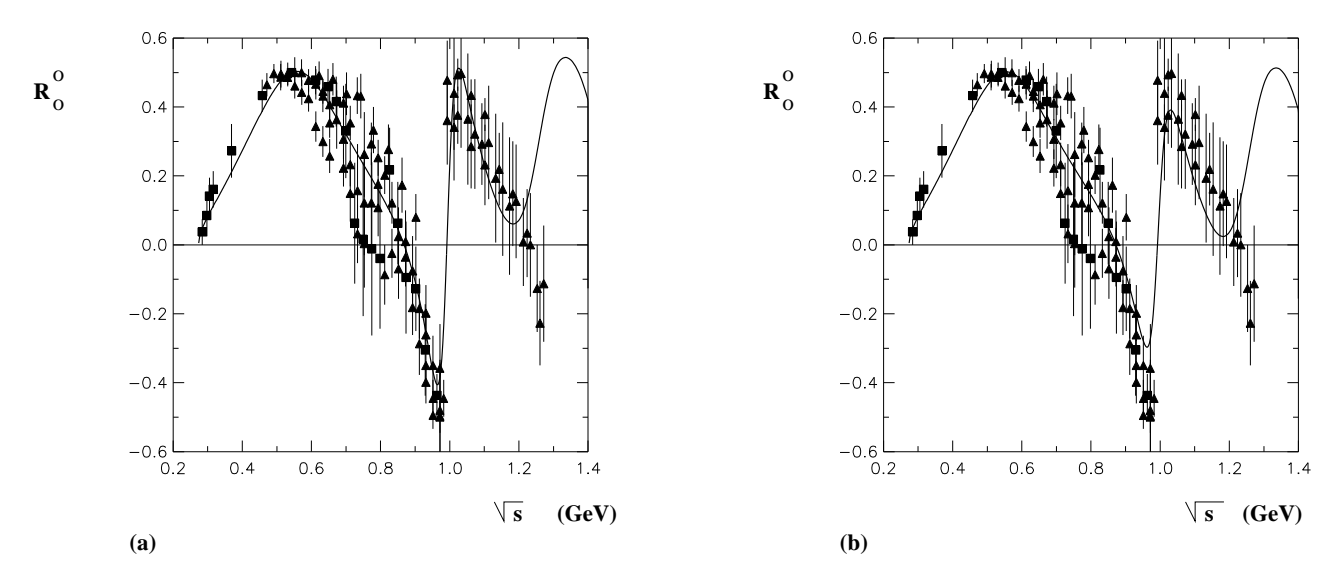


Figure 3.5: Prediction for  $R_0^0$  with the *next group* of resonances. (a) assumes (column 5 in Table 3.2)  $(BR(f_0(980) \to 2\pi) = 100\%)$  while (b) assumes (column 6)  $(BR(f_0(980) \to 2\pi) = 78.1\%)$ .

1500 MeV region, which have *not* been taken into account here, would presumably also have an important effect in the region above 1.2 GeV. Clearly there is not much sense, at the present stage, in trying to produce a fit above 1.2 GeV. In the last column of Table 3.2 we have neglected the effect of the  $\rho(1450)$ . The resulting fit is shown in the last column of Table 3.2 and it is seen to leave the other parameters essentially unchanged.

It thus seems that the results are consistent with the hypothesis of local cancellation, wherein the physics up to a certain energy E is described by including only those resonances up to slightly more than E and it is furthermore hypothesized that the individual particles cancel in such a way that unitarity is maintained.

#### 3.3 Inelastic effects

Up to now we have completely neglected the effects of coupled inelastic channels. Of course the  $4\pi$  channel opens at 540 MeV, the  $6\pi$  channel opens at 810 MeV and, probably most significantly, the  $K\overline{K}$  channel opens at 990 MeV. We have seen that a nice undestanding of the  $\pi\pi$  elastic channel up to about 1.2 GeV can be gotten with complete disregard for inelastic effects. Nevertheless it is interesting to see how our results would change if experimental data on the elasticity parameter  $\eta_0^0$  are folded into the analysis. Figure 3.6 illustrates the results for  $\eta_0^0(s)$  obtained from an

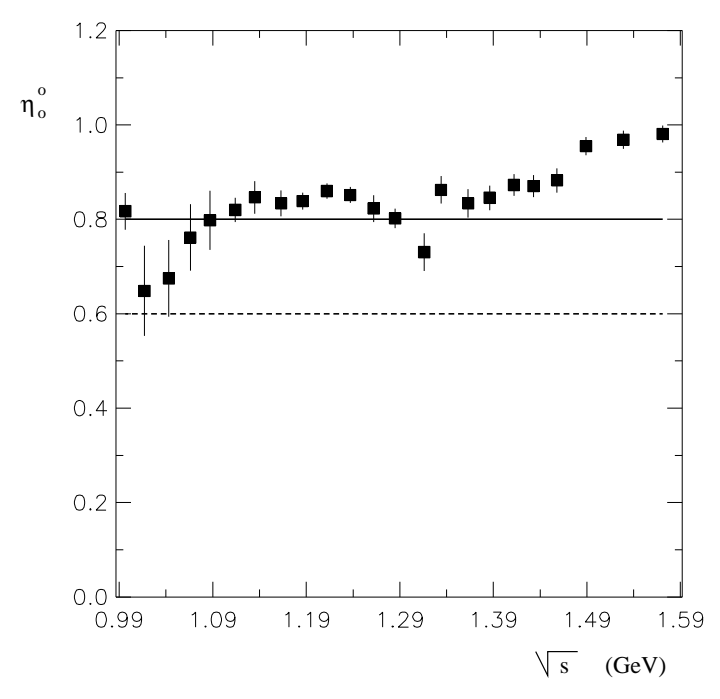


Figure 3.6: An experimental determination of  $\eta_0^0 = \sqrt{1 - 4|T_{12,0}^0|^2}$  [45].

experimental analysis [45] of  $\pi\pi \to K\overline{K}$  scattering. For simplicity, we approximated the data by a constant value  $\eta_0^0 = 0.8$  above the  $K\overline{K}$  threshold. Figure 3.7(a) shows the effect of this choice on  $R_0^0(s)$  computed without the inclusion of the *next group* of resonances, while Fig. 3.7(b) shows the effect when the *next group* is included.

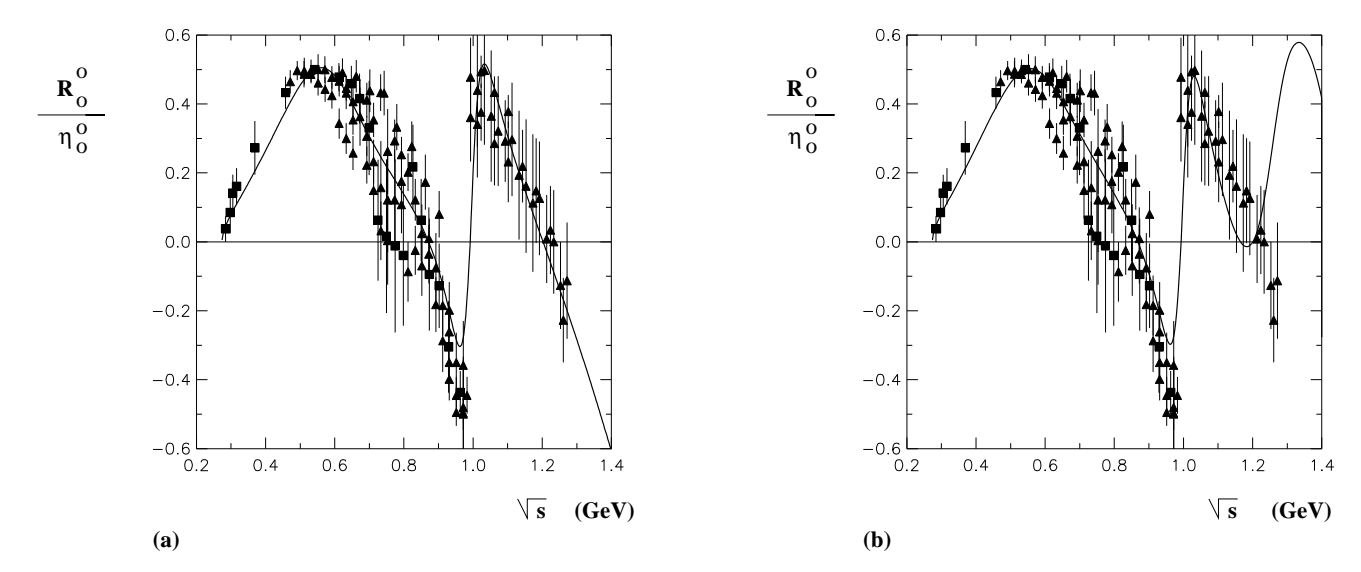


Figure 3.7: Predictions with phenomenological treatment of inelasticity  $(\eta_0^0 = 0.8)$  above  $K\overline{K}$  threshold. (a): without next group. (b): with next group.

Comparing with Fig. 3.1(b) and 3.5(b), we see that setting  $\eta_0^0 = 0.8$  has not made any substantial change. The parameters of the fit are shown in Table 3.2 as are the parameters for an alternative fit with  $\eta_0^0 = 0.6$ . The latter choice leads to a worse fit for  $R_0^0$ .

We conclude that inelastic effects are not very important for understanding the main features of  $\pi\pi$  scattering up to about 1.2 GeV. However, we will discuss the calculation of  $\eta_0^0(s)$  from our model in the  $\pi\pi \to K\overline{K}$  paragraph.

# 3.4 Phase Shifts

Strictly speaking the Chiral Resonance Model only entitles us to compare the real part of the predicted amplitude with the real part of the amplitude deduced from experiment. Since the predicted  $R_0^0(s)$  up to 1.2 GeV satisfies the unitarity bound

(within the fitting error) we can calculate the imaginary part  $I_0^0(s)$ , and hence the phase shift  $\delta_0^0(s)$  on the assumption that full unitarity holds. This is implemented by substituting  $R_0^0(s)$  into Eq. (2.1) and resolving the discrete sign ambiguities by demanding that  $\delta_0^0(s)$  be continuous and monotonically increasing (to agree with experiment). It is also necessary to know  $\eta_0^0(s)$  for this purpose; we will be content with the approximations above which seem sufficient for understanding the main features of  $\pi\pi$ -scattering up to 1.2 GeV.

In this procedure there is a practical subtlety already discussed at the end of section IV of Ref. [8]. In order for  $\delta_0^0(s)$  to increase monotonically it is necessary that the sign in front of the square root in Eq. (2.1) change. This can lead to a discontinuity unless  $2|R_0^0(s)|$  precisely reaches  $\eta_0^0(s)$ . However the phase shift is rather sensitive to small deviations from this exact matching. Since the fitting procedure does not enforce that  $|R_0^0(s)|$  go precisely to  $\eta_0^0(s)/2 \approx 0.5$ , this results in some small discontinuities. (These could be avoided by trying to fit the phase shift directly.)

Figure 3.8 shows the phase shift  $\delta_0^0(s)$  estimated in this manner for parameters in the first column of Table 3.2. As expected, the agreement is reasonable. A very similar estimate is obtained when (column 3 of Table 3.2)  $\eta_0^0$  is taken to be 0.8 while considering the  $\pi\pi$  branching ratio of  $f_0(980)$  to be its experimental value of 78.1%. It appears that these two parameter changes are compensating for one other so that one may again conclude that the turning on of the  $K\overline{K}$  channel really does not have a major effect. When the next group of resonances is included (column 7 of Table 3.2) the estimated  $\delta_0^0(s)$  is very similar up to about 1.2 GeV. Beyond this point it is actually somewhat worse, as we would expect by comparing Fig. 3.7(b) with Fig. 3.7(a).

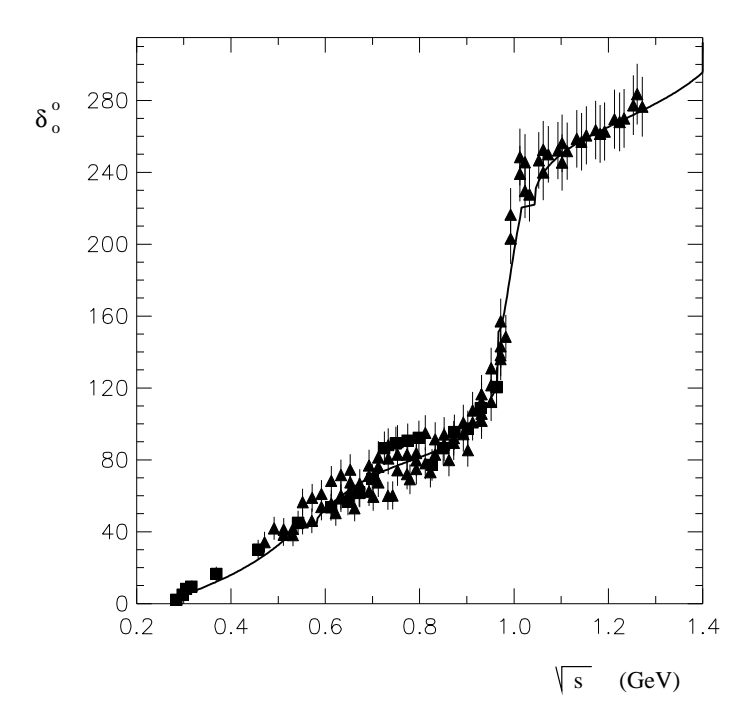


Figure 3.8: Estimated phase shift using the predicted real part and unitarity relation.

# 3.5 The inelastic channel $\pi\pi \to K\bar{K}$

We have seen that  $\pi\pi \to \pi\pi$  scattering can be understood up to about 1.2 GeV without including this inelastic channel. In particular, a phenomenological description of the inelasticity did not change the overall picture. However we would like to begin to explore the predictions of the present model for this channel also. The whole coupled channel problem is a very complicated one so we will be satisfied here to check that the procedure followed for the  $\pi\pi$  elastic channel can lead to an inelastic amplitude which also satisfies the unitarity bounds. Specifically we will confine our attention to the real part of the I = J = 0  $\pi\pi \to K\overline{K}$  amplitude,  $R_{12;0}^0$  defined in Eq. (A.11).

In exact analogy to the  $\pi\pi \to \pi\pi$  case we first consider the contribution of the contact plus the  $K^*(892)$  plus the  $\sigma(550)$  terms. It is necessary to know the coupling strength of the  $\sigma$  to  $K\overline{K}$ , defined by the effective Lagrangian piece

$$+\frac{\gamma_{\sigma K\overline{K}}}{2}\sigma\partial_{\mu}\overline{K}\partial^{\mu}K. \qquad (3.16)$$

If the  $\sigma$  is ideally mixed and there is no OZI rule-violating piece we would have  $\gamma_{\sigma K\overline{K}} = \gamma_0$  as defined in Eq. (1.25). For definiteness, we shall adopt this standard mixing assumption. The appropriate amplitudes are listed in Appendix A. Figure 3.9 shows the plots of  $R_{12;0}^0$  for the current algebra part alone, the current algebra plus  $K^*$  and the current algebra plus  $\sigma$  parts. Notice that unitarity requires

$$|R_{12;0}^0| \le \frac{\sqrt{1 - \eta_0^{0^2}}}{2} \le \frac{1}{2} \ . \tag{3.17}$$

The current algebra result already clearly violates this bound at 1.05 GeV. As before, this is improved by the  $K^*$  vector—meson exchange contribution and further improved by the very important tail of the  $\sigma$  contribution. The sum of all three shows a structure

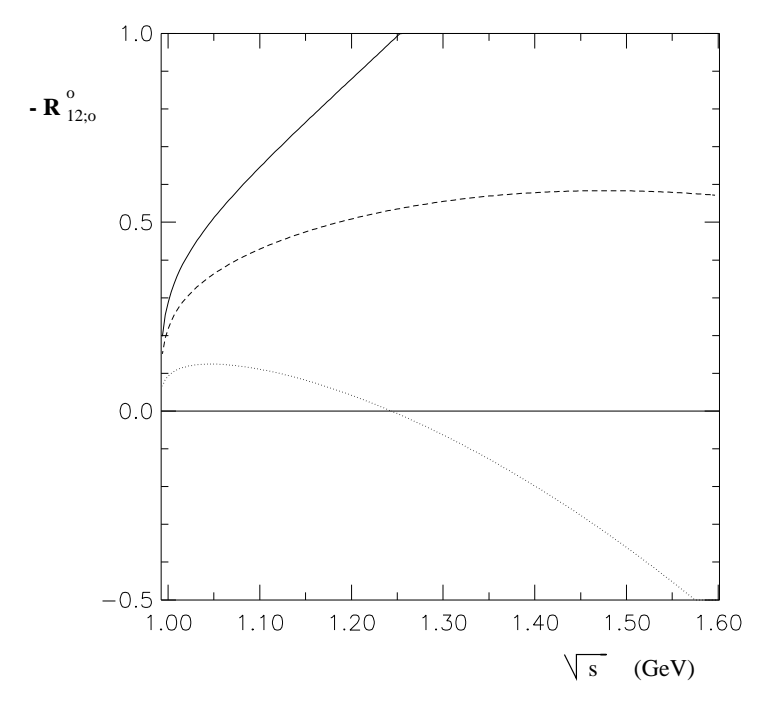


Figure 3.9: Contributions to  $\pi\pi \to K\overline{K}$   $(R_{12;0}^0)$ . The solid line shows the current algebra result, the dashed line represents the inclusion of  $K^*(892)$ , the dotted line includes the  $\sigma(550)$  too.

similar to the corresponding Fig. 2.8 in the  $\pi\pi \to \pi\pi$  case. The unitarity bound is not violated until about 1.55 GeV.

Next, let us consider the contribution of the  $f_0(980)$  which, since the resonance straddles the threshold, is expected to be important. We need to know the effective coupling constant of the  $f_0$  to  $\pi\pi$  and to  $K\overline{K}$ . As we saw in Eq. (3.3), and the subsequent discussion, the effective  $\pi\pi$  coupling should be taken as  $\gamma_{f_0\pi\pi}e^{i\frac{\pi}{2}}$ . Experimentally, only the branching ratios for  $f_0(980) \to \pi\pi$  and  $f_0(980) \to K\overline{K}$  are accurately known. We will adopt for definiteness the value of  $\gamma_{f_0\pi\pi}$  corresponding to the fit in the third column of Table 3.2  $(\Gamma_{tot}(f_0(980)) = 76~MeV)$ . It is more difficult to estimate the  $f_0(980) \to K\overline{K}$  effective coupling constant since the central value of the resonance may actually lie below the threshold. By taking account  $^2$  of the finite width of the  $f_0(980)$  we get the rough estimate  $|\gamma_{f_0K\overline{K}}| = 10~GeV^{-1} \approx 4|\gamma_{f_0\pi\pi}|$  for the choice in the third column,  $M_{f_0(980)} = 990~MeV$ . Of course, this estimate is very sensitive to the exact value used for  $M_{f_0(980)}$ . It seems reasonable to take  $\gamma_{f_0K\overline{K}}$  to be purely real. The results of including the  $f_0(980)$  contribution, for both sign choices of  $\gamma_{f_0K\overline{K}}$ , are shown in Fig. 3.10. The unitarity bounds are satisfied for the positive sign of  $\gamma_{f_0K\overline{K}}$  but slightly violated for the negative sign choice.

Finally, let us consider the contributions to  $\pi\pi \to K\overline{K}$  from the members of the

$$16.6 \ MeV = |\gamma_{f_0 K\overline{K}}|^2 \int_{2m_k}^{\infty} \rho(M) |A(f_0(M) \to K\overline{K})|^2 \Phi(M) dM ,$$

where  $A(f_0(M) \to K\overline{K})$  is the reduced amplitude for an  $f_0$  of mass M to decay to  $K\overline{K}$ ,  $\Phi(M)$  is the phase space factor and  $\rho(M)$  is the weighting function given by

$$\rho(M) = \sqrt{\frac{2}{\pi}} \frac{1}{\Gamma_{tot}} exp \left\{ -2 \left[ \frac{(M - M_0)^2}{\Gamma_{tot}^2} \right] \right\} .$$

Here,  $M_0$  is the central mass value of the  $f_0(980)$ .

With  $\Gamma_{tot}(f_0(980)) = 76~MeV$  we would have  $\Gamma(f_0(980) \to K\overline{K}) = 16.6~MeV$ . Then  $\gamma_{f_0K\overline{K}}$  is estimated from the formula:

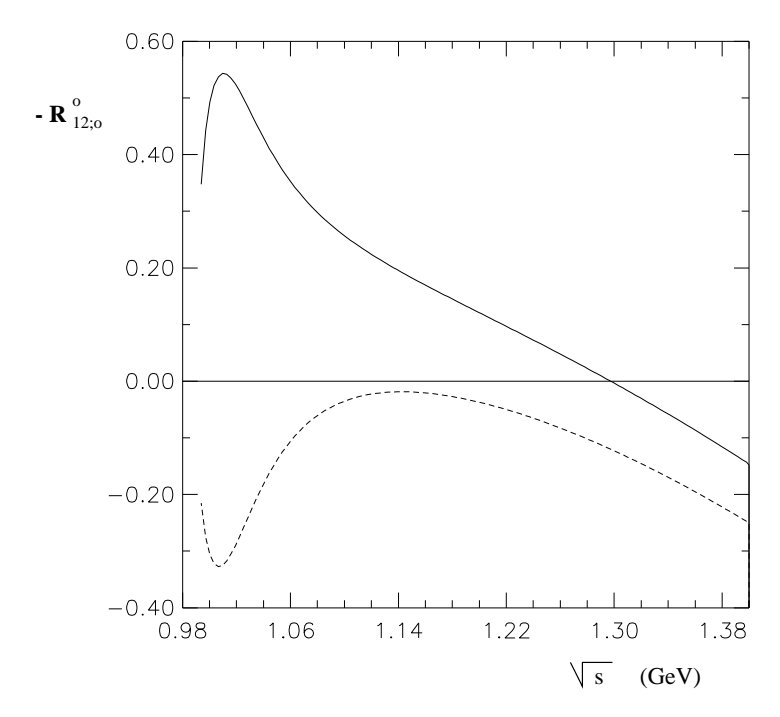


Figure 3.10: Effect of  $f_0(980)$  on  $\pi\pi \to K\overline{K}$ . The solid curve corresponds to a negative  $\gamma_{f_0K\overline{K}}$  and the dashed one to a positive sign.

multiplets containing the next group of particles. There will be a crossed channel contribution from the strange excited vector meson  $K^*(1410)$ . However it will be very small since  $K^*(1410)$  predominately couples to  $K^*\pi$  and has only a 7% branching ratio to  $K\pi$ . In addition there will be a crossed channel scalar  $K_0^*(1430)$  diagram as well as a direct channel scalar  $f_0(1300)$  diagram contributing to  $\pi\pi \to K\overline{K}$ . The  $f_0(1300)$  piece is small because  $f_0(1300)$  has a very small branching ratio to  $K\overline{K}$ . Furthermore the  $K_0^*(1430)$  piece turns out also to be small; we have seen that the crossed channel scalar gave a negligible contribution to  $\pi\pi \to \pi\pi$ . The dominant next group diagrams involve the tensor mesons. Near threshold, the crossed channel  $K_2^*(1430)$  diagram is the essential one since the direct channel  $f_2(1270)$  contribution for the J=0 partial wave is suppressed by a spin-2 projection operator. Above 1270 MeV the  $f_2(1270)$  contribution becomes increasingly important although it has the opposite sign to the crossed channel tensor piece. Figure 3.11 shows the net prediction for  $R_{12;0}^0$  obtained with the inclusion of the main next group contributions from the  $K_2^*(1430)$  and  $f_2(1270)$ . Both assumed signs for  $\gamma_{f_0K\overline{K}}$  are shown and other parameters correspond to column 3 of Table 3.2. Clearly there is an appreciable effect. Figure 3.12 shows the magnitude of  $|R_{12;0}^0|$  together with one experimental determination [45] of  $|T_{12;0}^0| = \sqrt{(R_{12;0}^0)^2 + (I_{12;0}^0)^2}$ . The positive sign of  $\gamma_{f_0K\overline{K}}$  is favored but, considering the uncertainty in  $|\gamma_{f_0K\overline{K}}|$  among other things, we shall not insist on this. It seems to us that the main conclusion is that the unitarity bound can be satisfied in the energy range of interest. In this analysis we have shown that the local cancellation principle is satisfied and that the  $\sigma$  plays an important role in the  $\pi\pi \to K\overline{K}$  channel.

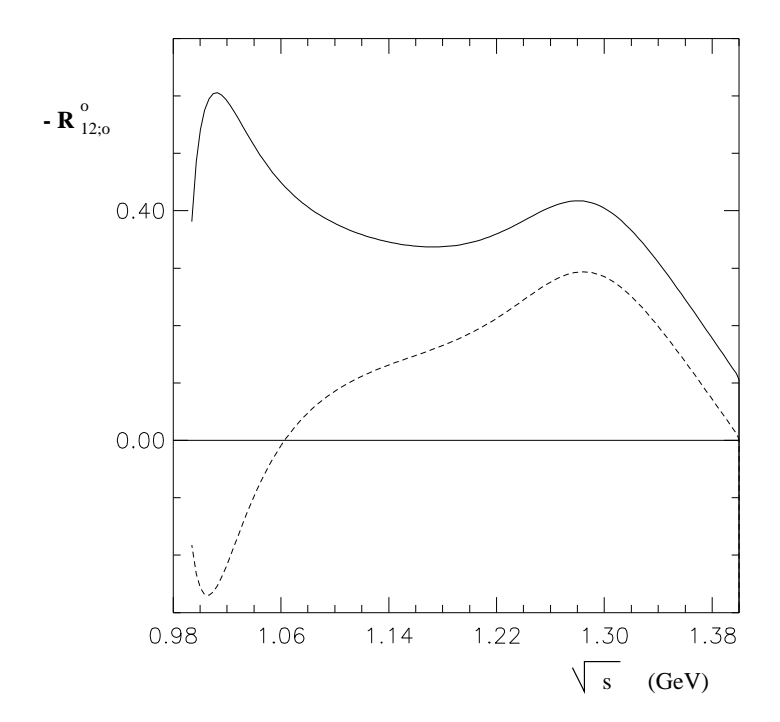


Figure 3.11: Effects on  $\pi\pi \to K\overline{K}$  due to the *next group* of resonances for the two different sign choices in Fig. 3.10.

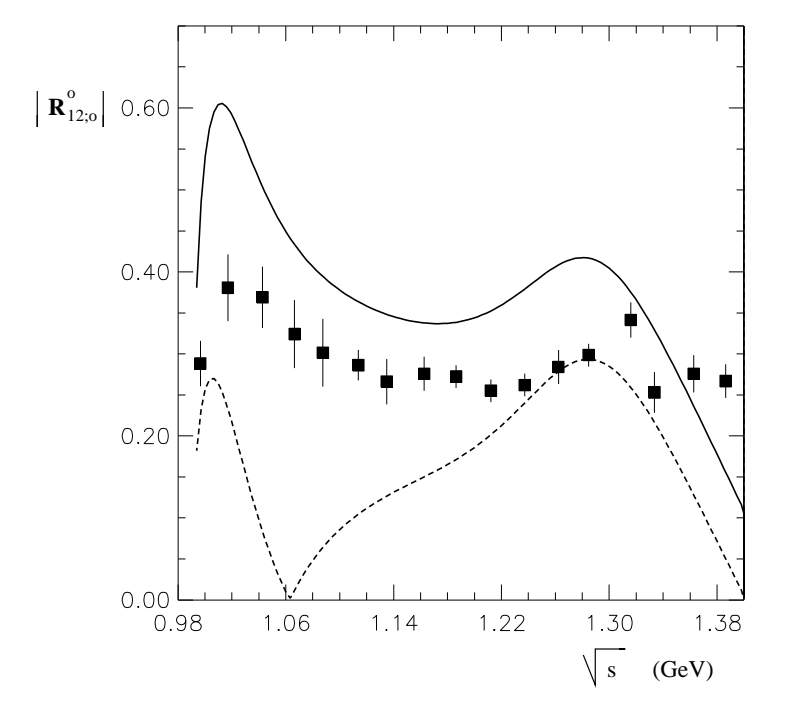


Figure 3.12:  $|R_{12;0}^0|$  together with one experimental determination [45] of  $|T_{12;0}^0| = \sqrt{(R_{12;0}^0)^2 + (I_{12;0}^0)^2}$ . Signs for  $\gamma_{f_0K\overline{K}}$  as in Fig. 3.10.

## 3.6 The lonely $\sigma$

In Reference [33], Törnqvist and Roos presented a model of  $\pi\pi$  scattering which supports the existence of the old  $\sigma$  meson at a pole position,  $s_0^{1/2}=0.470-i0.250$  GeV. While this model is constructed to satisfy unitarity, it does not explicitly take crossing symmetry into account. In particular, one may question [34] the validity of neglecting the crossed-channel  $\rho$  meson exchange contributions, which are generally considered to be important. It is actually very complicated, as noted by the authors themselves, to examine this question in their model. We can investigate this issue in the framework of the Chiral Resonance Model [8–10,55] We find that the consistent neglect of the  $\rho$  exchange does not destroy the existence of the  $\sigma$  meson but merely modifies its parameters so that they get close to the results of Ref. [33].

In the previous chapters [10] a best fit to the real part of the I=J=0 partial amplitude  $R_0^0$  was found for a mass  $M_\sigma=559$  MeV, a width G'=370 MeV and G/G'=0.29 (pole position  $s_0^{1/2}=0.585-i0.176$  GeV). It is an easy matter to neglect the  $\rho$  meson contributions (including the associated contact term needed for chiral symmetry) and make a new fit. The resulting  $R_0^0$  in comparison with the experimental data is shown in Fig. 3.13 and is about as good as the previous fit including the  $\rho$  meson. (Of course, the  $\rho$  meson is definitely present in nature.) The new fitted parameters are the mass  $M_\sigma=378$  MeV, the width G'=836 MeV and G/G'=0.08 (pole position  $s_0^{1/2}=0.495-i0.319$  GeV). The new mass and width are close to the values found in Ref. [33]. We therefore would expect that including the  $\rho$  exchange in their framework would raise their mass by roughly 100 MeV and lower their width prediction. This behavior can be easily understood in a qualitative sense, since the addition of the  $\rho$  raises the energy at which the unitarity bound is violated (see Fig. 2.6). Of course, in the previous chapters, the question of whether the  $\sigma$  and  $f_0(980)$  are  $q\bar{q}$ ,  $q^2\bar{q}^2$  states or some superposition is not directly addressed.

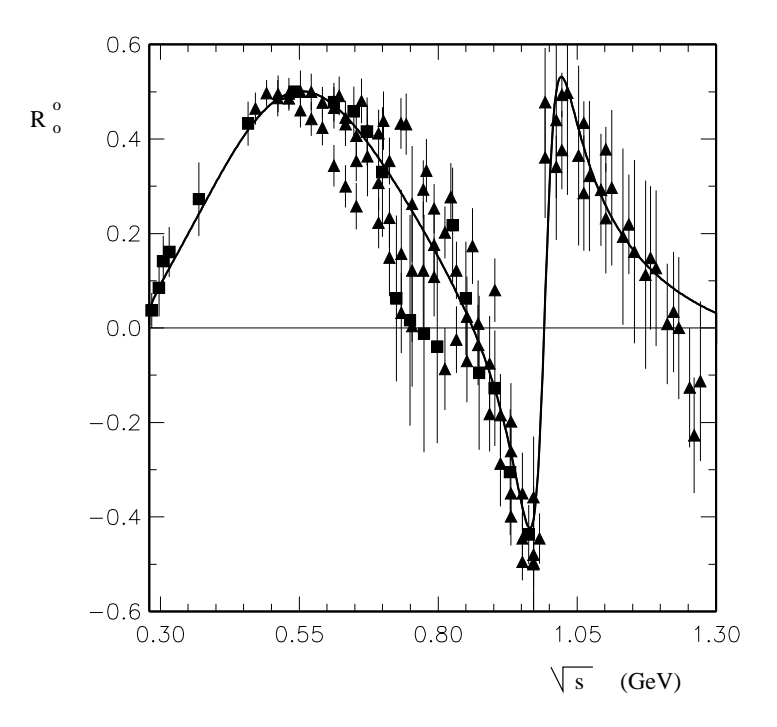


Figure 3.13: The solid line is the current algebra +  $\sigma$  +  $f_0(980)$  result for  $R_0^0$ .

### 3.7 Conclusions for the Chiral Resonance Model

We have used the Chiral Resonance scheme to obtain a simple approximate analytic form for the real part of the  $\pi\pi$ -scattering amplitude in the energy range from threshold to about 1.2 GeV. It satisfies both crossing symmetry and (more non-trivially) unitarity in this range. Inspired by the leading  $1/N_c$  approximation, we have written the amplitude as the sum of a contact term and poles. Of course the leading  $1/N_c$  amplitude can not be directly compared with experiment since it is purely real (away from the direct channel poles) and diverges at the pole positions. Furthermore, an infinite number of poles and higher derivative interactions are in principle needed. To overcome these problems we have employed the following Chiral Resonance Model procedure:

- a. We specialized to predicting the real part of the amplitude.
- b. We postulated that including only resonances from threshold to slightly more than the maximum energy of interest is sufficient. We have seen that this *local* cancellation appears stable under the addition of resonances in the 1300 MeV range. Beyond this range we would expect still higher resonances to add in such a way as to enforce unitarity at still higher energies.
- c. In the effective interaction Lagrangian we included only terms with the minimal number of derivatives consistent with the assumed chiral symmetry.
- d. The most subtle aspect concerns the method for regularizing the divergences at the direct channel resonance poles. In the simplest case of a single resonance dominating a particular channel (e.g. the  $\rho$  meson) it is sufficient to add the standard width term to the denominator (e.g. the real part of Eq. (1.10)). For an extremely broad resonance (like a needed low–energy scalar isosinglet)

the concept of width is not so clear and we employed the slight modification of the Breit-Wigner amplitude given in Eq. (1.11). Finally, for a relatively narrow resonance in the presence of a non-negligible background, we employed the regularization given in Eq. (1.12) which includes the background phase. Self-consistency is assured by requiring that the background phase should be predicted by the model itself.

All the regularizations introduced above are formally of higher than leading order in the  $1/N_c$  expansion (i.e. of order  $1/N_c^2$  and higher) and correspond physically to pion rescattering effects. This rescattering is schematically represented in Fig. 3.14. In the case of non-negligible background phase, there is an interesting difference

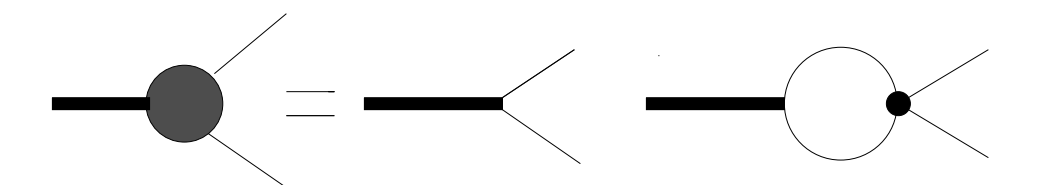


Figure 3.14: Effective resonance— $2\pi$  coupling due to the pions' rescattering effects. The latter has been shown schematically in a generic pertubative scheme. For simplicity we only considered the rescattering due to a four pion contact term ( $\bullet$ ).

from the usual tree-level treatment of pole diagrams. The effective squared coupling constant,  $g_{R\pi\pi}^2$  of such a resonance to two pions, is then not necessarily real and positive. Since this regularization is interpreted as a rescattering effect it does not mean that ghost fields are present in the theory. This formulation maintains crossing symmetry which is typically lost when a unitarization method is employed.

In this analysis, the most non-trivial point is the satisfaction of the unitarity bound for the predicted real part of the partial wave amlitude,

$$|R_l^I| \le \frac{\eta_l^I}{2} \,, \tag{3.18}$$

where  $\eta_l^I < 1$  is the elasticity parameter. The well–known difficulty concerns  $R_0^0$ . If  $\eta_l^I(s)$  is known or calculated, the imaginary part  $I_l^I(s)$  can be obtained, up to discrete ambiguities, by Eq. (2.1).

The picture of  $\pi\pi$  scattering in the threshold to slightly more than 1 GeV range which emerges from this model has four parts. Very near threshold the current algebra contact term approximates  $R_0^0(s)$  very well. The imaginary part  $I_0^0(s)$ , which is formally of order  $1/N_c^2$  can be obtained from unitarity directly using Eq. (2.1) or, equivalently, by chiral perturbation theory. At somewhat higher energies the most prominent feature is the  $\rho$  meson pole in the I=J=1 channel. The crossed channel  $\rho$  exchange is also extremely important in taming the elastic unitarity violation associated with the current algebra contact term (Fig. 2.6). Even with the  $\rho$  present, Fig. 2.6 shows that unitarity is still violated, though much less drastically. This problem is overcome by introducing a low mass  $\approx 550 \text{ MeV}$ , extremely broad sigma meson. It also has another desirable feature:  $R_0^0(s)$  is boosted (see Fig. 2.9) closer to experiment in the 400-500~MeV range. The three parameters characterizing this particle are essentially the only unknowns in the model and were determined by making a best fit. In the 1 GeV region it seems clear that the  $f_0(980)$  resonance, interacting with the predicted background in the Ramsauer-Townsend effect manner, dominates the structure of the I = J = 0 phase shift. The inelasticity associated with the opening of the  $K\overline{K}$  threshold has a relatively small effect. However we also presented a preliminary calculation which shows that the present approach satisfies the unitarity bounds in the inelastic  $\pi\pi \to K\overline{K}$  channel.

Other recent works [32, 42, 49, 51, 56, 57] which approach the problem in different ways, also contain a low mass broad sigma. The question of whether the lighter scalar mesons are of  $q\bar{q}$  type or meson-meson type has also been discussed [32, 42, 56]. In our model it is difficult to decide this issue. Of course, it is not a clean question from a field-theoretic standpoint. This question is important for understanding whether the contributions of such resonances are formally leading in the  $1/N_c$  expansion. We are postponing the answer as well as the answer to how to derive the rescattering effects that were used to regularize the amplitude near the direct channel poles as higher order in  $1/N_c$  corrections. Presumably, the rescattering effects could some day be calculated as loop corrections with a (very complicated) effective Wilsonian action. This would be a generalization of the chiral perturbation scheme of pions. Another aspect of the  $1/N_c$  picture concerns the infinite number of resonances which are expected to contribute already at leading order. One may hope that the idea of local cancellation will help in the development of a simple picture at high energies which might get patched together with the present one. Is the simple high energy theory a kind of string model?

In this first part of the thesis we have shown [8–10,55] that it is possible to build a reasonable model for light meson interactions, which we have called the Chiral Resonance Model (ChRM). Using the previous scheme we have demonstrated that it is possible to understand  $\pi\pi$ -scattering up to the 1 GeV region by shoehorning together poles and contact term contributions and employing a suitable regularization procedure. It seems likely that any crossing symmetric approximation will have a similar form. We will regard the ChRM as a leading order  $1/N_c$  mean field approximation for the Quantum Chromodynamics.

## Part II

Heavy Systems

## Chapter 4

# Heavy Baryons in the Bound State Approach

## 4.1 Brief Introduction to the Heavy Physics

In the second part of this thesis we will investigate the heavy baryon spectra. A heavy hadron schematically consists of a heavy quark Q of spin  $S_{\text{heavy}} = 1/2$  and a light cloud. The latter describes the light degrees of freedom with total light spin  $j_l$ . There also exist heavy hadrons which contain a higher number of heavy quarks, but we will not consider them here. The total hadron spin is obtained by adding together the heavy quark spin and the spin of the light cloud

$$\boldsymbol{J} = \boldsymbol{S}_{\text{heavy}} + \boldsymbol{j}_{l} . \tag{4.1}$$

A heavy baryon corresponds to an integer value of  $j_l$ , while a heavy meson to half-odd integer values of  $j_l$ .

In the heavy quark mass limit  $(m_Q/\Lambda \gg 1)$  the heavy spin commutes with the

68

QCD hamiltonian  $H_0$ 

$$[H_0, \mathbf{S}_{\text{heavy}}] = 0. \tag{4.2}$$

Hence the heavy spin is now a good quantum number leading to the heavy spin symmetry. Since in the heavy limit the hamiltonian cannot depend on the mass of the heavy quark it is not possible to distinguish among heavy hadrons made with different heavy quarks. We will indicate this symmetry as heavy flavor symmetry. Heavy spin symmetry predicts that for given  $j_l \neq 0$  and fixed parity, we have a degenerate doublet of total spin

$$J = j_l \pm \frac{1}{2} \ . \tag{4.3}$$

while for  $j_l = 0$  we have a heavy baryon with total spin J = 1/2 which we can identify as  $\Lambda_Q$ , where Q indicates the heavy quark contained in the heavy hadron. Let us explicitly demonstrate that the splitting between the  $J^P = 1^-$  and  $J^P = 0^-$  states of a  $Q\bar{q}$  meson must vanish in the limit of infinite heavy quark mass. Since the action of  $S_{\text{heavy}}^3$  on a  $0^-$  state produces a  $1^-$  state, i.e.  $|M_{1^-}\rangle = 2S_{\text{heavy}}^3|M_{0^-}\rangle$  we then have

$$H_0|M_{1^-}> = m_{1^-}|M_{1^-}> = 2S_{\text{heavy}}^3 H_0|M_{0^-}> = m_{0^-}|M_{1^-}>,$$
 (4.4)

implying that  $m_{1^-} - m_{0^-} \to 0$  as  $m_Q \to \infty$ . Experimentally [37] we have

$$\frac{m_{D^*} - m_D}{m_D} \approx 8\% , \qquad \frac{m_{B^*} - m_B}{m_B} \approx 1\% ,$$
 (4.5)

which indicates the goodness of the 1/M expansion. We also notice that the heavy spin breaking is O(1/M) as can be understood by looking at a one gluon exchange diagram.

## 4.2 Bound State Approach to the Heavy Baryon system

There has been recent interest in studying heavy baryons (those with the valence quark structure qqQ) in the bound state picture [59,60] together with heavy quark spin symmetry [61]. In this picture the heavy baryon is treated [62–67] as a heavy spin multiplet of mesons  $(Q\bar{q})$  bound in the background field of the nucleon (qqq), which in turn arises as a soliton configuration of light meson fields.

A nice feature of this approach is that it permits, in principle, an exact expansion of the heavy baryon properties in simultaneous powers of 1/M and  $1/N_c$ . In the simplest treatments, the light part of the chiral Lagrangian is made from only pion fields. However it has been shown that the introduction of light vector mesons [64–66] substantially improves the accuracy of the model. This is also true for the soliton treatment of the nucleon itself [68–70]. Furthermore finite M corrections as well as finite  $N_c$  (nucleon recoil) corrections are also important. This has been recently demonstrated for the hyperfine splitting problem [71,90] and it will be explained in some detail in the next chapter.

Since the bound state—soliton approach is somewhat involved it may be worthwhile to point out a couple of its advantages. In the first place, it is based on an effective chiral Lagrangian containing physical parameters which are in principle subject to direct experimental test. Secondly, the bound state approach models a characteristic feature of a confining theory. When the bound system is suitably "stretched" it does not separate into colored objects but into physical color singlet states.

#### 4.2.1 Effective Lagrangian for the Heavy-Light system

Here we will review the chiral Lagrangian for the low lying heavy mesons in the heavy limit. In the next chapter we will see how to include next to leading corrections in 1/M. The model is based on a chiral Lagrangian with two parts,

$$\mathcal{L} = \mathcal{L}_{\text{light}} + \mathcal{L}_{\text{heavy}} \tag{4.6}$$

The light part involves the chiral field  $U = \xi^2 = \exp(2i\phi/F_{\pi})$ , where  $\phi$  is the  $3 \times 3$  matrix of standard pseudoscalars. Relevant vector and pseudovector combinations are  $v_{\mu}$  and  $p_{\mu}$  defined in Eq. (1.17). In addition light vector mesons are included in a  $3 \times 3$  matrix field  $\rho_{\mu}$ . The explicit form of  $\mathcal{L}_{\text{light}}$  is as in Ref. [90].

The heavy field H, which describes the heavy multiplet which contains the heavy pseudoscalar P and a heavy vector meson  $Q_{\mu}$  is

$$H = \frac{1 + \gamma_{\mu} V^{\mu}}{2} [i\gamma_5 P' + \gamma^{\alpha} Q_{\alpha}'] ,$$

$$\overline{H} = \gamma_0 H^{\dagger} \gamma_0 , \qquad (4.7)$$

where in the leading order in 1/M the pseudoscalar fluctuation field (P') and the vector meson fluctuation  $(Q'_{\mu})$  are connected with the heavy fields via

$$P = e^{-iMV \cdot x} P'$$
,  $Q_{\mu} = e^{-iMV \cdot x} Q'_{\mu}$ . (4.8)

 $V_{\mu}$  is the super selected four velocity of the heavy meson.

Under a heavy spin transformation S, H transforms as

$$H \to SH$$
 , (4.9)

while under a chiral transformation H transforms as a matter field

$$H \to HK^{\dagger}$$
 , (4.10)

where K is defined in Eq. (1.15). The heavy spin and chiral preserving lagrangian takes the form [76]

$$\mathcal{L}_{\text{heavy}}/M = iV_{\mu}\text{Tr}\left[HD^{\mu}\bar{H}\right] - d\,\text{Tr}\left[H\gamma_{\mu}\gamma_{5}p^{\mu}\bar{H}\right] + \frac{ic}{m_{V}}\text{Tr}\left[H\gamma_{\mu}\gamma_{\nu}F^{\mu\nu}(\rho)\bar{H}\right] , (4.11)$$

where  $D_{\mu} \equiv \partial_{\mu} + i\alpha \tilde{g} \rho_{\mu} - i(1-\alpha)v_{\mu}$ , and  $F_{\mu\nu}(\rho) = \partial_{\mu}\rho_{\nu} - \partial_{\nu}\rho_{\mu} + i\tilde{g} [\rho_{\mu}, \rho_{\nu}]$ . Furthermore,  $m_V$  is the light vector meson mass while  $d \simeq 0.53$  and  $c \simeq 1.6$  are respectively the heavy meson–pion and magnetic type heavy meson–light vector meson coupling constants;  $\alpha$  is a coupling constant whose value has not yet been firmly established.

## 4.3 Mechanics of Baryon States

Following the Callan-Klebanov idea [59], we first find the classical solution of the light meson action and then obtain the classical approximation to the wave function in which this baryon as soliton is bound to a heavy meson (yielding a heavy baryon). The hedgehog ansatz for the classical light baryon in the SU(2) case simply corresponds to

$$\xi_{c}(\boldsymbol{x}) = \exp\left[\frac{i}{2}\hat{\boldsymbol{x}} \cdot \boldsymbol{\tau} F(|\boldsymbol{x}|)\right] ,$$

$$\rho_{ic}^{a} = \frac{1}{\sqrt{2}\tilde{g}|\boldsymbol{x}|} \epsilon_{ika}\hat{x}_{k} G(|\boldsymbol{x}|) ,$$

$$\omega_{0c} = \omega(|\boldsymbol{x}|) ,$$

$$\rho_{0c}^{a} = \omega_{ic} = 0 ,$$

$$(4.12)$$

where  $\rho_{\mu c} = \frac{1}{\sqrt{2}} \left( \omega_{\mu c} + \tau^a \rho_{\mu c}^a \right)$  and  $\tilde{g}$  is a coupling constant. The appropriate boundary conditions are

$$F(0) = -\pi$$
,  $G(0) = 2$ ,  $\omega'(0) = 0$ ,  
 $F(\infty) = G(\infty) = \omega(\infty) = 0$ , (4.13)

which correspond to unit baryon number. The wave function for the heavy meson bound to the background Skyrmion field (4.12) is conveniently presented in the rest frame,  $\mathbf{V} = 0$ . In this frame

$$\bar{H}_{\rm c} \to \begin{pmatrix} 0 & 0 \\ \bar{h}_{lh}^a & 0 \end{pmatrix} ,$$
 (4.14)

with a, l, h representing respectively the isospin, light spin and heavy spin bivalent indices. The calculation simplifies if we deal with a radial wave function obtained after removing the factor  $\hat{x} \cdot \tau$ :

$$\bar{h}_{lh}^{a} = \frac{u(|\boldsymbol{x}|)}{\sqrt{M}} \left( \hat{\boldsymbol{x}} \cdot \boldsymbol{\tau} \right)_{ad} \psi_{dl,h} , \qquad (4.15)$$

where  $u(|\mathbf{x}|)$  is a radial wave function, assumed to be very sharply peaked near  $|\mathbf{x}| = 0$  for large M (i.e.  $r^2|u(r)|^2 \approx \delta(r)$ ). The heavy spinor  $\chi_h$  can be trivially factored out

$$\psi_{dl,h} = \psi_{dl} \chi_h \tag{4.16}$$

in this expression as a manifestation of the heavy quark symmetry. We perform a partial wave analysis of the generalized "angular" wave function  $\psi_{dl}$ :

$$\psi_{dl}(g, g_3; r, k) = \sum_{r_3, k_3} C_{r_3, k_3; g_3}^{r, k; g} Y_r^{r_3} \xi_{dl}(k, k_3) . \tag{4.17}$$

Here  $Y_r^{r_3}$  stands for the standard spherical harmonic representing orbital angular momentum r while C denotes the ordinary Clebsch–Gordan coefficients.  $\xi_{dl}(k, k_3)$  represents a wave function in which the "light spin" and isospin (referring to the "light cloud" component of the heavy meson) are added vectorially to give

$$K = I_{\text{light}} + S_{\text{light}} , \qquad (4.18)$$

with eigenvalues  $\mathbf{K}^2 = k(k+1)$ . The total light "grand spin"

$$\boldsymbol{g} = \boldsymbol{r} + \boldsymbol{K} , \qquad (4.19)$$

is a *good* quantum number in the heavy limit. It is also convenient to define the total *grand spin* operator

$$G = g + S_{\text{heavy}} , \qquad (4.20)$$

where  $S_{\text{heavy}}$  is the spin of the heavy quark within the heavy meson. Substituting the wave–function (4.15) into  $\int d^3x \mathcal{L}_{\text{heavy}}$  given in Eq. (4.11) yields the potential operator

$$V = \int d\Omega \ \psi^* \left\{ \boldsymbol{\sigma} \cdot \boldsymbol{\tau} \Delta_1 + 1 \Delta_2 \right\} \psi$$

$$= \int d\Omega \ \psi^* \left\{ 4\Delta_1 \boldsymbol{S}_{light} \cdot \boldsymbol{I}_{light} + 1 \Delta_2 \right\} \psi$$

$$= 2\Delta_1 \left[ k(k+1) - \frac{3}{2} \right] + \Delta_2 , \qquad (4.21)$$

where  $\int d\Omega$  is the solid angle integration and Eq. (4.18) was used in the last step. In addition

$$\Delta_1 = \frac{1}{2} dF'(0) - \frac{c}{m_V \tilde{g}} G''(0) ,$$

$$\Delta_2 = -\frac{\alpha \tilde{g}}{\sqrt{2}} \omega(0) . \tag{4.22}$$

The  $\Delta_2$  term is relatively small [65, 66, 90]. Both terms in  $\Delta_1$  are positive with the second one (due to light vectors) slightly larger. There are just the two possibilities k=0 and k=1. It is seen that the k=0 states, for any orbital angular momentum r, will be bound with binding energy  $3\Delta_1$ . The k=1 states are unbound in this limit. The parity of the bound state wave function is

$$P_B = (-1)^r ,$$
 (4.23)

which emerges as a product of  $(-1)^r$  for  $Y_r^{r_3}$  in Eq. (4.17), -1 for the  $\hat{\boldsymbol{x}} \cdot \boldsymbol{\tau}$  factor in Eq. (4.15) and -1 due to the fact that the mesons (P,Q) bound to the soliton have negative parity.

## 4.4 Collective Quantization

In the soliton approach, the particle states with definite rotational and flavor quantum numbers appear after the so–called rotational collective modes are introduced and the theory is quantized. This is conveniently done by first finding the time independent parameters which leave the theory invariant, then those collective parameters are allowed to depend on time. The collective angle–type coordinate A(t) is introduced [77] as

$$\xi(\boldsymbol{x},t) = A(t)\xi_{c}(\boldsymbol{x})A^{\dagger}(t) ,$$

$$\boldsymbol{\tau} \cdot \boldsymbol{\rho}(\boldsymbol{x},t) = A(t)\boldsymbol{\tau} \cdot \boldsymbol{\rho}_{c}(\boldsymbol{x})A^{-1}(t) ,$$

$$\bar{H}(\boldsymbol{x},t) = A(t)\bar{H}_{c}(\boldsymbol{x}) ,$$

$$(4.24)$$

where  $\xi_c$  and  $\rho_c$  are defined in Eq. (4.12) and  $\bar{H}_c$  in Eqs. (4.14) and (4.15). For our purposes the important variable is the "angular–velocity"  $\Omega$  defined by

$$A^{\dagger} \dot{A} = \frac{i}{2} \boldsymbol{\tau} \cdot \boldsymbol{\Omega} , \qquad (4.25)$$

which measures the time dependence of the collective coordinates A(t). It should furthermore be mentioned that, due to the collective rotation, the vector meson field components which vanish classically ( $\rho_0^a$  and  $\omega_i$ ) get induced:

$$\omega_i = -\frac{\sqrt{2}}{r}\varphi(r)\epsilon_{ijk}\Omega_j\hat{r}_k \quad \text{and} \quad \rho_0^k = -\frac{1}{\sqrt{2}}\left(\xi_1(r)\Omega_k + \xi_2(r)\hat{\boldsymbol{r}}\cdot\boldsymbol{\Omega}\hat{r}_k\right) . \tag{4.26}$$

Substituting Eq. (4.24) and Eq. (4.26) into  $\int d^3x \left(\mathcal{L}_{light} + \mathcal{L}_{heavy}\right)$  gives an additional contribution to the lagrangian of the general form

$$L_{coll} = \frac{1}{2}\alpha^2 \mathbf{\Omega}^2 - \chi \mathbf{\Omega} \cdot \mathbf{G} , \qquad (4.27)$$

in which  $\alpha$  and  $\chi$  represent spatial integrals over the profiles in Eq. (4.12). The induced radial functions  $\varphi(r)$ ,  $\xi_1(r)$  and  $\xi_2(r)$  are obtained from a variational approach

to  $\alpha^2$  [85]. For each bound state solution  $\bar{H}_c$ , there will be a tower of states characterized by a soliton angular momentum  $\boldsymbol{J}^{\rm sol}$  and the total isospin  $\boldsymbol{I}$  satisfying  $I=J^{\rm sol}$ . The soliton angular momentum is computed from this collective Lagrangian as

$$\boldsymbol{J}^{\text{sol}} = \frac{\partial L_{\text{coll}}}{\partial \boldsymbol{\Omega}} , \qquad (4.28)$$

while the total baryon angular momentum is the sum

$$J = g + J^{\text{sol}} + S_{\text{heavy}}$$
 (4.29)

The rotational collective Hamiltonian is obtained by performing the standard Legendre transform

$$H_{coll} = \frac{1}{2\alpha^2} \left( \boldsymbol{J}^{\text{sol}} + \chi \boldsymbol{G} \right)^2 . \tag{4.30}$$

The moment of inertia  $\alpha^2$  is identified from the light soliton sector as  $\alpha^{-2} = \frac{2}{3}(m_{\Delta} - m_N)$  in terms of the nucleon and  $\Delta$  masses. Equation (4.27) can be simplified by noting that the total angular momentum is given by  $\mathbf{J} = \mathbf{J}^{\text{sol}} + \mathbf{G}$ . Then we deduce the heavy baryon mass formula [59]

$$H_{coll} = \frac{1}{3} (m_{\Delta} - m_N) \left[ (1 - \chi)I(I+1) + \chi J(J+1) + \cdots \right] , \qquad (4.31)$$

where the ellipsis stands for the  $\chi(\chi - 1)G(G + 1)$  term which does not split the heavy baryon masses. In the heavy limit  $\mathcal{L}_{\text{heavy}}$  leads to  $\chi = 0$ . Thus we have the final results

$$m(\Sigma_Q^*) - m(\Sigma_Q) = 0 , \qquad (4.32)$$

$$m(\Sigma_Q) - m(\Lambda_Q) = \frac{2}{3}(m_\Delta - m_N) , \qquad (4.33)$$

wherein the subscript Q denotes the heavy baryon which contains the heavy quark Q. It may be interesting to compare the experimental determination [37] for  $m(\Sigma_c)$  –  $m(\Lambda_c) \simeq 170$  MeV which the theoretical prediction in Eq. (4.33) which provides 195

MeV. The result  $m(\Sigma_Q^*) - m(\Sigma_Q) = 0$  is, of course, expected in the heavy quark spin symmetry limit. However if we consider heavy spin violating term (i.e.  $\chi \neq 0$ ) we get

$$m(\Sigma_Q^*) - m(\Sigma_Q) = \chi (m_\Delta - m_N) . \tag{4.34}$$

The next chapter will be devoted to the calculation of the hyperfine splitting parameter  $\chi$ .

## Chapter 5

## Heavy Baryon Hyperfine Splitting

## 5.1 Introduction

We have already noticed that a compelling feature of the heavy soliton approach is that it permits, in principle, an exact expansion of the heavy baryon properties in simultaneous powers of 1/M,  $1/N_c$  and, since it is based on a chiral Lagrangian, number of derivatives acting on the light components of the heavy system. In practice there are obstacles related to the large number of unknown parameters which must be introduced. Rather than treating the light soliton in a model with many derivatives of the light pseudoscalar fields it turns out to be much more efficient to use the light vector mesons. Based on a model [65] of the light vector interactions with the heavy multiplet, the leading order (in the  $1/N_c$  and 1/M expansions) heavy baryon mass splittings have been discussed [66], obtaining satisfactory agreement with experiment. Actually the need for light vector mesons is not surprising since, in the soliton approach, they are necessary to explain, for example, the neutron–proton mass difference [68] and the nucleon axial singlet matrix element [69].

In the present chapter we focus our attention on the hyperfine splitting, which is

of subleading order both in 1/M and  $1/N_c$ . This is a more complicated calculation and also involves using a cranking procedure [77] to obtain physical states which carry good spin and isospin quantum numbers. The first calculation of the heavy baryon hyperfine splitting in the perturbative bound state framework was carried out by Jenkins and Manohar [62] who got the formula

$$m(\Sigma_Q^*) - m(\Sigma_Q) = \frac{(m(\Delta) - m(N))(M^* - M)}{4d F'(0)},$$
 (5.1)

where  $M^* - M$  is the heavy vector-heavy pseudoscalar mass difference, d is the light pseudoscalar-heavy meson coupling constant and F'(0) is the slope of the Skyrme "profile function" at the origin. This formula is obtained (see also section 5) by using the leading order in number of derivatives (zero) and leading order in 1/M heavy spin violation term. Therefore it is expected to provide the dominant contribution. Unfortunately, on evaluation, it is found to provide only a small portion of the experimental  $\Sigma_c^* - \Sigma_c$  mass difference. This naturally suggests the need for including additional higher order in derivative heavy spin violation terms. However, there are many possible terms with unknown coefficients so that the systematic perturbative approach is not very predictive.

To overcome this problem we employ a relativistic Lagrangian model [65] which uses ordinary heavy pseudoscalar and vector fields rather than the heavy "fluctuation" field multiplet [61]. This model reduces to the heavy multiplet approach in leading order and does not contain any new parameters. We will show that [71] such a model (considered, for simplicity, to contain only light pseudoscalars; *i.e.*, the light part is the original Skyrme model [80]) yields a "hidden" heavy spin violation which is not manifest from the form of the Lagrangian itself. This hidden part involves two derivatives and is actually more important numerically than the zero derivative "manifest" piece which leads to Eq (5.1). However this new result is still not sufficient to bring the predicted  $\Sigma_c^* - \Sigma_c$  mass difference into agreement with experiment. The

prediction for this difference is actually correlated to those for  $\Sigma_c - \Lambda_c$  and  $\Delta - N$ , the  $\Delta$  - nucleon mass difference by [59]:

$$m\left(\Sigma_{c}^{*}\right) - m\left(\Sigma_{c}\right) = m\left(\Delta\right) - m\left(N\right) - \frac{3}{2}\left[m\left(\Sigma_{c}\right) - m\left(\Lambda\right)\right] . \tag{5.2}$$

This formula depends only on the collective quantization procedure being used rather than the detailed structure of the model. If  $m(\Sigma_c) - m(\Lambda)$  and  $m(\Delta) - m(N)$  are taken to agree with experiment, Eq (5.2) predicts 41 MeV rather than the experimental value of 66 MeV. This means that it is impossible to exactly predict, in models of the present type, all three mass differences which appear in Eq (5.2). The goodness of the overall fit must be judged by comparing all three quantities with experiment. Our focus, of course, is the left hand side of Eq (5.2) which is of order 1/M while the right hand side involves the difference of two order 1/M quantities. A similar calculation in the model with only light pseudoscalars was carried out by Oh and Park [67]. However, they did not make a 1/M expansion in order to reveal the hidden violation terms. They also introduced a one-derivative "manifest" heavy spin violation term with a new relatively large unknown constant in order to improve the agreement with experiment.

In the present chapter we show that it is not necessary to introduce any new violation terms to agree with experiment if a chiral Lagrangian including light vectors is employed. Typical results are summarized, compared with experiment and compared with the Skyrme model for the light sector in Table 5.1. A much more detailed discussion is given later in the text. We notice from the last row, that the model with light vectors gives a very satisfactory account of the  $\Sigma_c^*$ - $\Sigma_c$  hyperfine splitting in contrast to the model without light vectors. There are also noticeable effects when the use of the heavy meson reduced mass is taken as a simple approximation for kinematical corrections. Similarly, the first four rows of Table 5.1 show that the other predictions of the model with light vectors agree well with experiment.

mass difference	expt.	present model	present model + CM	Skyrme
$\Lambda_c - N$	1345	1257	1356	1553
$\Lambda_b - \Lambda_c$	$3356 \pm 50$	3164	3285	3215
$\Lambda_c' - \Lambda_c$	308	249	342	208
$\Sigma_c - \Lambda_c$	168	172	158	185
$\Sigma_c^* - \Sigma_c$	66	42	63	16

Table 5.1: Typical results for the present model (including light vectors) compared with model with light pseudoscalars only ("Skyrme" column) and compared with experiment. No "manifest" heavy spin violation effects other than  $M^* \neq M$  have been included. The column "present model + CM" simply takes into account recoil corrections by replacing the heavy meson mass by the reduced mass.  $\Lambda'_c$  denotes a negative parity, spin 1/2 state. The quantity  $\alpha$  in Eqs (5.4) was taken to be zero. All masses in MeV.

#### 5.1.1 Relativistic Lagrangian for the Heavy Mesons.

For the sector of the model describing the light pseudoscalar and vector mesons we adopt the chirally invariant Lagrangian discussed in detail in the literature [86,87,90]. We now present the relativistic Lagrangian, which describes the coupling between the light and heavy mesons [65]

$$\mathcal{L}_{H} = D_{\mu}PD^{\mu}\overline{P} - \frac{1}{2}Q_{\mu\nu}\overline{Q}^{\mu\nu} - M^{2}P\overline{P} + M^{*2}Q_{\mu}\overline{Q}^{\mu} 
+2iMd\left(Pp_{\mu}\overline{Q}^{\mu} - Q_{\mu}p^{\mu}\overline{P}\right) + \frac{d}{2}\epsilon^{\alpha\beta\mu\nu}\left[Q_{\nu\alpha}p_{\mu}\overline{Q}_{\beta} + Q_{\beta}p_{\mu}\overline{Q}_{\nu\alpha}\right] 
+ \frac{2icM}{m_{V}}\left\{2Q_{\mu}F^{\mu\nu}\left(\rho\right)\overline{Q}_{\nu} - \frac{i}{M}\epsilon^{\alpha\beta\mu\nu}\left[D_{\beta}PF_{\mu\nu}\left(\rho\right)\overline{Q}_{\alpha} + Q_{\alpha}F_{\mu\nu}\left(\rho\right)D_{\beta}\overline{P}\right]\right\}.$$
(5.3)

Here we have allowed the mass M of the heavy pseudoscalar meson P to differ from the mass  $M^*$  of the heavy vector meson  $Q_{\mu}$ . Note that the heavy meson fields are conventionally defined as row vectors in isospin space. The covariant derivative introduces the additional parameter  $\alpha$ :

$$D_{\mu}\left(\overline{P}, \overline{Q}_{\alpha}\right) = \left(\partial_{\mu} + i\alpha\widetilde{g}\rho_{\mu} - i\left(1 - \alpha\right)v_{\mu}\right)\left(\overline{P}, \overline{Q}_{\alpha}\right) . \tag{5.4}$$

The covariant field tensor of the heavy vector meson is then defined as

$$\overline{Q}_{\mu\nu} = D_{\mu}\overline{Q}_{\nu} - D_{\nu}\overline{Q}_{\mu} . \tag{5.5}$$

The coupling constants d, c and  $\alpha$ , which appear in the Lagrangian (5.3), have still not been very accurately determined. In particular there is no direct experimental evidence for the value of  $\alpha$ , which would be unity if a possible definition of light vector meson dominance for the electromagnetic form factors of the heavy mesons were to be adopted [88]. We will later adjust  $\alpha$  to the spectrum of the heavy baryons. The other parameters in (5.3) will be taken to be:

$$d = 0.53$$
,  $c = 1.60$ ;

$$M = 1865 \text{MeV}$$
,  $M^* = 2007 \text{ MeV}$ ,  $D - \text{meson}$ ;  
 $M = 5279 \text{MeV}$ ,  $M^* = 5325 \text{ MeV}$ ,  $B - \text{meson}$ . (5.6)

It should be stressed that the assumption of infinitely large masses for the heavy mesons has not been made in (5.3). However, a model Lagrangian which was only required to exhibit the Lorentz and chiral invariances would be more general than the relativistic Lagrangian (5.3). Actually the coefficients of the various Lorentz and chirally invariant pieces in the relativistic Lagrangian (5.3) have precisely been arranged to yield the spin–flavor symmetric model (4.11) in the heavy quark limit [76].

## 5.2 An apparent puzzle

In this paragraph we will resolve an apparent puzzle which arises when calculating the corrections to the hyperfine splitting using the relativistic lagrangian presented in Eq. (5.3). Here we will neglect the light vector contributions which is equivalent to set  $\alpha = 0$  and c = 0 in Eq. (5.3). Then the heavy Lagrangian in Eq. (5.3) becomes

$$\mathcal{L}(P,Q_{\mu}) = +D_{\mu}PD^{\mu}\overline{P} - M^{2}P\overline{P} - \frac{1}{2}Q_{\mu\nu}\overline{Q}^{\mu\nu} + M^{*2}Q_{\mu}\overline{Q}^{\mu}$$

$$+ 2iMd\left(Pp_{\mu}\overline{Q}^{\mu} - Q^{\mu}p_{\mu}\overline{P}\right)$$

$$+ d'\epsilon^{\alpha\beta\mu\nu}\left(D_{\alpha}Q_{\beta}p_{\mu}\overline{Q}_{\nu} - Q_{\alpha}p_{\beta}D_{\mu}\overline{Q}_{\nu}\right).$$

$$(5.7)$$

Here we have modified the coefficient of the fifth term in Eq. (5.3) to include a new source of heavy spin breaking. First let us consider the calculation of the hyperfine splitting in the heavy field approach. This, of course, arises at first sub-leading order in 1/M and violates the heavy spin symmetry. Thus we must add to Eq. (4.11) suitable heavy spin violating terms [62]:

$$\mathcal{L}'_{\text{heavy}}/M = \frac{M - M^*}{8} \text{Tr} \left[ H \sigma_{\mu\nu} \overline{H} \sigma^{\mu\nu} \right] + \frac{(d - d')}{2} \text{Tr} \left[ H p^{\mu} \overline{H} \gamma_{\mu} \gamma_5 \right] + \cdots$$
 (5.8)

The first term has no derivatives while the second term has one derivative. The hyperfine splitting is related to a collective Lagrangian parameter (see section 5.3 for details)  $\chi$  with a proportionality factor of the  $\Delta$ -N mass difference:

$$m(\Sigma_O^*) - m(\Sigma_O) = [m(\Delta) - m(N)] \chi . \tag{5.9}$$

(At present only  $\Sigma_c$  is well established experimentally.) For Eq. (5.8) we have

$$\chi = \frac{M^* - M}{4dF'(0)} + \frac{d - d'}{4d} \,. \tag{5.10}$$

The first term was obtained in Ref. [62] while the second seems to be new. Notice that  $(M^* - M)$  and (d - d') behave as 1/M. These quantities are the same as the ones appearing in the ordinary field Lagrangian (5.7). It would thus seem that  $\mathcal{L}'_{\text{heavy}}$  in Eq. (5.8) neatly summarizes the heavy spin violation in Eq. (5.7).

Now let us consider the calculation of  $\chi$  from Eq. (5.7) directly based on exact numerical solution of the associated coupled differential equations. We content ourselves with the graphical presentation of some results<sup>1</sup> and relegate the details to Ref. [90]<sup>2</sup>. Figure 5.1 shows  $\chi$  plotted against M for three cases: i)  $M^* = M$ , d' = d = 0.53, ii)  $M^* - M \simeq (0.258 \text{GeV})^2/M$  (a fit to experiment), d' = d = 0.53, iii)  $M^* = M$ , d' - d = (0.0991 GeV)/M (an arbitrary choice which sets the coupling constant splitting to be 10% at the D meson mass). We immediately notice that  $\chi$  does not vanish when there is no manifest heavy spin violation, i.e.,  $M = M^*$ , d = d'. In fact the dominant part of the contribution to  $\chi$  for realistic heavy meson masses is already present in this case. By subtracting out this piece we note that the signs of the contributions due to  $M^* \neq M$  and  $d' \neq d$  agree with those predicted in Eq. (5.10). It is interesting to note that all three curves in Fig. 5.1 fall off as 1/M for  $M \geq 10$  GeV.

<sup>&</sup>lt;sup>1</sup>For the Skyrme model parameters we use the experimental value of  $F_{\pi}$  and  $e_{Sk} = 6.0$ . This results in a profile with  $F'(0) = 1.20 \,\text{GeV}$ .

<sup>&</sup>lt;sup>2</sup>Similar calculations were done in Ref. [67] but they did not consider the  $M = M^*$ , d = d' case.

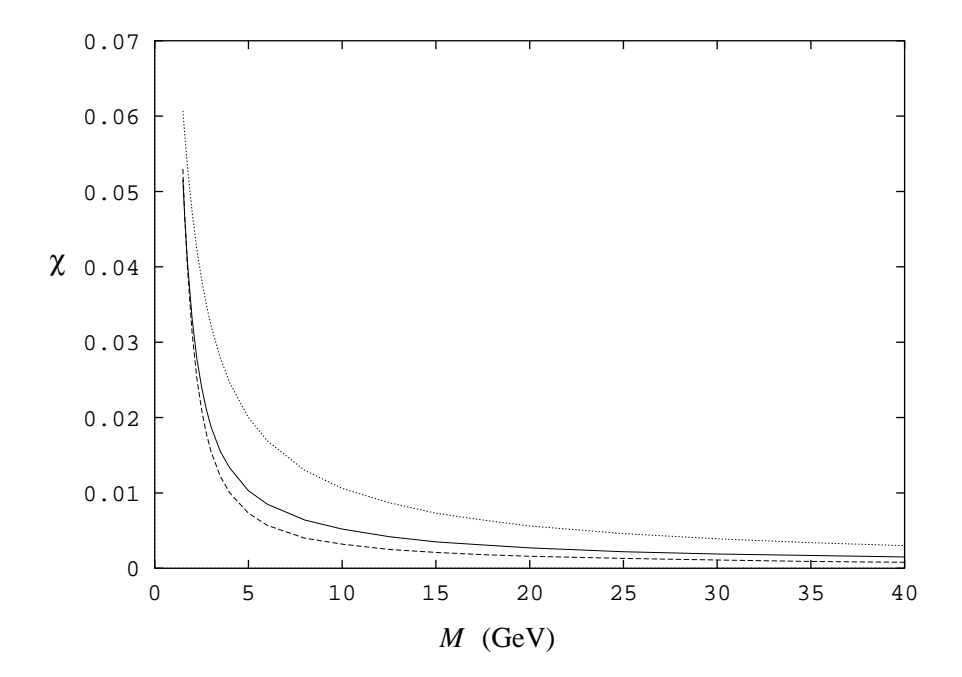


Figure 5.1:  $\chi$  vs. M computed by numerical integration. Solid line  $M^* = M$ , d' = d; dotted line  $M^* \neq M$ , d' = d, dashed line  $M^* = M$ ,  $d' \neq d$ .

But our main task is to understand the source of the puzzling non-zero contribution in case i. It is clear that the ordinary field Lagrangian (5.7) must contain heavy spin violating pieces which are not manifest. We will now explore this in detail by rewriting Eq. (5.7) in terms of the "fluctuation field" H and expanding it in powers of 1/M.

#### 5.2.1 Expansion of Lagrangian

Since the effects of  $M \neq M^*$  and  $d \neq d'$  were taken into account in Eq. (5.10) it is sufficient to expand Eq. (5.7) with  $M^* = M$  and d' = d. To describe the heavy particle moving with four-velocity  $V_{\mu}$ , we introduce the factorization

$$P = e^{-iMV \cdot x} P' , \qquad Q_{\mu} = e^{-iMV \cdot x} \tilde{Q}_{\mu} . \qquad (5.11)$$

P' is the pseudoscalar "fluctuation field".  $\widetilde{Q}_{\mu}$  is not exactly the vector fluctuation field since  $V \cdot \widetilde{Q}$  is not constrained to be zero. We therefore introduce the correct fluctuation field  $Q'_{\mu}$  by

$$\widetilde{Q}_{\mu} = Q'_{\mu} + V_{\mu}V \cdot \widetilde{Q} , \qquad (5.12)$$

which shows that  $V \cdot Q' = 0$ . Substituting Eqs (5.11) and (5.12) into the Lagrangian (5.3) gives, in addition to the leading terms of order M, the presently interesting terms of order  $M^0$ :

$$\mathcal{L}(P,Q) = (\text{order } M) - P'D^{2}\overline{P'} + Q'_{\mu}D^{2}\overline{Q'}^{\mu} - Q'^{\mu}D_{\nu}D_{\mu}\overline{Q'}^{\nu} 
- d\epsilon^{\alpha\beta\mu\nu} \left( D_{\alpha}Q'_{\beta}p_{\mu}\overline{Q'}_{\nu} - Q'_{\alpha}p_{\beta}D_{\mu}\overline{Q'}_{\nu} \right) 
+ M^{2}V \cdot \widetilde{Q}V \cdot \overline{\widetilde{Q}} + iM \left( D_{\mu}Q'^{\mu}V \cdot \overline{\widetilde{Q}} - V \cdot \widetilde{Q}D_{\mu}\overline{Q'}^{\mu} \right) 
+ 2iMd \left( P'V \cdot pV \cdot \overline{\widetilde{Q}} - V \cdot \widetilde{Q}V \cdot p\overline{P'} \right) + \cdots ,$$
(5.13)

where the three dots stand for terms of order 1/M. In contrast to the massless fields P' and Q',  $V \cdot \tilde{Q}$  is seen to have the large mass M. We thus integrate it out using

the equation of motion

$$V \cdot \tilde{Q} = -\frac{i}{M} D_{\mu} Q^{\prime \mu} - \frac{2id}{M} P^{\prime} V \cdot p . \qquad (5.14)$$

Substituting Eq. (5.14) back into Eq. (5.13) gives

$$\mathcal{L}(P,Q) = (\text{order } M) - P' D^2 \overline{P'} + Q'_{\mu} D^2 \overline{Q'}^{\mu} - i Q'_{\mu} F^{\mu\nu}(v) \overline{Q'}_{\nu} 
- 2d \left( P' V \cdot p D_{\mu} \overline{Q'}^{\mu} + D_{\mu} Q'^{\mu} V \cdot p \overline{P'} \right) 
- i d \epsilon^{\alpha\beta\mu\nu} \left( D_{\alpha} Q'_{\beta} p_{\mu} \overline{Q'}_{\nu} - Q'_{\alpha} p_{\beta} D_{\mu} \overline{Q'}_{\nu} \right) 
- 4d^2 P' (V \cdot p)^2 \overline{P'} + \cdots,$$
(5.15)

where  $F_{\mu\nu}(v) = \partial_{\mu}v_{\nu} - \partial_{\nu}v_{\mu} - i[v_{\mu}, v_{\nu}]$ . In order to extract the heavy spin violating pieces it is convenient to rewrite the order  $M^0$  Lagrangian in terms of the heavy multiplet field H Eq. (4.7). After some algebraic calculation we find

$$\mathcal{L}(H) = \mathcal{L}_{\text{heavy}} + \frac{1}{2} \text{Tr} \left[ H D^2 \overline{H} \right] + i \frac{1}{8} \text{Tr} \left[ [H, \gamma_{\mu} \gamma_{\nu}] F^{\mu\nu}(v) \overline{H} \right] 
+ d \left[ \frac{i}{2} \text{Tr} \left[ D_{\mu} H \gamma^{\mu} \gamma_5 (V \cdot p) \overline{H} \right] - \frac{i}{4} \text{Tr} \left[ \gamma \cdot D H \gamma_{\mu} \gamma_5 p^{\mu} \overline{H} \right] \right] 
- \frac{i}{4} \text{Tr} \left[ \gamma \cdot D H p_{\mu} \overline{H} \gamma^{\mu} \gamma_5 \right] - \frac{1}{8} \text{Tr} \left[ \sigma_{\mu\nu} D_{\alpha} H \gamma^{\alpha} V \cdot p \gamma_5 \sigma^{\mu\nu} \overline{H} \right] + \text{h.c.} \right] 
+ d^2 \left[ \frac{1}{2} \text{Tr} \left[ H \left( V \cdot p \right)^2 \overline{H} \right] + \frac{1}{4} \text{Tr} \left[ \sigma_{\mu\nu} H \sigma^{\mu\nu} \left( V \cdot p \right)^2 \overline{H} \right] \right] + \cdots , \quad (5.16)$$

where  $\mathcal{L}_{\text{heavy}}$  is given in Eq. (4.11) with  $c = \alpha = 0$ . At this stage we see that Eq. (5.16) actually contains pieces which are not manifestly invariant under the heavy spin transformations  $H \to SH$ ,  $\overline{H} \to \overline{H}S^{\dagger}$ . These pieces involve two derivatives.

## 5.3 Hyperfine splitting from the Hidden Terms

We now sketch the computation of the portion of  $\chi$  in Eq. (5.9) which results from the "hidden" heavy spin violation in Eq. (5.3) that has been made explicit in Eq. (5.16).

For this purpose one needs to collectively quantize the Lagrangian as described in paragraph 4.4. To leading order in M, the "angular part" of the ground state wave function in Eq. (4.15) is [64,65]

$$\psi_{dl,h}^{(1)} = \frac{1}{\sqrt{8\pi}} \epsilon_{dl} \delta_{2h} \ . \tag{5.17}$$

The specific value of the index h results from the choice  $G_3 = G = 1/2$  where G is the "grand spin". To next leading order in M the ground state wave function receives a heavy spin violating admixture of

$$\psi_{dl,h}^{(2)} = \frac{1}{\sqrt{4\pi}} \left[ \sqrt{\frac{2}{3}} \delta_{d1} \delta_{l1} \delta_{h1} + \frac{1}{\sqrt{6}} \left( \delta_{d2} \delta_{l1} + \delta_{d1} \delta_{l2} \right) \right] \delta_{h2} . \tag{5.18}$$

Finally, the hyperfine splitting parameter  $\chi$  is recognized by expanding the collective Lagrangian [59], in powers of  $\Omega$  and picking up the linear piece  $L_{\text{coll}} = (\chi/2)\Omega_3 + \cdots$ . Noting that the  $\Delta$ -nucleon mass difference is given by the moment of inertia, which relates the angular velocity to the spin operator [77], this piece of the Lagrangian yields Eq. (5.9) after canonical quantization of the collective coordinates [59]. There are two types of contribution to  $\chi$ . The first type, from the heavy spin violating terms proportional to d in Eq. (5.16), corresponds to the evaluation of heavy spin violating operators in the ground state (5.17). The second type corresponds to the evaluation of heavy spin conserving operators in the ground state which includes an admixture of Eq. (5.18) due to the Tr  $\left[\gamma_{\mu}\gamma_{\nu}HF^{\mu\nu}(v)\overline{H}\right]$  term in Eq. (5.16). The net result for the "hidden" part of  $\chi$  is

$$\chi = \frac{F'(0)}{4M} \left( d - \frac{1}{2d} \right) . {(5.19)}$$

This equation is expected to hold for large M. To this should be added the "manifest" part given in Eq. (5.10).

It is important to compare Eq. (5.19) with the result for  $\chi$  obtained by the exact numerical solution for the model based on Eq. (5.7). This is gotten as an integral over

the properly normalized radial functions  $\Phi(r), \ldots, \Psi_2(r)$  which appear in the P-wave solution of the bound state equation [66]:

$$\overline{P} = A(t) \frac{\Phi(r)}{\sqrt{4\pi}} \hat{\mathbf{r}} \cdot \boldsymbol{\tau} \rho e^{i\epsilon t}, \qquad \overline{Q}_0 = \frac{i}{\sqrt{4\pi}} A(t) \Psi_4(r) \rho e^{i\epsilon t}, 
\overline{Q}_i = \frac{1}{\sqrt{4\pi}} A(t) \left[ i \Psi_1(r) \hat{r}_i + \frac{1}{2} \Psi_2(r) \epsilon_{ijk} \hat{r}_j \tau_k \right] \rho e^{i\epsilon t} .$$
(5.20)

The spinor  $\rho$  labels the grand spin of the bound heavy meson. The choice  $G_3 = +1/2$  corresponds to  $\rho = (1,0)^{\dagger}$ . The heavy limit bound state wave function in Eq. (5.17) corresponds to the special choice

$$\Phi(r) \propto u(r)$$
,  $\Psi_1(r) = -\Phi(r)$ ,  $\Psi_2(r) = -2\Phi(r)$  and  $\Psi_4(r) = 0$ . (5.21)

The numerical solution to the bound state equations exactly exhibits these relations for  $M, M^* \to \infty$  [66].

Equation (5.19) has an interesting d-dependence and vanishes at  $d=1/\sqrt{2}$ , which actually is not too far from the experimental value of this quantity. In Fig. 5.2 we compare the d-dependence of the exact numerical calculation with the perturbative result of Eq. (5.19). It is seen that the large M perturbation approach works reasonably well and the gross structure of the hyperfine splitting is reproduced. For a detailed comparison of the two treatments it is important to note that for fixed  $M=M^*$  the binding of the heavy meson increases with d. In particular this implies that the wave function is only reasonably localized for large enough d. As a strong localization is a basic feature of the perturbative approach it is easy to understand why this calculation does not yield the exact (numerical) result for small d. In fact, as d increases the agreement expectedly improves. However, upon further increase of d (at finite  $M, M^*$ ), the numerical solution to the bound state equations shows noticeable deviations from the heavy limit relations (5.21), which causes the moderate differences at larger d.

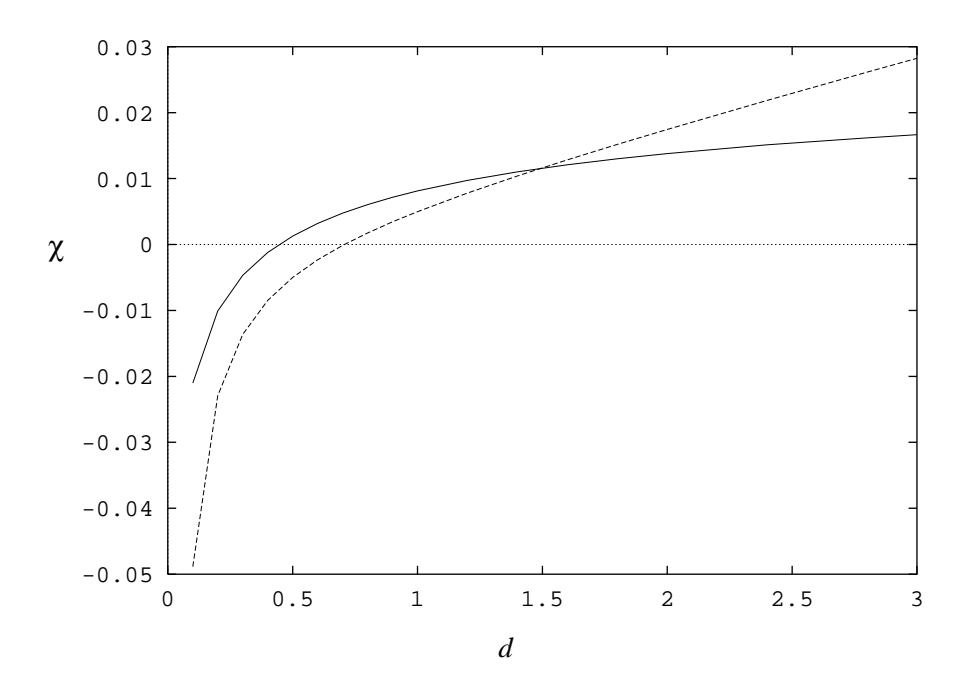


Figure 5.2: The d dependence of  $\chi$  for  $M=M^*=30\,\mathrm{GeV}$  and d=d'. Solid line is the exact numerical calculation. Dashed line is the large M perturbation formula given in Eq. (5.19).

We have solved [71] the apparent puzzle associated with the use of a model Lagrangian containing ordinary fields for computing the hyperfine splitting parameter  $\chi$  by carefully expanding the Lagrangian in powers of 1/M. The key point was the need to preserve the constraint  $V \cdot Q' = 0$  for the heavy vector fluctuation field.

Of course, such a model Lagrangian (which has been used in many calculations) is not exactly QCD. Nevertheless it seems reasonable since it automatically has the correct relativistic kinematics and satisfies the heavy spin symmetry at leading order. We have seen (Eq. (5.16)) that at next order in 1/M, it predicts the coefficients of many terms which otherwise would be unspecified by heavy spin symmetry.

It is amusing to note that these 1/M suppressed terms involve two derivatives and are actually more important for the computation of  $\chi$  than the zero derivative term in Eq. (5.10). This is readily understandable since the dynamical scale in this calculation is the binding energy,  $m(B) + m(N) - m(\Lambda_b) \simeq 620 \,\text{MeV}$  which is rather large for neglecting light vector mesons, higher derivatives etc. [See, for example, Ref. [10].]

We are regarding the Lagrangian (5.3) with  $\alpha = c = 0$  as an illustrative model rather than as a realistic one for comparison with experiment. As indicated earlier it seems necessary to include, in addition to finite M corrections, the effects of light vector mesons as well as nucleon recoil. The discussion of  $\chi$  in this more complicated model and further details of the present calculation will be given in the next paragraph [90].

## Perturbative Approach and the Vector contri-5.4 bution.

The perturbative approach can illuminate several aspects of the hyperfine splitting problem. This is due to the heavy quark symmetry which is naturally exploited by making an expansion in powers of 1/M using the heavy field formalism. Our starting Lagrangian (5.3) has been set up in such a way as to yield a heavy quark symmetric result as  $M \to \infty$  when  $M = M^*$  is assumed, cf. Eq. (4.11). The perturbative 1/M expansion is more general (presumably exact) but less predictive. Thus the 1/M expansion provides a useful calibration in the large M limit. Since it deals with perturbation matrix elements it provides us with a convenient classification of the various sources of hyperfine splitting. The method is also advantageous in that it can be extended, without too much algebraic work, to different channels of interest. On the other hand, once the particular channels of interest are settled on, it is clearly more convenient to employ the exact numerical solution, which efficiently sums up a class of 1/M corrections.

The leading order Lagrangian (4.11) can be supplemented by terms which manifestly break the heavy quark symmetry to leading order ( $M^0$  with the present normalization) as follows:

$$\frac{1}{M}\mathcal{L}'_{H} = \frac{M - M^{*}}{8} \operatorname{Tr} \left[ H \sigma_{\mu\nu} \overline{H} \sigma^{\mu\nu} \right] + \frac{(d - d')}{2} \operatorname{Tr} \left[ H p_{\mu} \overline{H} \gamma^{\mu} \gamma_{5} \right] 
+ i \frac{(c - c')}{m_{V}} \operatorname{Tr} \left[ \gamma_{\mu} \gamma_{\nu} H F^{\mu\nu} (\rho) \overline{H} \right] 
- \tilde{\alpha} V^{\beta} \operatorname{Tr} \left[ H \sigma_{\mu\nu} \left( \tilde{g} \rho_{\beta} + v_{\beta} \right) \overline{H} \sigma^{\mu\nu} \right] .$$
(5.22)

Here the  $(M - M^*)$  term measures the heavy spin violation due to the heavy pseudoscalar – heavy vector mass difference. The (d-d') term measures the heavy spin violation induced by choosing different coefficients for the fifth and sixth terms in Eq. (5.3), while the (c-c') term corresponds to choosing different coefficients for the last and next-to last terms in Eq. (5.3). Finally the  $\tilde{\alpha}$  term corresponds to the leading term obtained by using different values of  $\alpha$  in Eqs (5.4) for P and Q. Note that  $(M-M^*)$ , (d-d'), (c-c') and  $\tilde{\alpha}$  all behave as 1/M.

In addition to the terms in Eq. (5.22), which manifestly break the heavy quark symmetry, there are, in fact, "hidden" violation terms contained in Eq. (5.3). The explicit expression for the hidden terms in the model without light vectors is given in Eq. (5.16) [71]. These were shown to exist (for the model without light vectors) in Ref. [71] and arise from performing a detailed 1/M expansion of the relativistic Lagrangian. In Reference [90] the numerical study has confirmed that this is also true when light vector mesons are included. In the last paragraph we have shown (cf. Fig. 5.2) [71]) that the dependence on d of the hyperfine splitting computed from these hidden terms using the perturbative approach generally matched the exact numerical calculation. Hence we shall not explicitly isolate the extra hidden terms due to the addition of the light vectors but shall content ourselves with the numerical treatment given in Ref. [90].

Here we discuss the computation of  $\chi$  in some detail. We have already noticed that the dynamics of the model dictates that the bound-states occur for k = 0, in which case  $\xi_{dl}(0,0) = \epsilon_{dl}/\sqrt{2}$ . For reader's convenience we display again the relevant wave functions. The bound-state wave–function simply is

$$\psi_{dl,h}(0,0,0,0) = \frac{1}{\sqrt{8\pi}} \epsilon_{dl} \chi_h . \qquad (5.23)$$

The k=1 unbound wave–function with no orbital excitation (r=0) is

$$\psi_{dl,h}(1,g_3,0,1) = \frac{1}{\sqrt{4\pi}} \xi_{dl}(1,g_3) \chi_h . \tag{5.24}$$

When violations of the heavy quark symmetry are included, g is no longer a good

quantum number. The grand spin, is a good quantum number

$$G' = g + S_{\text{heavy}}. \tag{5.25}$$

In the notation of Eqs (5.23) and (5.24) we have the grand spin eigenstates

$$\psi_{dl,h}^{(1)}(G' = G_3' = 1/2) = \frac{1}{\sqrt{8\pi}} \epsilon_{dl} \delta_{2h} ,$$
 (5.26)

$$\psi_{dl,h}^{(2)}(G' = G_3' = 1/2) = \frac{1}{\sqrt{4\pi}} \left[ \sqrt{\frac{2}{3}} \delta_{d1} \delta_{l1} \delta_{h1} + \frac{1}{\sqrt{6}} \left( \delta_{d2} \delta_{l1} + \delta_{d1} \delta_{l2} \right) \delta_{h2} \right] . (5.27)$$

Note that in Eq. (5.26) the  $G'_3 = +1/2$  wave function is  $\delta_{2h}$  since the index 2 corresponds to +1/2 for the anti-quark wave-function. The two states (5.26) and (5.27) differ with respect to their  $\boldsymbol{g}$  and  $\boldsymbol{K}$  labels.

Now let us consider the potential for the bound-state wave–function in the presence of the first heavy quark symmetry violating term in Eq. (5.22). Substituting the G'–eigenstates  $\psi^{(1)}$  and  $\psi^{(2)}$  from Eqs (5.26) and (5.27) into Eq. (4.11) and the first term of Eq. (5.22) yields, after a spatial integration, the potential matrix in the  $\psi^{(1)}$ – $\psi^{(2)}$  space:

$$V = -\frac{dF'(0)}{2} \begin{pmatrix} 3 & 0 \\ 0 & -1 \end{pmatrix} + \frac{M - M^*}{4} \begin{pmatrix} 0 & \sqrt{3} \\ \sqrt{3} & 2 \end{pmatrix} , \qquad (5.28)$$

where F(r) is defined in Eq. (4.12) and F' = dF/dr. The first matrix shows that  $\psi^{(1)}$  is bound while  $\psi^{(2)}$  is unbound in the heavy spin limit. Since the second matrix gives mixing between  $\psi^{(1)}$  and  $\psi^{(2)}$  the latter must be included in the presence of effects which break the heavy quark symmetry. The diagonalized bound wave function is seen to be

$$\psi^{(1)} - \frac{\sqrt{3}}{8} \frac{M - M^*}{dF'(0)} \psi^{(2)} . \tag{5.29}$$

This is the proper wave–function to be "cranked" in order to generate the heavy spin violation. Using it in Eq. (4.24), which is then substituted into the  $\alpha = 0$  limit of the

first term of Eq. (4.11), contributes a term in the collective Lagrangian

$$\frac{\chi}{2}\Omega_3$$
 where  $\chi = \frac{M^* - M}{4d F'(0)}$ . (5.30)

By using the Wigner–Eckart theorem we may express this for states of either  $G_3'$  as the matrix element of the operator  $\chi \Omega \cdot G'$ . For convenience we have chosen to consider our wave–function as representing the conjugate particle in Eq. (4.15). Hence the matrix element of G' in this section differs by a minus sign from that of G defined in  $J = G + J^{\text{sol}}$ , with  $J_i^{\text{sol}} \equiv (\partial L/\partial \Omega_i)$ , which is the appropriate one when we form the total heavy baryon spin. Then the collective Lagrangian,  $L_{\text{coll}}$  may be written (see section 4.4)

$$L_{\text{coll}} = \frac{1}{2}\alpha^2 \mathbf{\Omega}^2 - \chi \mathbf{\Omega} \cdot \mathbf{G}$$
 (5.31)

which again leads to the Hamiltonian (4.31) and hence to the well known formula cf. Eq. (5.1)

$$m(\Sigma_Q^*) - m(\Sigma_Q) = [m(\Delta) - m(N)] \chi . \qquad (5.32)$$

The purpose in deriving this again was to explain the perturbative method and our notation.

Next we shall give some new perturbative "manifest" contributions to  $\chi$  from Eq. (5.22). When all these terms are included the potential V in Eq. (5.28) is modified so that the properly diagonalized wave–function which replaces Eq. (5.29) becomes

$$\psi^{(1)} + \epsilon \psi^{(2)} , \qquad (5.33)$$

with

$$\epsilon = \frac{-\frac{\sqrt{3}}{4}(M - M^*) + \frac{\sqrt{3}}{4}(d - d') F'(0) + \sqrt{3}\tilde{\alpha}\omega(0) + \frac{\sqrt{3}(c - c')}{m_V} \frac{G''(0)}{\tilde{g}}}{2dF'(0) - \frac{2cG''(0)}{\tilde{g}m_V}}.$$
 (5.34)

There are two types of contribution to  $\chi$ . The first type is analogous to Eq. (5.30) and arises when Eq. (5.33) is cranked and substituted into Eq. (4.11). The second type

is obtained by substituting the leading order wave function  $\psi^{(1)}$  into the (c-c') and  $\tilde{\alpha}$  terms in Eq. (5.22). The complete expression for  $\chi$  resulting from the "manifest" heavy spin violation is

$$\chi = \epsilon \left[ \frac{2}{\sqrt{3}} \left( 1 - \frac{4}{3} \alpha \right) + \frac{2\sqrt{2}}{3\sqrt{3}} \alpha \tilde{g} \left( \xi_1(0) - \xi_2(0) \right) - 8\sqrt{\frac{2}{3}} \frac{c}{m_V} \varphi''(0) \right] + \frac{\tilde{\alpha}}{3} \left[ 8 - 2\sqrt{2} \tilde{g} \left( \xi_1(0) - \xi_2(0) \right) \right] - 4\sqrt{2} \frac{c - c'}{m_V} \varphi''(0) . \tag{5.35}$$

The quantities  $\xi_1(0)$ ,  $\xi_2(0)$  and  $\varphi''(0)$  are defined in Eq. (4.26). This formula may be useful for quickly estimating the effects of heavy spin violation in the coupling constants, which were not explicitly given in the previous discussion. Unfortunately there is no determination of the magnitude of these effects from the mesonic sector at present. In the previous paragraphs [71] the discussion of the "hidden" heavy contributions to  $\chi$  was given for the Lagrangian with only light pseudoscalars.

The hyperfine splitting just discussed is for the ground state or P-wave heavy baryons. It is of some interest to briefly consider the negative parity heavy baryons with one unit of orbital excitation (S-wave). In the heavy spin limit these bound states correspond to the r = 1 and k = 0 choice in Eq. (4.15):

$$\psi_{dl,h}(1,g_3,1,0) = \frac{\epsilon_{dl}}{\sqrt{2}} Y_1^{g_3} \chi_h . {(5.36)}$$

The spin,  $J_{\text{light}}$  of the "light cloud" part of the heavy baryon is gotten by adding this g=1 piece to the soliton spin  $J^{\text{sol}}$ . For the I=0 (which implies  $J^{\text{sol}}=0$ ) heavy baryons one finds  $J_{\text{light}}=1$  and the degenerate multiplet

$$\left\{ \Lambda_{Q}'(1/2) \,,\, \Lambda_{Q}'(3/2) \right\} \,.$$
 (5.37)

For the  $I=J^{\rm sol}=1$  heavy baryons,  $J_{\rm light}$  can be either 0, 1 or 2 and we find the degenerate heavy multiplets

$$\Sigma_O'(1/2)$$
,

$$\left\{ \Sigma_{Q}'(1/2), \Sigma_{Q}'(3/2) \right\},$$
  
 $\left\{ \Sigma_{Q}'(3/2), \Sigma_{Q}'(5/2) \right\}.$  (5.38)

In general, the situation is even more complicated and the subject will be fully investigated in the next chapter. At present there are experimental candidates [37] for a negative parity spin 1/2 baryon  $\Lambda'_c$  at 2593.6  $\pm$  1.0 MeV and a negative parity spin 3/2 baryon  $\Lambda'_c$  at 2626.4  $\pm$  0.9 MeV.

Since experimental information is available, it is especially interesting to consider the splitting between the two  $\Lambda'_Q$  states in Eq. (5.37). This splitting stems from the violation of the heavy quark symmetry. For the  $\Lambda_Q$  type states the total spin coincides with the grand spin G so that Eq. (5.37) may be alternatively considered a G = 1/2, G = 3/2 multiplet. Since the good quantum number is G, we may in general expect the hyperfine parameter  $\chi$  to depend on G. The collective Hamiltonian takes the form

$$H_{\text{coll}} = \frac{\left(\boldsymbol{J}^{\text{sol}} + \chi_G \boldsymbol{G}\right)^2}{2\alpha^2} \ . \tag{5.39}$$

On general grounds we see that for the case of the  $\Lambda'_Q$ 's the collective Hamiltonian contribution to the hyperfine splitting will be suppressed. Setting  $J^{\rm sol} = 0$  in Eq. (5.39) shows that the hyperfine splitting is of order  $(\chi^2)$  or equivalently of order  $(1/M^2)$ . Unlike the ground state which involves only the G = 1/2 P—wave channel, there is another possibility for hyperfine splitting here. It is allowed for the G = 1/2 and G = 3/2 bound state energies to differ from each other. In the Lagrangian with only light pseudoscalars this does not happen and the  $\Lambda'_Q(1/2) - \Lambda'_Q(3/2)$  splitting is of order  $1/M^2$ . However when light vectors are added, there are "hidden" 1/M terms, which violate the heavy quark symmetry as e.g.

$$i \operatorname{Tr} \left[ \sigma_{\alpha\mu} H \gamma_{\nu} F^{\mu\nu}(\rho) D^{\alpha} \overline{H} \right] + \text{h.c.}$$
 (5.40)

This term is likely to generate splitting for the multiplet (5.37) to order 1/M by

giving different binding energies to the G = 1/2 and G = 3/2 channels. It would be very interesting to investigate this in more detail.

Finally, we add a remark concerning an amusing conceptual feature in the computation of hyperfine splitting among the five  $\Sigma'_{Q}$ 's in Eq. (5.38). The total angular momentum of each state is given by

$$J = \underbrace{J^{\mathrm{sol}} + \overbrace{g + S_{\mathrm{heavy}}}^{G}}_{\mathrm{light}},$$
 (5.41)

where we are now considering each operator to be acting on the wave–function rather than its complex conjugate. We have illustrated two different intermediate angular momenta which can alternatively be used to label the final state. If  $J_{\text{light}}$  is used, we get the heavy-spin multiplets in Eq. (5.38). On the other hand, when the hyperfine splitting is turned on, the choice G is convenient, because it remains a good quantum number. According to the laws of quantum mechanics, we cannot simultaneously use both to specify the states, since the commutator

$$\left[ \boldsymbol{J}_{\text{light}}^{2} , \boldsymbol{G}^{2} \right] = 4i \boldsymbol{J}_{\text{light}} \cdot (\boldsymbol{S}_{\text{heavy}} \times \boldsymbol{g})$$
 (5.42)

is generally non–vanishing. This means that we cannot uniquely trace the splitting of, say, the  $\left\{\Sigma_Q'(1/2), \Sigma_Q'(3/2)\right\}$  heavy multiplet in Eq (5.38), as hyperfine splitting interactions are turned on. Physically, this causes a mixing between the  $\Sigma_Q'$ 's of the same spin. Rather, we must look at the whole pattern of the five masses. On the other hand, the problem simplifies for the computation of the ground state hyperfine splitting in Eq. (5.32). In that case the bound state wave function is characterized by g=0. Thus the commutator in Eq. (5.42) vanishes, and it is "trivially" possible to track the hyperfine splitting as a mass difference.

#### 5.5 Numerical Results

In this section we will briefly comment on the numerical results obtained in [90] for the masses of the heavy baryons within the relativistic Lagrangian model discussed above. The numerical procedure requires the solution of coupled inhomogeneous differential equations; the details are provied in Ref. [90]. In particular we will concentrate on the spin and isospin splitting in the realistic case of finite heavy meson masses (5.6). It should be noted that sizable quantum corrections occur for the classical soliton mass  $M_{\rm cl}$  [89]. It seems that these corrections are (approximately) equal for all baryons. Hence we will only consider mass differences between various baryons. In that case the absolute value of the classical mass  $M_{\rm cl}$  is redundant. The parameters in the light sector can completely be determined from properties of the corresponding mesons and by the  $\frac{1}{2}^+$  and  $\frac{3}{2}^+$  light baryons [90]. The corresponding moment of inertia is  $\alpha^2 = 5.00 {\rm GeV}^{-1}$ . In the preceding paragraphs Ref. [71] we have shown (in the case without light vectors) that a major fraction of the P-wave hyperfine constant is due to terms in the relativistic Lagrangian (5.3) which do not manifestly break the heavy spin symmetry rather than to terms, which explicitly break this symmetry; as for example  $M \neq M^*$ . The numerical results in Ref. [90] provide a quantitative extimate of the hidden contribution, when the light vectors are also included, by performing the calculation using identical masses from the charm sector i.e.  $M=M^*=1.865 {\rm GeV}$ and furthermore  $\alpha = 0.3$ . All other parameters are as in Eq. (5.6). This results in  $\chi_P=0.080$  ( $\chi$  for the P–wave). From table 5.2 we recognize that this is about 80% of the value obtained using the physical masses M = 1.865 GeV and  $M^* = 2.007 \text{GeV}$ . In the case of the S-wave the hidden piece is even more dominant. For the symmetric choice of the mass parameters one finds  $\chi_S = 0.175$  ( $\chi$  for the S-waves) which is more than 90% of the value displayed in Table 5.2 for  $\alpha = 0.3$ . It is also possible to show [90] that the light vector model predicts a substantially larger  $\chi_P$ .

Since the contribution of the manifest  $(M^* - M)$  breaking term is relatively small it is reasonable to expect that the others will be small too.

Let us next discuss the spectrum of the baryons containing a single heavy quark. For this case we assume the realistic masses as in Eq. (5.6). In Table 5.2 the numerical results for the lowest S– and P–wave bound states in the charm sector are displayed. As already noted in Ref. [65] the binding energy ( $\omega$ ) decreases with growing coupling constant  $\alpha$ . This is the case for both the P– and S–wave channels. For  $M \to \infty$  the heavy limit (see Eq. (4.22))

$$\omega \longrightarrow \frac{3}{2}dF'(0) + \frac{3c}{\tilde{g}m_V}G''(0) + \frac{\alpha\tilde{g}}{\sqrt{2}}\omega(0) = 3\Delta_1 - \Delta_2$$
 (5.43)

will be attained. We note that the hyperfine parameters in these two channels behave oppositely as functions of  $\alpha$ . Here we have chosen to measure the mass differences with respect to the lightest charmed baryon,  $\Lambda_c$ . Hence the mass differences with respect to  $\Sigma_c$  and  $\Sigma_c^*$  directly reflect the  $\alpha$ -dependence of hyperfine parameter  $\chi_P$  while the corresponding dependence of the binding energy  $\omega_P$  can be extracted from the splitting relative to the nucleon. In addition the splitting with respect to the negative parity charmed baryons reflects the  $\alpha$ -dependence of the S-wave channel binding energy  $\omega_S$ . Finally the mass difference to  $\Lambda_b$  contains the energy eigenvalues and hyperfine parameters computed with the B and  $B^*$  meson masses in Eq. (5.6).

While the mass difference to the nucleon is improved with a positive value for  $\alpha$ , the agreement for the mass differences between the heavy baryons slightly deteriorates when increasing this parameter. Nevertheless, fair agreement with the experimental data is achieved for quite a range of  $\alpha$ .

Table 5.2 also contains the model predictions when the background soliton is taken from the basic Skyrme model [77, 80] which does not include the light vector mesons. Here we have adjusted the only free parameter ( $e_{\text{Skyrme}} = 4.25$ ) to reproduce the  $\Delta$ -nucleon mass difference. From the  $\Lambda_c$ -nucleon mass difference we observe

$\alpha$	-0.1	0.0	0.1	0.2	0.3	Expt.	Skyrme
$\omega_P$	564	544	522	500	478		243
$\chi_P$	0.147	0.140	0.131	0.123	0.114		0.053
$\omega_S$	316	298	281	264	247		57
$\chi_S$	0.172	0.181	0.189	0.197	0.205		0.346
$\Sigma_c$	171	172	174	175	177	168	185
$\Sigma_c^*$	215	214	213	212	211	233	201
$\Lambda_c'$	250	249	245	242	238	308	208
$\Sigma_c'$	415	413	408	402	397	?	335
$\Sigma_c^{\prime*}$	468	467	464	461	458	?	437
$\overline{N}$	-1237	-1257	-1278	-1299	-1321	-1345	-1553
$\Lambda_b$	3160	3164	3167	3170	3173	$3356 \pm 50$	3215

Table 5.2: Parameters for heavy baryons and mass differences with respect to  $\Lambda_c$ . Primes indicate negative parity baryons, *i.e.* S—wave bound states. All energies are in MeV.

$\alpha$	-0.1	0.0	0.1	0.2	0.3
$\omega_P$	811	786	762	737	713
$\chi_P$	0.055	0.053	0.050	0.048	0.045
$\omega_S$	639	617	595	573	552
$\chi_S$	0.043	0.046	0.049	0.052	0.055
$\Sigma_b$	189	189	190	190	191
$\Sigma_b^*$	206	205	205	205	205
$\Lambda_b'$	171	168	167	164	161
$\Sigma_b'$	363	359	358	354	351
$\Sigma_b^{\prime*}$	375	373	371	369	367
$\overline{N}$	-4397	-4422	-4446	-4471	-4494

Table 5.3: Parameters for heavy baryons and mass differences with respect to  $\Lambda_b$ . Primes indicate negative parity baryons, *i.e.* S—wave bound states. All energies are in MeV. The empirical value for the relative position of the nucleon is  $4701 \pm 50 \text{MeV}$  [37].

that in comparison with the nucleon the masses of the heavy baryons are predicted about 200 MeV too large. This confirms the above statement that the spectra of both the light and the heavy baryons can only be reasonably reproduced when light vector mesons are included. This conclusion can already be drawn from the too small binding energies [66]. The hyperfine corrections make only minor changes in the  $\Lambda_b$ - $\Lambda_c$  splitting.

In Table 5.3 we display the analogous predictions for the bottom sector. According to the heavy spin symmetry the binding energies of the P– and S–wave channels approach each other. Hence the mass differences between the even and odd parity baryons containing a bottom quark correspondingly decrease. From Table 5.2 we can infer that  $\chi_P$  decreases less quickly with the heavy meson mass than  $\chi_S$ . Except for  $\Lambda_b$ 

no empirical data for the masses of these baryons are known at present. These results for the mass differences among the bottom baryons are predictions of the model which can, in the future, be compared with experiment. As could have been inferred from the next to last row in Table 5.2 the absolute position of the bottom multiplet is about  $200 \pm 50 \text{MeV}$  too low. On the absolute scale this apparently is only a 5% deviation from the data. Certainly a larger value  $\alpha \approx 1$ , which corresponds to a model for light vector resonance dominance of the heavy meson form factor [88], would yield an excellent agreement for the mass difference between  $\Lambda_b$  and the nucleon. On the other hand such a choice would slightly spoil the nice picture for the charm multiplet.

The preceding calculations are based on the  $N_c \to \infty$  limit in which the nucleon is infinitely heavy. From a common sense point of view this is peculiar since the nucleon is actually lighter than the heavy mesons being bound to it in the model. Hence, for comparison with experiment it is desirable to estimate kinematic effects associated with the nucleon's motion. These are expected [65] to lower the binding energy of the heavy baryons which have up to now come out too high (see  $\Lambda_c$ -N mass difference in Table 5.2, for example.). In order to estimate these kinematical effects in the bound state approach we have substituted the reduced masses

$$\frac{1}{M} \longrightarrow \frac{1}{M_{\rm cl}} + \frac{1}{M} \quad \text{and} \quad \frac{1}{M^*} \longrightarrow \frac{1}{M_{\rm cl}} + \frac{1}{M^*}$$
 (5.44)

into the bound state equations. In a non-relativistic treatment this corresponds to the elimination of the center of mass motion [65]. The results for the spectrum of the heavy baryons obtained from the replacement (5.44) are in displayed in Table 5.4. Again we consider  $\alpha$  as a free parameter. We notice that there is a remarkable improvement in the prediction for the  $\Lambda_b$  mass, which was previously the worst one. The changes in some of the mass parameters can approximately be compensated by a suitable re-adjustment of  $\alpha$ . For  $\alpha \approx 0.0$  to -0.4 the agreement with the existing data is quite reasonable. When using the reduced meson masses the  $\Sigma_c$  baryon is

α	0.0	-0.1	-0.2	-0.3	-0.4	-0.5	-0.6	-0.7	Expt.
$\omega_P$	450	469	488	508	527	546	566	585	
$\chi_P$	0.212	0.232	0.246	0.260	0.273	0.286	0.299	0.312	
$\omega_S$	123	134	146	158	171	184	197	210	
$\chi_S$	0.410	0.399	0.387	0.374	0.361	0.346	0.331	0.315	
$\Sigma_c$	158	154	151	148	145	143	140	138	168
$\Sigma_c^*$	221	223	225	226	227	229	230	231	233
$\Lambda_c'$	342	346	353	359	363	367	371	375	308
$\Sigma_c'$	460	468	475	484	490	497	505	512	?
$\Sigma_c^{\prime*}$	583	587	591	596	599	601	605	607	?
N	-1356	-1338	-1320	-1302	-1283	-1265	-1246	-1228	-1345
$\Lambda_b$	3285	3282	3280	3278	3275	3272	3271	3269	$3356 \pm 50$

Table 5.4: Parameters for heavy baryons and mass differences with respect to  $\Lambda_c$ . Primes indicate negative parity states, *i.e.* S—wave bound states. All energies are in MeV. In this calculation the reduced masses (5.44) enter the bound state equations from which the binding energies are extracted. The physical meson masses 1865MeV and 5279MeV are used when computing the mass differences to the nucleon and the  $\Lambda_b$  from these binding energies. Radially excited states are omitted because they are only very loosely bound, if at all. The empirical data are taken from the PDG [37], see also [92].

$\alpha$	0.0	-0.1	-0.2	-0.3	-0.4	-0.5	-0.6	-0.7	Expt.
			109						
$\chi_P$	0.346	0.371	0.394	0.417	0.439	0.460	0.479	0.498	
$\sum$	131	126	121	117	112	108	104	100	77
$\Sigma^*$	235	237	239	242	244	246	248	250	269
$\overline{N}$	-366	-354	-341	-327	-313	-300	-285	-269	-177

Table 5.5: Same as Table 5.4 for even parity baryons in the kaon sector.

always predicted a bit too light while it is too heavy when the physical masses are substituted in the bound state equation. For  $\Lambda'_c$  the situation is opposite. While the use of the physical meson masses gives too small a mass, the substitution of the reduced masses gives too large a prediction for the mass of this baryon. These results indicate that kinematical corrections are indeed important.

It is interesting to see how far the heavy quark approach can be pushed to lighter quarks. To answer this question we have considered the strange quark. In the corresponding kaon sector the P-wave is only very loosely bound when the physical masses are substituted. On the other hand sizable binding energies are obtained when the reduced masses are used [66]. This behavior is somewhat different from the charm and bottom sector and can be understood by noting that the difference  $M^* - M$  is considerably reduced when using (5.44). In the heavy sectors (charm and bottom) this difference is small in any event. The resulting spectrum for the strange baryons is shown in Table 5.5. The comparison with the experimental data shows that even the use of the reduced masses does not provide sufficient binding. In the S-wave channel the situation is worse, even when the reduced masses are substituted bound states are not detected unless  $\alpha \leq -1.0$ . The failure of the present approach in the strange sector strongly suggests that for these baryons a chirally invariant set-up [81] is more appropriate.

# Chapter 6

# Generalization of the Bound State Model

#### 6.1 Introduction

Here we shall investigate the spectrum of excited states in the bound state–soliton framework. Some aspects of this problem have already been treated [65,67,71,72,90]. We will deal with an aspect which does not seem to have been previously discussed in the literature. This emerges when one compares the excited heavy baryon spectrum with that expected in the constituent quark model (CQM) [73]. We do not have in mind specific dynamical treatments of the CQM but rather just its general geometric structure. Namely we shall just refer to the counting of states which follows from considering the baryon as a three body system obeying Fermi–Dirac statistics. We shall restrict our attention to the physical states for  $N_c = 3$ . In this framework the CQM counting of the heavy excited baryon multiplets has been recently discussed [74]. At the level of two light flavors there are expected to be seven negative parity first excited  $\Delta$ -type heavy baryons and seven negative parity first excited  $\Sigma$ -type heavy

baryons. On the other hand a similar counting [65,90] in the bound state treatments mentioned above yields only two of the  $\Lambda$ -type and five of the  $\Sigma$ -type. Thus there are seven missing first excited states. One thought is that these missing states should be unbound and thus represent new dynamical information with respect to the simple geometrical picture. There is certainly not enough data for the charmed baryons to decide this issue. However for the strange baryons there are ten established particles for these fourteen states. Hence it is reasonable to believe that these states exist for the heavy baryons too. In the CQM one may have two different sources of orbital angular momentum excitation; for example the relative angular momentum of the two light quarks,  $L_I$  and the angular momentum,  $L_E$  of the diquark system with respect to the heavy quark. The parity of the heavy baryon is given by  $P = (-1)^{L_I + L_E}$ . However, in the bound state models considered up to now there is only room for one relative angular momentum, r associated with the wave function of the heavy meson with respect to the soliton. The parity is given by  $P = (-1)^r$ . Both models agree on the counting of the "ground" states  $(L_I = L_E = r = 0)$ . Also the counting of the states with  $(L_I = 0, L_E = 1)$  agrees with those of r = 1 in the bound state model. However, the bound state model has no analog of the  $(L_I = 1, L_E = 0)$  states and, in general, no analog of the higher  $L_I \neq 0$  states either.

It is clear that we must find a way of incorporating a new angular momentum quantum number in the bound state picture. One might imagine a number of different ways to accomplish this goal. Here we will investigate a method which approximates a three body problem by an effective two body problem. Specifically we will consider binding excited heavy mesons with orbital angular momentum  $\ell$  to the soliton. The excited heavy mesons may be interpreted as bound states of the original heavy meson and a surrounding light meson cloud. Then the baryon parity comes out to be  $(-1)^{r+\ell}$ . This suggests a correspondence (but not an identity)  $r \leftrightarrow L_E$ ,  $\ell \leftrightarrow L_I$  and

additional new states. An interesting conceptual point of the model is that it displays a correspondence between the excited heavy mesons and the excited heavy baryons.

Almost immediately one sees that the model is considerably more complicated than the previous one in which the single heavy field multiplet H is bound to the soliton. Now, for each value of  $\ell \neq 0$ , there will be two different higher spin heavy multiplets which can contribute. In fact there is also a mixing between multiplets with different  $\ell$ , which is therefore not actually a good quantum number for the model (unless the mixing is neglected).

Thus we will make a number of approximations which seem reasonable for an initial analysis. For one thing we shall neglect the light vector mesons even though we know they may be important. We shall also neglect the possible effects of higher spin light mesons, which one might otherwise consider natural when higher spin heavy mesons are being included. Since there is a proliferation of interaction terms among the light and heavy mesons we shall limit ourselves to those with the minimum number of derivatives. Finally, 1/M and nucleon recoil corrections will be neglected. The resulting model is the analog of the initial one used previously. Even though the true picture is likely to be more involved than our simplified model, we feel that the general scheme presented here will provide a useful guide for further work.

We would like to stress that this bound state model goes beyond the kinematical enumeration of states and contains dynamical information. Specifically, the question of which states are bound depends on the magnitudes and signs of the coupling constants. There is a choice of coupling constants yielding a natural pattern of bound states which includes the missing ones. It turns out that it is easier to obtain the precise missing state pattern for the  $\Lambda$ -type heavy particles. Generally, there seem to be more than just the missing  $\Sigma$ -type heavy baryons present. However we show that the collective quantization, which is anyway required in the bound state approach,

leads to a splitting which may favor the missing heavy spin multiplets.

This chapter is organized in the following way. Section 6.2 starts with a review of the CQM geometrical counting of excited heavy baryon multiplets. It continues with a quick summary of the treatment of heavy baryons in the existing bound state models. The comparison of the mass spectrum in the two different approaches reveals that there is a large family of "missing" excited states. This is discussed in general terms in section 6.3 where a proposal for solving the problem by considering the binding of heavy excited mesons to the Skyrmion is made. A correspondence between the angular momentum variables of the CQM and of the new model is set up. A detailed treatment of the proposed model for the case of the first excited heavy baryons is given in section 6.4. This includes discussion of the heavy meson bound state wave function, the classical potential energy as well as the energy corrections due to quantization of the collective variables of the model. It is pointed out that there is a possible way of choosing the coupling constants so as to bind all the missing states. The generalization to the excited heavy baryon states of arbitrary spin is given in section 6.5. This section also contains some new material on the interactions of the heavy meson multiplets with light chiral fields. Section 6.6 contains a discussion of the present status of the model introduced here. Finally, some details of the calculations are given in Appendices B.1 and B.2.

## 6.2 The Enigma of the Excited Missing States

In this section, for the reader's convenience, we will briefly discuss which heavy baryon states are predicted by the CQM as well as some relevant material needed for the bound state approach to the heavy baryon states.

It is generally agreed that the geometrical structure of the CQM provides a reason-

able guide for, at least, counting and labeling the physical strong interaction ground states. When radial excitations or dynamical aspects are considered the model predictions are presumably less reliable. In the CQM the heavy baryons consist of two light quarks (q) and a heavy quark (Q) in a color singlet state. Since the color singlet states are antisymmetric on interchange of the color labels of any two quarks, the overall wave function must, according to Fermi-Dirac statistics, be fully symmetric on interchange of flavor, spin and spatial indices. Here we will consider the case of two light flavors. For counting the states we may choose coordinates [74] so that the total angular momentum of the heavy baryon, J is decomposed as

$$\boldsymbol{J} = \boldsymbol{L}_I + \boldsymbol{L}_E + \boldsymbol{S} + \boldsymbol{S}_H , \qquad (6.1)$$

where  $L_I$  represents the relative orbital angular momentum of the two light quarks,  $L_E$  the orbital angular momentum of the light diquark center of mass with respect to the heavy quark, S the total spin of the diquarks and  $S_H$  the spin of the heavy quark. In the "heavy" limit where the heavy quark becomes infinitely massive  $S_H$  completely decouples. The parity of the heavy baryon is given by

$$P_B = (-1)^{L_I + L_E} (6.2)$$

Since we are treating only the light degrees of freedom as identical particles it is only necessary to symmetrize the diquark product wave function with respect to the  $L_I$ , S and isospin I labels. Note that the diquark isospin I equals the baryon isospin. There are four possible ways to build an overall wave function symmetric with respect to these three labels:

a) 
$$I = 0$$
,  $S = 0$ ,  $L_I = \text{even}$ ,

b) 
$$I=1$$
,  $S=1$ ,  $L_I=\text{even}$ ,

c) 
$$I = 0$$
,  $S = 1$ ,  $L_I = \text{odd}$ ,

d) 
$$I = 1$$
,  $S = 0$ ,  $L_I = \text{odd}$ . (6.3)

There is no kinematic restriction on  $L_E$ .<sup>1</sup>

Let us count the possible baryon states. The  $L_I = L_E = 0$  heavy baryon ground state consists of  $\Lambda_Q$  ( $J^P = \frac{1}{2}^+$ ) from a) and the heavy spin multiplet  $\left\{\Sigma_Q\left(\frac{1}{2}^+\right), \ \Sigma_Q\left(\frac{3}{2}^+\right)\right\}$  from b). It is especially interesting to consider the first orbitally excited states. These all have negative parity with either ( $L_E = 1, \ L_I = 0$ ) or ( $L_E = 0, \ L_I = 1$ ). For  $L_E = 1$ , a) provides the heavy spin multiplet  $\left\{\Lambda_Q\left(\frac{1}{2}^-\right), \ \Lambda_Q\left(\frac{3}{2}^-\right)\right\}$  and b) provides  $\Sigma_Q\left(\frac{1}{2}^-\right), \ \left\{\Sigma_Q\left(\frac{1}{2}^-\right), \ \Sigma_Q\left(\frac{3}{2}^-\right)\right\}, \ \left\{\Sigma_Q\left(\frac{3}{2}^-\right), \ \Sigma_Q\left(\frac{5}{2}^-\right)\right\}$ . For  $L_I = 1$  c) provides  $\Lambda_Q\left(\frac{1}{2}^-\right), \ \left\{\Lambda_Q\left(\frac{1}{2}^-\right), \ \Lambda_Q\left(\frac{3}{2}^-\right)\right\}, \ \left\{\Lambda_Q\left(\frac{3}{2}^-\right), \ \Lambda_Q\left(\frac{5}{2}^-\right)\right\}$ , while d) provides  $\left\{\Sigma_Q\left(\frac{1}{2}^-\right), \ \Sigma_Q\left(\frac{3}{2}^-\right)\right\}$ . Altogether there are fourteen different isotopic spin multiplets at the first excited level. The higher excited levels can be easily enumerated in the same way. For convenient reference these are listed in Table 6.1.

It is natural to wonder whether all of these states should actually exist experimentally. This is clearly a premature question for the c and b baryons. However an indication for the first excited states can be gotten from the ordinary hyperons (or s baryons). In this case there are six well established candidates [75] for the  $\Lambda$ 's [ $\Lambda$ (1405),  $\Lambda$ (1520),  $\Lambda$ (1670),  $\Lambda$ (1690),  $\Lambda$ (1800) and  $\Lambda$ (1830)]; only one  $\frac{3}{2}^-$  state has not yet been observed. For the  $\Sigma$ 's there are four well established candidates [ $\Sigma$ (1670),  $\Sigma$ (1750),  $\Sigma$ (1775) and  $\Sigma$ (1940)]; two  $\frac{1}{2}^-$  states and one  $\frac{3}{2}^-$  state have not yet been observed. Thus it seems plausible to expect that all fourteen of the first excited negative parity heavy baryons do indeed exist. We might also expect higher excited states to exist.

What is the situation in the bound state approach? To study this we shall briefly summarize the usual approach [65,67,90] to the excited heavy baryons in the bound state picture. In this model the heavy baryon is considered to be a heavy meson

<sup>&</sup>lt;sup>1</sup>We are adopting a convention where bold–faced angular momentum quantities are vectors and the regular quantities stand for their eigenvalues.

	$L_E = 0$	$L_E = 1$
$L_I = 0$	$\Lambda_{Q}\left(\frac{1}{2}^{+}\right) \left\{ \Sigma_{Q}\left(\frac{1}{2}^{+}\right),  \Sigma_{Q}\left(\frac{3}{2}^{+}\right) \right\}$	$ \left\{ \Lambda_{Q} \left( \frac{1}{2}^{-} \right), \Lambda_{Q} \left( \frac{3}{2}^{-} \right) \right\}  \Sigma_{Q} \left( \frac{1}{2}^{-} \right)  \left\{ \Sigma_{Q} \left( \frac{1}{2}^{-} \right), \Sigma_{Q} \left( \frac{3}{2}^{-} \right) \right\}  \left\{ \Sigma_{Q} \left( \frac{3}{2}^{-} \right), \Sigma_{Q} \left( \frac{5}{2}^{-} \right) \right\} $
$L_I = 1$	$\begin{split} & \Lambda_Q\left(\frac{1}{2}^-\right) \\ & \left\{\Lambda_Q\left(\frac{1}{2}^-\right) \;,\; \Lambda_Q\left(\frac{3}{2}^-\right)\right\} \\ & \left\{\Lambda_Q\left(\frac{3}{2}^-\right) \;,\; \Lambda_Q\left(\frac{5}{2}^-\right)\right\} \\ & \left\{\Sigma_Q\left(\frac{1}{2}^-\right) \;,\; \Sigma_Q\left(\frac{3}{2}^-\right)\right\} \end{split}$	
:		
$L_I = 2n - 1$	$ \left\{ \Lambda_Q \left( \left( 2n - \frac{5}{2} \right)^- \right), \Lambda_Q \left( \left( 2n - \frac{3}{2} \right)^- \right) \right\}  \left\{ \Lambda_Q \left( \left( 2n - \frac{3}{2} \right)^- \right), \Lambda_Q \left( \left( 2n - \frac{1}{2} \right)^- \right) \right\}  \left\{ \Lambda_Q \left( \left( 2n - \frac{1}{2} \right)^- \right), \Lambda_Q \left( \left( 2n + \frac{1}{2} \right)^- \right) \right\}  \left\{ \Sigma_Q \left( \left( 2n - \frac{3}{2} \right)^- \right), \Sigma_Q \left( \left( 2n - \frac{1}{2} \right)^- \right) \right\} $	•••
$L_I = 2n$	$ \left\{ \Lambda_Q \left( \left( 2n - \frac{1}{2} \right)^+ \right), \Lambda_Q \left( \left( 2n + \frac{1}{2} \right)^+ \right) \right\}  \left\{ \Sigma_Q \left( \left( 2n - \frac{3}{2} \right)^+ \right), \Sigma_Q \left( \left( 2n - \frac{1}{2} \right)^+ \right) \right\}  \left\{ \Sigma_Q \left( \left( 2n - \frac{1}{2} \right)^+ \right), \Sigma_Q \left( \left( 2n + \frac{1}{2} \right)^+ \right) \right\}  \left\{ \Sigma_Q \left( \left( 2n + \frac{1}{2} \right)^+ \right), \Sigma_Q \left( \left( 2n + \frac{3}{2} \right)^+ \right) \right\} $	
:		

Table 6.1: Examples of the heavy baryon multiplets predicted by the  $\mathbf{CQM}$ .

bound, via its interactions with the light mesons, to a nucleon treated as a Skyrme soliton. The total baryon angular momentum is the sum (see Eq. (4.29))

$$\boldsymbol{J} = \boldsymbol{g} + \boldsymbol{J}^{\text{sol}} + \boldsymbol{S}_{\text{heavy}} , \qquad (6.4)$$

where  $S_{\text{heavy}}$  is the spin of the heavy quark within the heavy meson.

Now we can list the bound states of this model. First consider the r=0 states. According to Eq. (4.23), they have positive parity. Since Eq. (4.21) shows that k=0 for binding, Eq. (4.19) tells us that the light "grand spin" g=0. Equation (4.29) indicates (noting  $I=J^{\rm sol}$ ) that there will be a  $\Lambda_Q\left(\frac{1}{2}^+\right)$  state as well as a  $\left\{\Sigma_Q\left(\frac{1}{2}^+\right),\ \Sigma_Q\left(\frac{3}{2}^+\right)\right\}$  heavy spin multiplet. Actually the model also predicts a whole tower of states with increasing isospin. Next there will be an I=2 heavy spin multiplet with spins and parity  $\frac{3}{2}^+$  and  $\frac{5}{2}^+$ , and so forth. Clearly the isospin zero and one states correspond exactly to the  $L_I=L_E=0$  ground states of the constituent quark model. The isotopic spin two states would also be present if we were to consider the ground state heavy baryons in a constituent quark model with number of colors,  $N_c=5$ . This is consistent with the picture [77] of the Skyrme model as a description of the large  $N_c$  limit.

Next, consider the r=1 states. These all have negative parity and (since the bound states have k=0) light grand spin, g=1. The  $J^{\rm sol}=I=0$  choice yields a heavy multiplet  $\left\{\Lambda_Q\left(\frac{1}{2}^-\right), \Lambda_Q\left(\frac{3}{2}^-\right)\right\}$  while the  $J^{\rm sol}=I=1$  choice yields the three heavy multiplets  $\left\{\Sigma_Q\left(\frac{1}{2}^-\right)\right\}$ ,  $\left\{\Sigma_Q\left(\frac{1}{2}^-\right), \Sigma_Q\left(\frac{3}{2}^-\right)\right\}$  and  $\left\{\Sigma_Q\left(\frac{3}{2}^-\right), \Sigma_Q\left(\frac{5}{2}^-\right)\right\}$ . These three multiplets are associated with the intermediate sums  $|\boldsymbol{g}+\boldsymbol{J}^{\rm sol}|=0,1,2,1$  respectively. It is evident that the seven states obtained have the same quantum numbers as the seven constituent quark states with  $L_I=0$  and  $L_E=1$ . Proceeding in the same way, it is easy to see that the bound states with general r agree with those states in the constituent quark model which have  $L_I=0$  and  $L_E=r$ . This

may be understood by rewriting Eqs. (4.29) and (4.19) as

$$J = r + J^{\text{sol}} + S_{\text{heavy}}$$
, (6.5)

where k = 0 for the bound states was used. Comparing this with the  $L_I = 0$  limit of the constituent quark model relation (6.1) shows that there seems to be a correspondence

$$egin{array}{lcl} m{S}_{
m heavy} & \leftrightarrow & m{S}_H \; , \\ & m{r} & \leftrightarrow & m{L}_E \; , \\ & m{J}^{
m sol} & \leftrightarrow & m{S} \; . \end{array} \eqno(6.6)$$

This correspondence is reinforced when we notice that  $I = J^{\text{sol}}$  in the bound state model and, for the relevant cases a) and b) in Eq. (6.3) of the constituent quark model, I = S also. We stress that Eq. (6.6) is a correspondence rather than an exact identification of the same dynamical variables in different models. It should be remarked that in the exact heavy and large  $N_c$  limits the heavy baryons for all values of r = g will have the same mass. When finite 1/M corrections are taken into account, there will always be, in addition to other things, a "centrifugal term" in the effective potential of the form  $g(g+1)/(2M|\mathbf{x}|^2)$ , which makes the states with larger values of g, heavier. It should also be remarked that the above described ordering of heavy baryon states in the bound state approach applies only to the heavy limit, where  $\mathbf{S}_{\text{heavy}}$  decouples. For finite heavy quark masses, multiplets are characterized by the total grand spin  $\mathbf{g} + \mathbf{S}_{\text{heavy}}$ . Then states like  $\Lambda_Q\left(\frac{1}{2}^-\right)$  and  $\Lambda_Q\left(\frac{3}{2}^-\right)$  no longer constitute a degenerate multiplet.

### 6.3 The Planetary Conjecture

It is clear that the bound state model discussed above contains only half of the fourteen negative parity, first excited states predicted by the CQM. The states with  $L_I \neq 0$  are all missing. Since the enumeration of states in the CQM was purely kinematical one might at first think that the bound state model (noting that the dynamical condition k = 0 was used) is providing a welcome constraint on the large number of expected states. However, experiment indicates that this is not likely to be the case. As pointed out in the last section, there are at present good experimental candidates for ten out of the fourteen negative parity, first excited ordinary hyperons. Thus the missing excited states appear to be a serious problem for the bound state model.

The goal of the present work is to find a suitable extension of the bound state model which gives the same spectrum as the CQM. Reference to Eq. (6.1) suggests that we introduce a new degree of freedom which is related in some way to the light diquark relative angular momentum  $L_I$ . To gain some perspective, and because we are working in a Skyrme model overall framework, it is worthwhile to consider the heavy baryons in a hypothetical world with  $N_c$  quark colors. In such a case there would be  $N_c - 1$  relative angular momentum variables and we would require  $N_c - 2$  additional degrees of freedom. Very schematically we might imagine, as in Fig. 6.1, one heavy meson H and  $N_c - 2$  light mesons  $\mathcal{M}_i$  orbiting around the nucleon. One might imagine a number of different schemes for treating the inevitably complicated bound state dynamics of such a system. Even in the  $N_c = 3$  case it is much simpler if we can manage to reduce the three body problem to an effective two body problem. This can be achieved, as schematically indicated in Fig. 6.2, if we link the two "orbiting" mesons together in a state which carries internal angular momentum. The "linked mesons" will be described mathematically by a single excited heavy meson multiplet

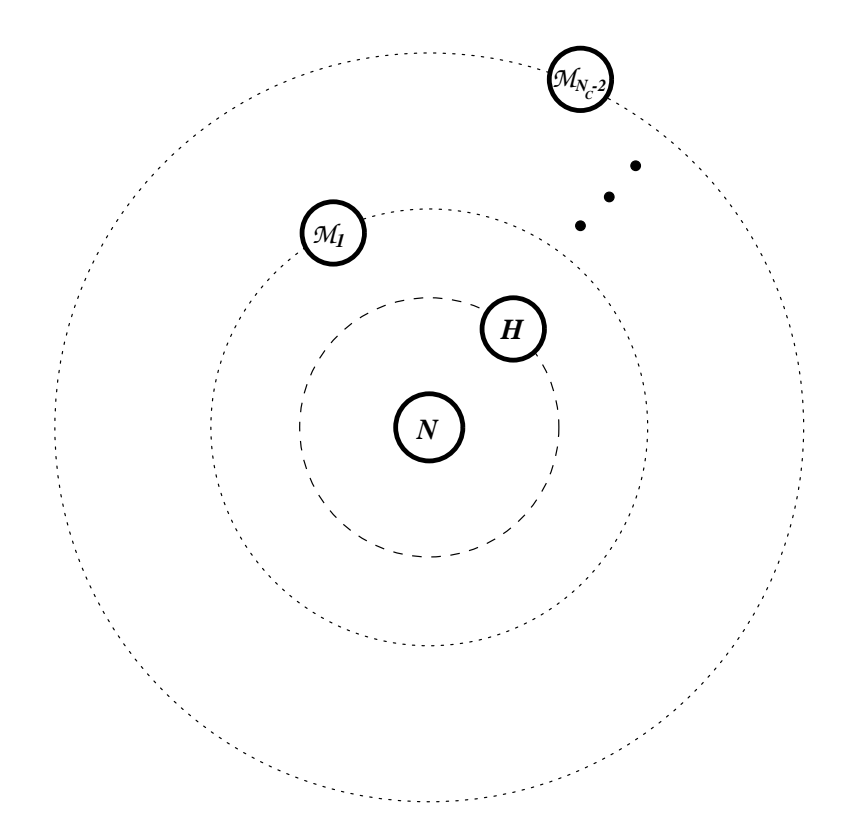


Figure 6.1: Schematic planetary picture for large  $N_c$  excited heavy baryons in the bound state approach.

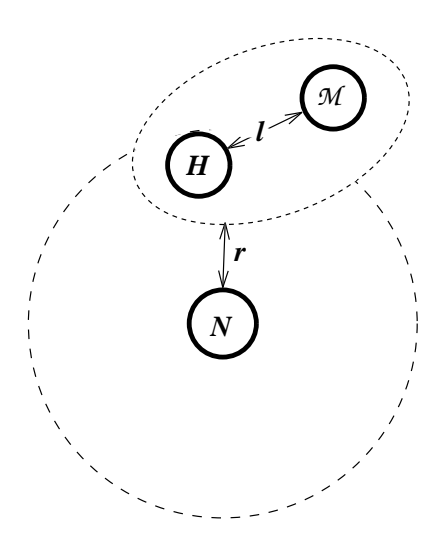


Figure 6.2: Schematic picture of the "two body" approximation for the  $N_c=3$  excited heavy baryons.

field. One may alternatively consider these "linked mesons" as bare heavy mesons surrounded by a light meson cloud. Such fields are usually classified by the value<sup>2</sup>,  $\ell$  of the relative orbital angular momentum of a  $\bar{q}Q$  pair which describes it in the CQM. We will not attempt to explain the binding of these two mesons but shall simply incorporate the "experimental" higher spin meson fields into our chiral Lagrangian. Different  $\ell$  excitations will correspond to the use of different meson field multiplets. From now on we will restrict our attention to  $N_c = 3$ .

Taking the new degree of freedom  $\ell$  into account requires us to modify the previous formulas describing the heavy baryon. Now the parity formula (4.23) is modified to

$$P_B = (-1)^{\ell+r} \ , \tag{6.7}$$

which is seen to be compatible with the CQM relation (6.2). Now Eq. (4.29) holds

<sup>&</sup>lt;sup>2</sup>Actually if we want to picture the linked mesons as literally composed of a meson–meson pair, we should assign relative orbital angular momentum  $\ell-1$  to these bosonic constituents and allow for both light pseudoscalars and vectors.

but with the light grand spin g modified to,

$$g = r + K'. (6.8)$$

Note that K in Eq. (4.18) has been incorporated in

$$K' = I_{\text{light}} + S_{\text{light}} + \ell$$
 (6.9)

The new correspondence between the bound–state picture variables and those of the CQM is:

Previously  $I_{\text{light}} + S_{\text{light}} = K$  had zero quantum numbers on the bound states; now the picture is a little more complicated. We will see that the dynamics may lead to new bound states which are in correspondence with the CQM. Equation (6.10) should be interpreted in the sense of this correspondence.

It is easiest to see that the lowest new states generated agree with the CQM for  $\ell = \text{even}$ , which corresponds to negative parity heavy mesons. In this case k = 0 or equivalently  $k' = \ell$  may be favored dynamically. Then the last line in Eq. (6.10) indicates that  $J^{\text{sol}}$ , which can take on the values 0 and 1, corresponds to the light diquark spin S in the CQM. This leads to the CQM states of type a) and b) in Eq. (6.3). This is just a generalization of the discussion for the ground state given in section 6.2. Now let us discuss how the states corresponding to c) and d) can be constructed in the bound state scenario. Apparently we require  $\ell = \text{odd}$ , i.e. positive parity heavy mesons. For I = 0 we also have  $J^{\text{sol}} = 0$ . Hence the last line in Eq. (6.10)

requires k = 1 for S = 1. To generate states of type d) also k = 1 would be needed in order to accommodate  $I = J^{\text{sol}} = 1$  and S = 0. Actually for the case k = 1 and  $J^{\text{sol}} = 1$  states with S = 0, 1, 2 would be possible. The states with S = 1, 2 should be ruled out by the dynamics of the model.

One may perhaps wonder whether we are pushing the bound state picture too far; since things seem to be getting more complicated why not just use the constituent quark model? Apart from the intrinsic interest of the soliton approach there are two more or less practical reasons for pursuing the approach. The first is that the parameters of the underlying chiral Lagrangian are, unlike parameters such as the constituent quark masses and inter–quark potentials of the CQM, physical ones and in principle subject to direct experimental test. The second reason is that the bound state approach actually models the expected behavior of a confining theory; namely, when sufficient energy is applied to "stretch" the heavy baryon it does not come apart into a heavy quark and two light quarks but rather into a nucleon and a heavy meson. The light quark–antiquark pair which one usually imagines popping out of the vacuum when the color singlet state has been suitably stretched, was there all the time, waiting to play a role, in the bound state picture. The model may therefore be useful in treating reactions of this sort.

#### 6.4 Model for the Missing First Excited States

Before going on to the general orbital excited states it may be helpful to see how the dynamics could work out for explaining the missing seven  $\Lambda_Q$  and  $\Sigma_Q$  type, negative parity, excited states. In the *new* bound state picture these correspond to the choices<sup>3</sup>

<sup>&</sup>lt;sup>3</sup>Actually,  $\ell$  was introduced for convenience in making a comparison with the constituent quark model. It is really hidden in the heavy mesons which, strictly speaking, are specified by the light cloud angular momentum  $J_{\text{light}}$  and parity. We can perform the calculation without mentioning  $\ell$ .

 $\ell=1,\ r=0$ . As discussed, we are considering that the orbital angular momentum  $\ell$  is "locked-up" in suitable excited heavy mesons. As in Eq. (4.17), r appears as a parameter in the new heavy meson wave–function. The treatment of the excited heavy mesons in the effective theory context, has been given already by Falk and Luke [78]. For a review see [79]. The case (for orbital angular momentum=1) where the light cloud spin of the heavy meson is 1/2 is described by the heavy multiplet

$$\mathcal{H} = \frac{1 + \gamma_{\mu} V^{\mu}}{2} \left( S + \gamma_5 \gamma_{\nu} A^{\nu} \right) , \qquad (6.11)$$

where S is the fluctuation field for a scalar  $(J^P = 0^+)$  particle and  $A_{\mu}$ , satisfying  $V_{\mu}A^{\mu} = 0$ , similarly corresponds to an axial  $(J^P = 1^+)$  particle. The case where the light cloud spin is 3/2 is described by

$$\mathcal{H}_{\mu} = \frac{1 + \gamma_{\alpha} V^{\alpha}}{2} \left( T_{\mu\nu} \gamma^{\nu} - i \sqrt{\frac{3}{2}} B^{\nu} \gamma_{5} \left[ g_{\mu\nu} - \frac{1}{3} \gamma_{\nu} \left( \gamma_{\mu} - V_{\mu} \right) \right] \right) \tag{6.12}$$

satisfying the Rarita-Schwinger constraints  $\mathcal{H}_{\mu}\gamma^{\mu} = \mathcal{H}_{\mu}V^{\mu} = 0$ . The field  $T_{\mu\nu} = T_{\nu\mu}$  (with  $V^{\mu}T_{\mu\nu} = T^{\mu}_{\mu} = 0$ ) is a spin 2 tensor  $(J^P = 2^+)$  and  $B_{\mu}$  (with  $V_{\mu}B^{\mu} = 0$ ) is another axial  $(J^P = 1^+)$ . Currently, experimental candidates exist for the tensor and an axial.

In order to prevent the calculation from becoming too complicated we will adopt the approximation of leaving out the light vector mesons. This is a common approximation used by workers in the field but it should be kept in mind that the effect of the light vectors is expected to be substantial.

The kinetic terms of the effective chiral Lagrangian (analogous to the first term of Eq. (4.11)) are:

$$\mathcal{L}_{kin} = -i\mathcal{M}V^{\mu} \text{Tr} \left[ \mathcal{H} D_{\mu} \bar{\mathcal{H}} \right] - i\mathcal{M} V^{\mu} \text{Tr} \left[ \mathcal{H}^{\alpha} D_{\mu} \bar{\mathcal{H}}_{\alpha} \right] , \qquad (6.13)$$

where  $\mathcal{M}$  is a characteristic heavy mass scale for the excited mesons. For simplicity<sup>4</sup>

<sup>4</sup>A more general approach is to replace  $\mathcal{M}$  on the right hand side of Eq. (6.13) by the same M used in Eq. (4.11) and to add the splitting terms  $-2M(M_S-M)\mathrm{Tr}\left[\mathcal{H}\bar{\mathcal{H}}\right]-2M(M_T-M)\mathrm{Tr}\left[\mathcal{H}_{\mu}\bar{\mathcal{H}}^{\mu}\right]$ .

we are neglecting mass differences between the  $\ell = 1$  heavy mesons. The interaction terms involving only the  $\mathcal{H}$  and  $\mathcal{H}_{\mu}$  fields, to lowest order in derivatives, are

$$\mathcal{L}_{\text{int}}/\mathcal{M} = -d_{S} \text{Tr} \left[ \mathcal{H} \gamma^{\mu} \gamma_{5} p_{\mu} \bar{\mathcal{H}} \right] - d_{T} \text{Tr} \left[ \mathcal{H}^{\mu} \gamma^{\alpha} \gamma_{5} p_{\alpha} \bar{\mathcal{H}}_{\mu} \right]$$

$$+ \left[ f_{ST} \text{Tr} \left[ \mathcal{H} \gamma_{5} p^{\mu} \bar{\mathcal{H}}_{\mu} \right] + \text{h.c.} \right] .$$

$$(6.14)$$

These generalize the second term in Eq. (4.11) and  $d_{\rm S}$ ,  $d_{\rm T}$  and  $f_{\rm ST}$  (which may be complex) are the heavy meson–pion coupling constants. Similar terms which involve  $\ell \neq 1$  multiplets are not needed for our present purpose but will be discussed in the next section.

As in section 6.2, the wave–functions for the excited heavy mesons bound to the background Skyrmion are conveniently presented in the rest frame  $\mathbf{V} = 0$ . The analogs of Eq. (4.14) become

$$\bar{\mathcal{H}}_{c} \rightarrow \begin{pmatrix} \bar{f}_{lh}^{a} & 0 \\ 0 & 0 \end{pmatrix} , \quad (\bar{\mathcal{H}}_{i})_{c} \rightarrow \begin{pmatrix} 0 & 0 \\ \bar{f}_{i,lh}^{a} & 0 \end{pmatrix} ,$$
 (6.15)

and  $(\bar{\mathcal{H}}_0)_c \to 0$ . Now the wave–functions in Eq. (6.15) are expanded as:

$$\bar{f}_{lh}^{a} = \frac{u(|\boldsymbol{x}|)}{\sqrt{\mathcal{M}}} (\hat{\boldsymbol{x}} \cdot \boldsymbol{\tau}_{ad}) \Phi_{ld} (k', k'_{3}; r) \chi_{h} ,$$

$$\bar{f}_{i,lh}^{a} = \frac{u(|\boldsymbol{x}|)}{\sqrt{\mathcal{M}}} (\hat{\boldsymbol{x}} \cdot \boldsymbol{\tau}_{ad}) \Phi_{i,ld} (k', k'_{3}; r) \chi_{h} , \qquad (6.16)$$

where u stands for a sharply peaked radial wave–function which may differ for the two cases. Other notations are as in Eq. (4.15). Note that the constraint  $\gamma^{\mu}\bar{\mathcal{H}}_{\mu}=0$  implies that

$$(\sigma_i)_{ll'} \Phi_{i,l'd} = 0 . (6.17)$$

It is interesting to see explicitly how the extra angular momentum  $\ell=1$  is "locked—up" in the heavy meson wave–functions. For the  $\mathcal{H}$  wave–function, the fact that

 $J_{\text{light}} = \ell + S_{\text{light}}$  takes the value 1/2 leads, using Eq. (6.9), to the possible values k' = 0 or 1. The corresponding wave–functions are

$$\Phi_{ld}(k' = k_3' = 0) = \frac{\epsilon_{ld}}{\sqrt{8\pi}}, \quad \Phi_{ld}(k' = k_3 = 1) = \frac{\delta_{l1}\delta_{d1}}{\sqrt{4\pi}},$$
(6.18)

where, for the present case, we are taking r=0. For the  $\bar{\mathcal{H}}_i$  wave–function it is important to satisfy  $j_l=|\boldsymbol{J}_{\text{light}}|=3/2$  condition (6.17). This may be accomplished by combining with suitable Clebsch-Gordan coefficients an  $\ell=1$  wave–function with the  $S_{\text{light}}=1/2$  spinor to give

$$\Phi_{i,ld}(k' = k'_3 = 2) = w_i^{(+1)} \delta_{l1} \delta_{d1} ,$$

$$\Phi_{i,ld}(k' = k'_3 = 1) = \frac{\sqrt{3}}{2} w_i^{(+1)} \delta_{l1} \delta_{d2} - \frac{1}{2\sqrt{3}} w_i^{(+1)} \delta_{l2} \delta_{d1} - \frac{1}{\sqrt{6}} w_i^{(0)} \delta_{l1} \delta_{d1} , (6.19)$$

where  $w_j^{(\pm 1)} = \frac{\mp 1}{\sqrt{8\pi}} (\delta_{j1} \pm i\delta_{j2})$  and  $w_i^{(0)} = \frac{\delta_{i3}}{\sqrt{4\pi}}$  is a spherical decomposition.

The main question is: Which of the channels contain bound states? Note that, for the reduced space in which  $\hat{x} \cdot \tau$  has been removed as in Eq. (6.16), k' is a good quantum number. Furthermore, because the wave–function u(|x|) is sharply peaked, the relevant matrix elements are actually independent of the orbital angular momentum r. The classical potential for each k' channel may be calculated by setting r=0 and substituting the appropriate reduced wave–functions from Eqs. (6.18) and (6.19) into the interaction Lagrangian (6.14). (see Appendix B.1 for more details.) The k'=0 channel gets a contribution only from the  $d_S$  term in Eq. (6.14) while the k'=2 channel receives a contribution only from the  $d_T$  term. On the other hand, all three terms contribute to the k'=1 channel. The resulting potentials are:

$$V(k'=0) = -\frac{3}{2}d_{\rm S}F'(0) , \qquad (6.20)$$

$$V(k'=2) = -\frac{1}{2}d_{\rm T}F'(0)$$
, (6.21)

$$V(k'=1) = \begin{pmatrix} \langle \mathcal{H}|V|\mathcal{H}\rangle & \langle \mathcal{H}|V|\mathcal{H}_{\mu}\rangle \\ \langle \mathcal{H}_{\mu}|V|\mathcal{H}\rangle & \langle \mathcal{H}_{\mu}|V|\mathcal{H}_{\mu}\rangle \end{pmatrix} = \begin{pmatrix} \frac{1}{2}d_{\mathrm{S}} & \sqrt{\frac{2}{3}}f_{\mathrm{ST}} \\ \sqrt{\frac{2}{3}}f_{\mathrm{ST}}^{*} & \frac{5}{6}d_{\mathrm{T}} \end{pmatrix} F'(0) . \quad (6.22)$$

The classical criterion for a channel to contain a bound state is that its potential be negative. Since F'(0) > 0 we require for bound states in the k' = 0 and k' = 2 channels

$$d_{\rm S} > 0 \; , \quad d_{\rm T} > 0 \; , \tag{6.23}$$

respectively<sup>5</sup>. For bound states in the k' = 1 channel we must examine the signs of the eigenvalues of Eq. (6.22). Assuming that Eq. (6.23) holds (as will be seen to be desirable) it is easy to see that there is, at most, one k' = 1 bound state. The condition for this bound state to exist is

$$|f_{\rm ST}|^2 > \frac{5}{8} d_S d_T \ .$$
 (6.24)

The (primed) states which diagonalize Eq. (6.22) are simply related to the original ones by

$$\begin{pmatrix} \Phi \\ \Phi_i \end{pmatrix} = \begin{pmatrix} \cos \theta & \sin \theta \\ -p^* \sin \theta & p \cos \theta \end{pmatrix} \begin{pmatrix} \Phi' \\ \Phi'_i \end{pmatrix} , \qquad (6.25)$$

$$\tan 2\theta = \frac{4\sqrt{6}|f_{\rm ST}|}{5d_{\rm T} - 3d_{\rm S}} \,, \tag{6.26}$$

where p is the phase of  $f_{\rm ST}$ .  $\Phi$  and  $\Phi_i$  are shorthand notations<sup>6</sup> for the appropriate wave–functions. Clearly, the results for which states are bound depend on the numerical values and signs of the coupling constants. At the moment there is no purely experimental information on these quantities. However, it is very interesting to observe that if Eqs. (6.23) and (6.24) hold, then the missing first excited  $\Lambda_Q$  states are bound. To see this note that the heavy baryon spin is given by Eq. (4.29) with g

<sup>&</sup>lt;sup>5</sup>In a more general picture where  $\ell = 3$  excited heavy mesons are included, the k' = 2 channel will also be described by a potential matrix. Then the criterion for  $d_T$  is modified. (See next section.)

<sup>&</sup>lt;sup>6</sup>Strictly speaking, to put  $\Phi_{ld}$  on a parallel footing to  $\Phi_{i,ld}$  we should replace  $\Phi_{ld} \rightarrow \sqrt{\frac{3}{8}} \left(P^{3/2}\right)_{ik;ll'} (\tau_k)_{dd'} \Phi_{l'd'}$  with the spin 3/2 projection operator,  $\left(P^{3/2}\right)_{ik;ll'} = \frac{2}{3} \left(\delta_{ik}\delta_{ll'} - \frac{i}{2}\epsilon_{jik} \left(\sigma_j\right)_{ll'}\right)$  (see Appendix B.1).

defined in Eqs. (6.8) and (6.9). For the  $\Lambda_Q$ -type states, noting that  $I = J^{\text{sol}} = 0$  in the Skyrme approach gives the baryon spin as

$$J = g + S_{\text{heavy}} \quad (\Lambda_Q \text{ states}) .$$
 (6.27)

The r=0 choice enables us to set g=k'. With just the three attractive channels  $k'=0,\ k'=1$  and k'=2 we thus end up with the missing first three excited  $\Lambda_Q$  heavy multiplets  $\Lambda_Q\left(\frac{1}{2}^-\right), \left\{\Lambda_Q\left(\frac{1}{2}^-\right), \Lambda_Q\left(\frac{3}{2}^-\right)\right\}$  and  $\left\{\Lambda_Q\left(\frac{3}{2}^-\right), \Lambda_Q\left(\frac{5}{2}^-\right)\right\}$ . It should be stressed that this counting involves dynamics rather than pure kinematics. For example, it may be seen from Eqs. (6.20)–(6.22) that it is dynamically impossible to have four bound heavy multiplets  $(k'=0,\ k'=2)$  and two k'=1 channels). The missing first excited  $\Sigma_Q$ –type states comprise the single heavy multiplet  $\left\{\Sigma_Q\left(\frac{1}{2}^-\right), \Sigma_Q\left(\frac{3}{2}^-\right)\right\}$ . At the classical level there are apparently more bound multiplets present. However, we will now see that the introduction of collective coordinates, as is anyway required in the Skyrme model [80] to generate states with good isospin quantum number, will split the heavy multiplets from each other. Thus, deciding which states are bound actually requires a more detailed analysis.

We need to extend Eq. (4.24) in order to allow the  $\ell = 1$  heavy meson fields to depend on the collective rotation variable A(t):

$$\bar{\mathcal{H}}(\boldsymbol{x},t) = A(t)\bar{\mathcal{H}}_{c}(\boldsymbol{x}) , \quad \bar{\mathcal{H}}_{i}(\boldsymbol{x},t) = A(t)\bar{\mathcal{H}}_{ic}(\boldsymbol{x}) ,$$
 (6.28)

where  $\bar{\mathcal{H}}_c$  and  $\bar{\mathcal{H}}_{ic}$  are given in Eq. (6.15). Note, again, that the matrix A(t) acts on the isospin indices. We also have  $\bar{\mathcal{H}}_{0c} = 0$  due to the rest frame constraint  $V^{\mu}\bar{\mathcal{H}}_{\mu c} = 0$ . Now substituting Eq. (6.28) as well as the first of Eq. (4.24) into the heavy field Lagrangian<sup>7</sup> yields [59] the collective Lagrangian<sup>8</sup>

$$L_{\text{coll}} = \frac{1}{2} \alpha^2 \mathbf{\Omega}^2 - \chi(k') \mathbf{K'} \cdot \mathbf{\Omega} , \qquad (6.29)$$

<sup>&</sup>lt;sup>7</sup>Note that Eq. (6.13) contributes but Eq. (6.14) does not contribute.

<sup>&</sup>lt;sup>8</sup>In Eq. (6.29) k' is defined to operate on the heavy particle wave–functions rather than on their conjugates. This is required when the heavy meson is coupled to the Skyrme background field since

where  $\Omega$  is defined in Eq. (4.25) and  $\alpha^2$  is the Skyrme model moment of inertia. In the vector meson model the induced fields ( $\rho_0^a$  and  $\omega_i$ ) are determined from a variational approach to  $\alpha^2$ . The quantities  $\chi(k')$  are given by (see Appendix B.2).

$$\chi(k') = \begin{cases}
0 & k' = 0 \\
\frac{1}{4} (3 \cos^2 \theta - 1) & k' = 1 \\
\frac{1}{4} & k' = 2
\end{cases} ,$$
(6.30)

where the angle  $\theta$  is defined in Eq. (6.26). (Note that if light vector mesons are included the expressions for  $\chi$  would be more involved as the induced fields will also contribute.) In writing Eq. (6.30) it was assumed that the first state in Eq. (6.25) (i.e.  $\Phi'$  rather than  $\Phi'_i$ ) is the bound one; the collective Lagrangian is constructed as an expansion around the bound state solutions. We next determine from Eq. (4.28), the canonical (angular) momentum  $J^{\text{sol}}$  as  $\alpha^2 \Omega - \chi(k') K'$ . The usual Legendre transform then leads to the collective Hamiltonian

$$H_{\text{coll}} = \frac{1}{2\alpha^2} \left( \boldsymbol{J}^{\text{sol}} + \chi \left( k' \right) \, \boldsymbol{K'} \right)^2 \,. \tag{6.31}$$

Again we remark that  $J^{\text{sol}} = I$ . It is useful to define the light part of the total heavy baryon spin as

$$j = r + K' + J^{\text{sol}} , \qquad (6.32)$$

and rewrite Eq. (6.31) as

$$H_{\text{coll}} = \frac{1}{2\alpha^2} \left[ (1 - \chi(k')) \mathbf{I}^2 + \chi(k') (\mathbf{j} - \mathbf{r})^2 + \chi(k') (\chi(k') - 1) \mathbf{K'}^2 \right] . \tag{6.33}$$

The mass splittings within each given k' multiplet due to  $H_{\text{coll}}$  are displayed in Table 6.2. This table also shows the splitting of the k' multiplets from each other due to  $\overline{\Lambda_Q}$  is made as (qqq)  $(\overline{q}Q)$  rather than (qqq)  $(\overline{Q}q)$ . For convenience in Eqs. (4.15) and (6.16) we have considered the conjugate wave–functions (since they are usual in the light sector). This has been compensated by the minus sign in the second term of Eq. (6.29).

I	k'	$\left m{K}'+m{J}^{ m sol} ight $	V	$\alpha^2 H_{\rm coll}$	Candidates for $r = 0$
$=J^{\mathrm{sol}}$					missing states
	0	0	$-\frac{3}{2}d_{\rm S}F'(0)$	0	$\Lambda_Q\left(rac{1}{2}^- ight)$
0	1	1	$\lambda$	$\chi^2$	$\left\{\Lambda_Q\left(rac{1}{2}^- ight),\Lambda_Q\left(rac{3}{2}^- ight) ight\}$
	2	2	$-\frac{1}{2}d_{\mathrm{T}}F'(0)$	$\frac{3}{16}$	$\left\{\Lambda_Q\left(rac{3}{2}^- ight),\Lambda_Q\left(rac{5}{2}^- ight) ight\}$
	0	1	$-\frac{3}{2}d_{\rm S}F'(0)$	1	$\left\{ \Sigma_Q \left( \frac{1}{2}^- \right), \Sigma_Q' \left( \frac{3}{2}^- \right) \right\}_1$
	1	0	$\lambda$	$(\chi-1)^2$	-
	1	1	"	$(\chi - 1)^2 + \chi$	$\left\{ \Sigma_Q \left( \frac{1}{2}^- \right), \Sigma_Q \left( \frac{3}{2}^- \right) \right\}_2$
1	1	2	"	$(\chi - 1)^2 + 3\chi$	_ · · · · · · <u>-</u>
	2	1	$-\frac{1}{2}d_{\mathrm{T}}F'(0)$	$\frac{7}{16}$	$\left\{ \Sigma_Q \left( \frac{1}{2}^- \right), \Sigma_Q \left( \frac{3}{2}^- \right) \right\}_3$
	2	2	"	$\frac{15}{16}$	
	2	3	"	$\frac{27}{16}$	

Table 6.2: Contributions to energies of new predicted  $\ell=1$  states. Here,  $\lambda=\frac{1}{4}F'(0)\left[\left(d_{\rm S}+\frac{5}{3}d_{\rm T}\right)-\sqrt{\left(d_{\rm S}-\frac{5}{3}d_{\rm T}\right)^2+\frac{32}{3}|f_{\rm ST}|^2}\right]$  is the presumed negative binding potential in the k'=1 channel. Furthermore  $\chi=\chi(1)$  in Eq. (6.30); it satisfies  $-\frac{1}{4}\leq\chi\leq\frac{1}{2}$ .

the classical potential in Eqs. (6.20)–(6.22). Note that the slope of the Skyrme profile function F'(0) is of order 1 GeV. The coupling constants  $d_S$ ,  $d_T$ ,  $f_{ST}$ , based on  $d \simeq 0.5$ for the ground state heavy meson, are expected to be of the order unity. Hence the binding potentials V are expected to be of the rough order of 500 MeV. The inverse moment of inertia  $1/\alpha^2$  is of the order of 200 MeV which (together with  $-\frac{1}{4} \le \chi \le \frac{1}{2}$ ) sets the scale for the " $1/N_c$ " corrections due to  $H_{coll}$ . As mentioned before, if the coupling constants satisfy the inequalities (6.23) and (6.24), all the  $\Lambda_Q$  multiplets shown will be bound. At first glance we might expect all the  $\Sigma_Q$  states listed also to be bound. However the  $H_{\text{coll}}$  corrections increase as I increases, which is a possible indication that many of the  $\Sigma_Q$ 's might be only weakly bound. In a more complete model they may become unbound. Hence it is interesting to ask which of the three displayed candidates for the single missing  $\Sigma_Q$  multiplet is mostly tightly bound in the present model. Neglecting the effect of V we can see that  $H_{\rm coll}$  raises the energy of candidate 3 less than those of candidates 1 and 2. Furthermore, for the large range of  $\chi$ ,  $-\frac{1}{4} \le \chi \le 1 - \frac{\sqrt{7}}{4}$ , candidate 3 suffers the least unbinding due to  $H_{\text{coll}}$  of any of the I=1 heavy baryons listed. The  $\Lambda_Q$  states suffer still less unbinding due to  $H_{\rm coll}$ .

### 6.5 Extension to the Higher Orbital Excitations

We have already explicitly seen that the "missing" first orbitally excited heavy baryon states in the bound state picture might be generated if the model is extended to also include binding the first orbitally excited heavy mesons in the background field of a Skyrme soliton. From the correspondence (6.10) and associated discussion we expect that any of the higher excited heavy baryons of the CQM might be similarly generated by binding the appropriately excited heavy mesons. In this section we will show in detail how this result can be achieved in the general case. An extra complication,

which was neglected for simplicity in the last section, is the possibility of baryon states constructed by binding heavy mesons of different  $\ell$ , mixing with each other. For example  $\{r=1, \ell=0\}$  type states can mix with  $\{r=1, \ell=2\}$  type states, other quantum numbers being the same. Since  $r+\ell$  must add to 1, this channel could not mix with  $\{r=1, \ell=4\}$ . An identical type of mixing – between  $\{L_E=1, L_I=0\}$  and  $\{L_E=1, L_I=2\}$  – may also exist in the CQM. The present model, however, provides a simple way to study this kind of mixing as a perturbation.

To start the analysis it may be helpful to refer to Table 6.3, which shows our notations for the excited heavy meson multiplet "fluctuation" fields. The straight H's contain negative parity mesons and the curly  $\mathcal{H}$ 's contain positive parity mesons. Further details are given in Ref. [78]. Note that each field is symmetric in all Lorentz indices and obeys the constraints

$$V^{\mu_1} H_{\mu_1 \cdots \mu_n} = H_{\mu_1 \cdots \mu_n} \gamma^{\mu_1} = 0 , \qquad (6.34)$$

as well as for  $\mathcal{H}_{\mu_1\cdots\mu_n}$ . The general chiral invariant interaction with the lowest number of derivatives is

$$\mathcal{L}_d + \mathcal{L}_f + \mathcal{L}_g \ , \tag{6.35}$$

where

$$\mathcal{L}_{d} = -M \sum_{n=0} d_{Pn} \operatorname{Tr} \left[ H^{\mu_{1} \cdots \mu_{n}} p^{\mu} \gamma_{\mu} \gamma_{5} \bar{H}_{\mu_{1} \cdots \mu_{n}} \right]$$

$$-M \sum_{n=0} d_{Sn} \operatorname{Tr} \left[ \mathcal{H}^{\mu_{1} \cdots \mu_{n}} p^{\mu} \gamma_{\mu} \gamma_{5} \bar{\mathcal{H}}_{\mu_{1} \cdots \mu_{n}} \right] ,$$

$$\mathcal{L}_{f} = M \sum_{n=0} f_{Pn} \operatorname{Tr} \left[ H^{\mu_{1} \cdots \mu_{n}} p^{\mu} \gamma_{5} \bar{\mathcal{H}}_{\mu_{1} \cdots \mu_{n} \mu} \right] + \text{h.c.}$$

$$+ M \sum_{n=0} f_{Sn} \operatorname{Tr} \left[ \mathcal{H}^{\mu_{1} \cdots \mu_{n}} p^{\mu} \gamma_{5} \bar{\mathcal{H}}_{\mu_{1} \cdots \mu_{n} \mu} \right] + \text{h.c.} .$$

$$(6.36)$$

The final piece,

$$\mathcal{L}_{g} = M \sum_{n=0} g_{n} \operatorname{Tr} \left[ \mathcal{H}^{\mu_{1} \cdots \mu_{n}} p^{\mu} \gamma_{\mu} \gamma_{5} \bar{H}_{\mu_{1} \cdots \mu_{n}} \right] + \text{h.c.}$$
 (6.37)

field	$\ell$	$j_l$	$J^P$
H	0	1/2	$0^-, 1^-$
${\cal H}$	1	1/2	$0^+, 1^+$
${\cal H}_{\mu}$	1	3/2	$1^+, 2^+$
$H_{\mu}$	2	3/2	$1^-, 2^-$
$H_{\mu  u}$	2	5/2	$2^-, 3^-$
:			
$H_{\mu_1\cdots\mu_{\ell-1}}$	$\ell = \mathrm{even}$	$\ell - 1/2$	$(\ell-1)^-,\ell^-$
$H_{\mu_1 \cdots \mu_\ell}$	$\ell = \mathrm{even}$	$\ell + 1/2$	$\ell^-,(\ell+1)^-$
$\mathcal{H}_{\mu_1 \cdots \mu_{\ell-1}}$	$\ell = \text{odd}$	$\ell - 1/2$	$(\ell-1)^+,\ell^+$
$\mathcal{H}_{\mu_1 \cdots \mu_\ell}$	$\ell = \text{odd}$	$\ell + 1/2$	$\ell^+,(\ell+1)^+$
÷			

Table 6.3: Notation for the heavy meson multiplets.  $j_l$  is the angular momentum of the "light cloud" surrounding the heavy quark while  $J^P$  is the spin parity of each heavy meson in the multiplet.

exists in general, but does not contribute for our ansatz. Terms of the form

$$\operatorname{Tr}\left[H^{\mu_{1}\cdots\mu_{n}\mu}p_{\mu}\gamma_{5}\bar{\mathcal{H}}_{\mu_{1}\cdots\mu_{n}}\right], \qquad \operatorname{Tr}\left[\mathcal{H}^{\mu_{1}\cdots\mu_{n}\mu}p_{\mu}\gamma_{5}\bar{H}_{\mu_{1}\cdots\mu_{n}}\right]$$
(6.38)

can be shown to vanish by the heavy spin symmetry. In the notation of Eq. (6.14),  $d_{\rm S} = d_{\rm S0}$ ,  $d_{\rm T} = d_{\rm S1}$  and  $f_{\rm ST} = f_{\rm S0}$ . A new type of coupling present in Eq. (6.36) also connects multiplets to others differing by  $\Delta \ell = \pm 2$ . These are the terms with odd (even) n for H ( $\mathcal{H}$ )-type fields. The interactions in Eq. (6.37) connecting multiplets differing by  $\Delta \ell = \pm 1$  turn out not to contribute in our model. In the interest of simplicity we will consider all heavy mesons to have the same mass. This is clearly an approximation which may be improved in the future.

The rest frame ansätze for the bound state wave functions which generalize Eq. (6.15) are (note  $j_l = n + 1/2$ ):

$$\left(\bar{H}_{i_{1}\cdots i_{n}}\right)_{c} \to \begin{cases}
\bar{h}_{i_{1}\cdots i_{n},lh}^{a} \otimes \begin{pmatrix} 0 & 0 \\ 1 & 0 \end{pmatrix}, & j_{l} = \ell + \frac{1}{2}, \\
\bar{h}_{i_{1}\cdots i_{n},lh}^{a} \otimes \begin{pmatrix} 1 & 0 \\ 0 & 0 \end{pmatrix}, & j_{l} = \ell - \frac{1}{2},
\end{cases}$$
(6.39)

with identical structures for  $\bar{H} \to \bar{\mathcal{H}}$ . Note that again a, l, h represent respectively the isospin, light spin and heavy spin bivalent indices. Extracting a factor of  $\hat{x} \cdot \tau$  as we did before in Eqs. (4.15) and (6.16) leads to

$$\bar{h}_{i_1\cdots i_n,lh}^a = \frac{u\left(|\boldsymbol{x}|\right)}{\sqrt{M}} \left(\hat{\boldsymbol{x}}\cdot\boldsymbol{\tau}\right)_{ad} \psi_{i_1\cdots i_n,dl}\left(k',k_3',r\right) \chi_h \tag{6.40}$$

with similar notations. The relevant wave–functions are the  $\psi_{i_1\cdots i_n,dl}$   $(k',k'_3,r)$ . k' was defined in Eq. (6.9); we will see that it remains a good quantum number. Since the terms which connect the positive parity (H type) and negative parity (H type) heavy mesons (Eq. (6.37)) vanish when the  $ans\ddot{a}tze$  (6.39) are substituted, the baryon states associated with each type do not mix with each other in our model. We thus list

separately the potentials for each type. For the  $\ell =$  even baryons (associated with H mesons),

$$V[k'=0] = -\frac{3}{2}d_{P0}F'(0) ,$$

$$V[k'\neq 0] = F'(0) \begin{bmatrix} -(-1)^{k'}\frac{d_{P(k'-1)}}{2} & \sqrt{\frac{2}{3}}f_{P(k'-1)} \\ \sqrt{\frac{2}{3}}f_{P(k'-1)}^* & -(-1)^{k'}\frac{2k'+3}{2k'+1}\frac{d_{Pk'}}{2} \end{bmatrix} , \quad (6.41)$$

while for the  $\ell = \text{odd}$  baryons (associated with  $\mathcal{H}$  mesons),

$$V[k'=0] = -\frac{3}{2}d_{S0}F'(0),$$

$$V[k'\neq 0] = F'(0)\begin{bmatrix} -(-1)^{k'}\frac{d_{S(k'-1)}}{2} & \sqrt{\frac{2}{3}}f_{S(k'-1)} \\ \sqrt{\frac{2}{3}}f_{S(k'-1)}^* & -(-1)^{k'}\frac{2k'+3}{2k'+1}\frac{d_{Sk'}}{2} \end{bmatrix}. \quad (6.42)$$

Details of the derivations of Eqs. (6.41) and (6.42) are given in Appendix B.1. The ordering of matrix elements in Eqs. (6.41) and (6.42), for a given k', is such that the first heavy meson has a light spin,  $j_l = k' - \frac{1}{2}$  while the second has  $j_l = k' + \frac{1}{2}$ . The H type ( $\mathcal{H}$  type) channels with k' = even (odd) involve two mesons with the same  $\ell = k'$ . The H type ( $\mathcal{H}$  type) channels with k' = odd (even) involve two mesons differing by  $\Delta \ell = 2$ , i.e.,  $\ell = k' - 1$  and  $\ell = k' + 1$ . This pattern is, for convenience, illustrated in Table 6.4. Also shown, for each k', are the number of channels which are expected to be bound according to the CQM.

It is important to note that Table 6.4 holds for any value of the angular momentum r, which is a good quantum number in our model. For the reader's orientation, we now locate the previously considered cases in Table 6.4. The standard "ground state" heavy baryons discussed in section 6.2 are made from the H meson with  $\ell = 0$  and  $j_{\ell} = 1/2$ . They have r = 0 and k' = 0. The seven negative parity heavy baryons discussed in section 6.2 also are made from the H meson with  $\ell = 0$  and  $j_{\ell} = 1/2$ .

		H mesons		$\mathcal{H}$ mesons	
<i>k</i> ′	$j_l$	$\ell$	#	$\ell$	#
0	1/2	0	1	1	1
1	1/2	0	0	1	1
	$\frac{1/2}{3/2}$	2		1	1
2	3/2	2	1	1	2
	3/2 $5/2$	2		3	2
3	5/2 $7/2$	2	0	3	1
	7/2	4		3	1

Table 6.4: Pattern of states for Eqs. (6.41) and (6.42). Note that  $j_l = n + \frac{1}{2}$  is the light cloud spin of the heavy meson. The columns marked # stand for the number of channels which are expected to be bound, for that particular k', according to the CQM.

They still have k'=0, but now r=1. The seven "missing" first excited heavy baryons discussed in section 6.4 have r=0 and are made from the  $\ell=1$ ,  $\mathcal{H}$  and  $\mathcal{H}_{\mu}$  mesons with  $j_{\ell}=1/2$  and  $j_{\ell}=3/2$ . There should appear one bound state for k'=0, one bound state for k'=1 and one bound state for k'=2 in the " $\mathcal{H}$ -meson" section of Table 6.4. Note that the number of states expected in the CQM model for k'=2 is listed in Table 6.4 as two, rather than one. In the absence of  $\Delta \ell=2$  terms connecting  $\mathcal{H}_{\mu}$  and  $\mathcal{H}_{\mu\nu}$  (see the last term in Eq. (6.36))  $\ell$  would be conserved for our model and only the  $\ell=1$  state would be relevant. This was the approximation we made, for simplicity, in section 6.4. The other entry would have  $\ell=3$  and would decouple. When the  $\Delta \ell=2$  mixing terms are turned on, the  $\ell=1$  and  $\ell=3$ , k'=2 channels will mix. One diagonal linear combination should be counted against the  $L_I=1$  CQM states and one against the  $L_I=3$  CQM states.

To summarize: for the H-type mesons, the even k' channels should each have one bound state, while the odd k' channels should have none. The situation is very different for the  $\mathcal{H}$ -type mesons; then the even  $k' \neq 0$  channels should contain two bound states while the odd k' channels should contain one bound state. The k' = 0 channel should have one bound state.

For the H-type meson case, the pattern of bound states mentioned above would be achieved dynamically if the coupling constants satisfied:

$$d_{P0} > 0 ,$$

$$(-1)^{k'} \left[ d_{P(k'-1)} d_{Pk'} \left( \frac{2k'+3}{2k'+1} \right) - \frac{8}{3} \left| f_{P(k'-1)} \right|^2 \right] < 0 , \quad (k' > 0)$$

$$d_{P(k'-1)} + \left( \frac{2k'+3}{2k'+1} \right) d_{Pk'} > 0 , \quad (k' = \text{odd}) .$$

$$(6.43)$$

These follow from requiring only one negative eigenvalue of Eq. (6.41) for k' = even and none for k' = odd. Similarly requiring for the  $\mathcal{H}$ -type meson case in Eq. (6.42), a negative eigenvalue for k' = 0, one negative eigenvalue for k' = odd and two negative

eigenvalues for k' > 0 and even leads to the criteria,

$$d_{S0} > 0 ,$$

$$(-1)^{k'} \left[ d_{S(k'-1)} d_{Sk'} \left( \frac{2k'+3}{2k'+1} \right) - \frac{8}{3} \left| f_{S(k'-1)} \right|^2 \right] > 0 , \quad (k' > 0)$$

$$d_{S(k'-1)} + \left( \frac{2k'+3}{2k'+1} \right) d_{Sk'} > 0 , \quad (k' = \text{even} \neq 0) . \tag{6.44}$$

From Eqs. (6.43) and (6.44) it can be seen that all the d's are required to be positive. Furthermore these equations imply that the |f|'s which connect heavy mesons with  $\Delta \ell = 2$  are relatively small (compared to the d's) while the |f|'s which connect heavy mesons with  $\Delta \ell = 0$  are relatively large. In detail this means that  $|f_{P(k'-1)}|$  should be small for odd k' and large for even k' with just the reverse for  $|f_{S(k'-1)}|$ . This result seems physically reasonable.

As in the example in the preceding section we should introduce the collective variable A(t) in order to define states of good isospin and angular momentum. This again yields some splitting of the different  $|\mathbf{K}' + \mathbf{J}^{\text{sol}}|$  members of each k' bound state. Now, each k' channel (except for k' = 0) is described by a  $2 \times 2$  matrix. Thus there will be an appropriate mixing angle  $\theta$ , analogous to the one introduced in Eq. (6.25), for each k' and parity choice (i.e., H-type or  $\mathcal{H}$ -type field). The collective Lagrangian is still given by Eq. (6.29) but, in the general case,

$$\chi_{\pm}(k') = \frac{1}{2k'(k'+1)} \left[ \frac{1}{2} \pm \left( k' + \frac{1}{2} \right) \cos 2\theta \right] . \tag{6.45}$$

In this formula the different signs correspond to the two possible eigenvalues,

$$\lambda_{\pm} = \left[ \frac{(-1)^{k'-1}}{4} \left( d_{(k'-1)} + \frac{2k'+3}{2k'+1} d_{k'} \right) \pm \frac{1}{4} \sqrt{\left( d_{(k'-1)} - \frac{2k'+3}{2k'+1} d_{k'} \right)^2 + \frac{32}{3} \left| f_{(k'-1)} \right|^2} \right] F'(0)$$
(6.46)

of the potential matrix. For example, referring to Table 6.4, we would expect the k'=2,  $\mathcal{H}$ -type meson case to provide two distinct bound states and hence both

 $\chi_{+}(2,\mathcal{H})$  and  $\chi_{-}(2,\mathcal{H})$  would be non-zero. On the other hand, we would expect no bound states in the k'=3, H-type meson case so  $\chi_{\pm}(3,H)$  should be interpreted as zero.

It is convenient to summarize the energies of the predicted states in tabular form, generalizing the example presented in Table 6.2. The situation for baryons with parity =  $-(-1)^r$  ( $\mathcal{H}$ -type mesons) is presented in Table 6.5. For definiteness we have made the assumption that the constraints (6.44) above are satisfied. In order

I	k'	$oxed{K'+J^{\mathrm{sol}}}$	V	$\alpha^2 \times H_{\text{coll}}$	Candidates for $r=0$
$=J^{\mathrm{sol}}$					missing states
	2n-1	2n - 1	$\lambda_+$	$n(2n-1)\chi_{-}^{2}$	$\{\Lambda\left((2n-3/2)^-\right), \Lambda\left((2n-1/2)^-\right)\}$
0	2n	2n	$\lambda_+$	$n(2n+1)\chi_+^2$	$\{\Lambda ((2n-1/2)^-), \Lambda ((2n+1/2)^-)\}$
			$\lambda_{-}$	$n(2n+1)\chi^2$	"
	2n-1	2n-2		$n(2n-1)\chi_+^2 + 1 - 2n\chi_+$	
		2n - 1	$\lambda_{+}$	$n(2n-1)\chi_+^2 + 1 - \chi_+$	$\left\{\Sigma\left((2n-3/2)^-\right),\Sigma\left((2n-1/2)^-\right)\right\}_1$
		2n		$n(2n-1)\chi_{+}^{2} + 1 + (2n-1)\chi_{+}$	
	2n	2n - 1		$n(2n+1)\chi_+^2 + 1 - (2n+1)\chi_+$	$\{\Sigma ((2n-3/2)^{-}), \Sigma ((2n-1/2)^{-})\}_{2}$
1		2n	$\lambda_{+}$	$n(2n+1)\chi_+^2 + 1 - \chi_+$	
		2n + 1		$n(2n+1)\chi_+^2 + 1 + 2n\chi_+$	$\{\Sigma ((2n+1/2)^{-}), \Sigma ((2n+3/2)^{-})\}_{3}$
		2n - 1		$n(2n+1)\chi_{-}^{2} + 1 - (2n+1)\chi_{-}$	$\{\Sigma ((2n-3/2)^-), \Sigma ((2n-1/2)^-)\}_4$
		2n	$\lambda_{-}$	$n(2n+1)\chi_{-}^{2} + 1 - \chi_{-}$	
		2n+1		$n(2n+1)\chi_{-}^{2} + 1 + 2n\chi_{-}$	$\{\Sigma ((2n+1/2)^{-}), \Sigma ((2n+3/2)^{-})\}_{5}$

Table 6.5: Contributions to energies of the new predicted states made from  $\mathcal{H}$ -type heavy mesons. Note that n is a positive integer. The n=0 case is given in Table 6.2. The  $\lambda_+$  entries in the V column are more tightly bound than the  $\lambda_-$  entries.  $|\mathbf{K}' + \mathbf{J}^{\text{sol}}|$  is the light part of the heavy baryon angular momentum for r=0 (See Eq. (6.32).).

to explain Table 6.5 let us ask which states correspond to the  $(L_I = 3, L_E = 0)$  states in the CQM. Reference to Table 6.1 shows that three negative parity  $\Lambda$ -type heavy multiplets and one negative parity  $\Sigma$ -type heavy multiplet should be present. The correspondence in Eq. (6.10) instructs us to set r = 0 and, noting Eq. (6.9), to identify

$$\mathbf{K}' + \mathbf{J}^{\text{sol}} \leftrightarrow \mathbf{L}_I + \mathbf{S} \ . \tag{6.47}$$

The  $\Lambda$ -type particles are of type c) in Eq. (6.3) so we must take S=1. Hence, since  $J^{\rm sol}=0$  for  $\Lambda$ -type particles, we learn that k' can take on the values 2, 3 and 4. For k'=2, the second line of the k' column yields two possible multiplets (energies  $\lambda_+$ and  $\lambda_{-}$ ) with n=1 and structure  $\left\{\Lambda\left(\frac{3}{2}^{-}\right), \Lambda\left(\frac{5}{2}^{-}\right)\right\}$ . We should choose one of these to be associated with  $(L_I = 3, L_E = 0)$  and the other with  $(L_I = 1, L_E = 0)$  in the CQM. We remind the reader that  $\ell$  is not a good quantum number so that the correspondence  $\ell \leftrightarrow \mathbf{L}_I$  in Eq. (6.10) only holds when the  $\Delta \ell = 2$  mixing terms are neglected. For k'=3, the first line of the k' column correctly yields one multiplet with n=2 and structure  $\left\{\Lambda\left(\frac{5}{2}\right), \Lambda\left(\frac{7}{2}\right)\right\}$ . For k'=4, the second line of the k'column yields two multiplets with n=2 and structure  $\left\{\Lambda\left(\frac{7}{2}\right), \Lambda\left(\frac{9}{2}\right)\right\}$ . One of these is to be associated with  $(L_I = 3, L_E = 0)$  and the other with  $(L_I = 5, L_E = 0)$ in the CQM. Now let us go on to the  $\Sigma$ -type heavy multiplets. These are of type d) in Eq. (6.3) and yield S = 0. Hence  $\mathbf{K}' + \mathbf{J}^{\text{sol}} \leftrightarrow \mathbf{L}_I$  and  $\left| \mathbf{K}' + \mathbf{J}^{\text{sol}} \right| = 3$ . Five candidates for this  $\left\{\Sigma\left(\frac{5}{2}^{-}\right), \Sigma\left(\frac{7}{2}^{-}\right)\right\}$  multiplet are shown in the last column of Table 6.5. These consecutively correspond to the choices n=2, 2, 1, 2, 1 in the  $|K'+J^{\text{sol}}|$  column. As before it is necessary for an exact correspondence with the CQM that one of these should be dynamically favored (much more tightly bound) over the others. Again, note that the choice  $\left| \mathbf{K}' + \mathbf{J}^{\mathrm{sol}} \right| = 3$  does not uniquely constrain the value of  $\ell$ .

Next, the situation for baryons with parity =  $(-1)^r$  (*H*-type baryons) is presented in Table 6.6.. For definiteness we have made the assumption that the constraints

I	k'	$\left oldsymbol{K}'+oldsymbol{J}^{\mathrm{sol}} ight $	V	$\alpha^2 \times H_{\text{coll}}$	Candidates for $r = 0$
$=J^{\mathrm{sol}}$					missing states
0	2n	2n	$\lambda_{+}$	$n(2n+1)\chi_+^2$	$\{\Lambda ((2n-1/2)^+), \Lambda ((2n+1/2)^+)\}$
		2n - 1		$n(2n-1)\chi_+^2 + 1 - (2n+1)\chi_+$	$\{\Sigma ((2n-3/2)^+), \Sigma ((2n-1/2)^+)\}_1$
1	2n	2n	$\lambda_{+}$	$n(2n+1)\chi_+^2 + 1 - \chi_+$	$\{\Sigma\left((2n-1/2)^+\right), \Sigma\left((2n+1/2)^+\right)\}_2$
		2n + 1		$n(2n+1)\chi_+^2 + 1 + 2n\chi_+$	$\{\Sigma\left((2n+1/2)^+\right), \Sigma\left((2n+3/2)^+\right)\}_3$

Table 6.6: Contributions to energies of the new predicted states made from H-type heavy mesons. Other details as for Table 6.5.

(6.43) above are satisfied. This eliminates the odd k' states and agrees with the CQM counting. For example, we ask which states correspond to the  $(L_I = 2, L_E = 0)$  states in the CQM. Reference to Table 6.1 shows that one positive parity  $\Lambda$ -type heavy multiplet and three positive parity  $\Sigma$ -type heavy multiplets should be present. For r = 0 we have the correspondence  $\mathbf{K}' + \mathbf{J}^{\text{sol}} \leftrightarrow \mathbf{L}_I + \mathbf{S}$ . The  $\Lambda$ -type particles are of type a) in Eq. (6.3) so we must set k' = 2. The first line in Table 6.6 then yields, with n = 1 the desired  $\left\{\Lambda\left(\frac{3}{2}^+\right), \Lambda\left(\frac{5}{2}^+\right)\right\}$  heavy multiplet. The  $\Sigma$  particles are of type b) in Eq. (6.3) so that  $\left|\mathbf{K}' + \mathbf{J}^{\text{sol}}\right|$  can take on the values 1, 2 and 3. The last three lines in Table 6.6, with n = 1, give the desired multiplets:  $\left\{\Sigma\left(\frac{1}{2}^+\right), \Sigma\left(\frac{3}{2}^+\right)\right\}$ ,  $\left\{\Sigma\left(\frac{3}{2}^+\right), \Sigma\left(\frac{5}{2}^+\right)\right\}$  and  $\left\{\Sigma\left(\frac{5}{2}^+\right), \Sigma\left(\frac{7}{2}^+\right)\right\}$ . In this case all the states should be bound so that the splittings due to  $H_{\text{coll}}$  are desired to be relatively small. The present structure is simpler than the one shown in Table 6.5 for the  $\mathcal{H}$ -type cases.

# 6.6 Conclusions for the Generalized Heavy Baryon Model

In this chapter [91] we have pointed out the problem of getting, in the framework of a bound state picture, the excited states which are expected on geometrical grounds from the constituent quark model. We treated the heavy baryons and made use of the Isgur–Wise heavy spin symmetry. The approach may also provide some insight into the understanding of light excited baryons. The key problem to be solved is the introduction of an additional "source" of angular momentum in the model. It was noted that this might be achieved in a simple way by postulating that excited heavy mesons, which have "locked–in" angular momentum, are bound in the background Skyrmion field. The model was seen to naturally have the correct kinematical structure in order to provide the excited states which were missing in earlier models.

An important aspect of this work is the investigation of which states in the model are actually bound. This is a complicated issue since there are many interaction terms present with  $a\ priori$  unknown coupling constants. Hence, for the purpose of our initial investigation we included only terms with the minimal interactions of the light pseudoscalar mesons. The large M limit was also assumed and nucleon recoil as well as mass splittings among the heavy excited meson multiplets were neglected. We expect, based on previous work, that the most important improvement of the present calculation would be to include the interactions of the light vector mesons. It is natural to expect that possible interactions of the light higher spin mesons also play a role. In the calculation of the ground state heavy baryons the light vectors were actually slightly more important than the light pseudoscalars and reinforced the binding due to the latter. Another complicating factor is the presence, expected from phenomenology, of radially excited mesons along with orbitally excited ones.

It is interesting to estimate which of the first excited states, discussed in section 6.4, are bound. The criteria for actually obtaining the missing states in the model with only light pseudoscalars present are given in Eqs. (6.23) and (6.24). Based on the use of chiral symmetry for relating the coupling constants to axial matrix elements and using a quark model argument to estimate the axial matrix elements, Falk and Luke [78] presented the estimates (their Eqs. (2.23) and (2.24))  $d_{\rm T}=3d_{\rm S}=d$ and  $|f_{ST}| = \frac{2}{\sqrt{3}}d$ . With these estimates Eqs. (6.23) and (6.24) are satisfied. Note that d > 0 provides binding for the ground state heavy baryons. However we have checked this and find that, although we are in agreement for  $|f_{ST}|$  we obtain instead  $d_{\rm T}=3d_{\rm S}=-d$ . Assuming that this is the case then it is easy to see that the only bound multiplet will have k'=1. This leads to the desired  $\Sigma$ -type multiplet and one of the three desired  $\Lambda$ -type multiplets being bound, but not the k'=0 and 2, Λ-type multiplets. Clearly, it is important to make a more detailed calculation of the light meson–excited heavy meson coupling constants. We also plan to investigate the effects of including light vector mesons in the present model. It is hoped that the study of these questions will lead to a better understanding of the dynamics of the excited heavy particles.

Finally we would like to add a few remarks on studies of the excited "light" hyperons within the bound state approach to the SU(3) Skyrme model. In that model the heavy spin symmetry is not maintained since the vector counterpart of the kaon, the  $K^*$ , is omitted; while the kaons themselves couple to the pions as prescribed by chiral symmetry. On the other hand the higher orbital angular momentum channels (i.e.  $r \geq 2$ ) have been extensively studied. The first study was performed by the SLAC group [82]. However, they were mostly interested in the amplitudes for kaon–nucleon scattering and for simplicity omitted flavor symmetry breaking terms in the effective Lagrangian. Hence they did not find any bound states, except for zero modes.

#### 6.6. CONCLUSIONS FOR THE GENERALIZED HEAVY BARYON MODEL 139

These symmetry breaking terms were, however, included in the scattering analysis of all higher orbital angular momentum channels by Scoccola [83]. The only bound states he observed were those for P- and S-waves. After collective quantization these are associated with the ordinary hyperons and the  $\Lambda(1405)$ . As a matter of fact these states were already found in the original study by Callan and Klebanov [59]. It is clear that the orbital excitations found in the bound state approach to the Skyrme model should be identified as the  $\ell=0$  states. Furthermore when the dynamical coupling of the collective coordinates  $(A, \Omega)$  is included in the scattering analysis [84] the only resonances which are observed obey the selection rule  $|J-1/2| \le r \le |J+1/2|$ , where r denotes the kaon orbital angular momentum. This rule is consistent with  $\ell=0$  in our model. In order to find states with  $\ell\neq 0$  in this model one would also have to include pion fluctuations besides the kaon fluctuations for the projectile-state. As indicated in the previous sections, these fluctuating fields should be coupled to carry the good quantum number  $\ell$ . The full calculation would not only require this complicated coupling but also an expansion of the Lagrangian up to fourth order in the meson fluctuations off the background soliton. Such a calculation seems impractical, indicating that something like our present approximation, which treats these coupled states as elementary particles, is needed.

# Appendix A

# Part I Appendix

## A.1 Scattering kinematics

The general partial wave scattering matrix for the multichannel case can be written as:

$$S_{ab} = \delta_{ab} + 2iT_{ab} . (A.1)$$

For simplicity, the diagonal isospin and angular momentum labels have not been indicated.

By requiring the unitarity condition  $S^{\dagger}S=1$  one deduces for the two–channel case the following relations:

$$Im(T_{11}) = |T_{11}|^2 + |T_{21}|^2,$$
  
 $Im(T_{22}) = |T_{22}|^2 + |T_{12}|^2,$   
 $Im(T_{12}) = T_{11}^* T_{12} + T_{12}^* T_{22},$ 
(A.2)

where  $T_{12} = T_{21}$ . In the present case we will identify 1 as the  $\pi\pi$  channel and 2 as the  $K\overline{K}$  channel. In order to get the relations between the relative phase shifts and

the amplitude we need to consider the following parameterization of the scattering amplitude:

$$S = \begin{pmatrix} \eta e^{2i\delta_{\pi}} & \pm i\sqrt{1-\eta^2} e^{i\delta_{\pi K}} \\ \pm i\sqrt{1-\eta^2} e^{i\delta_{\pi K}} & \eta e^{2i\delta_{K}} \end{pmatrix} , \qquad (A.3)$$

where  $\delta_{\pi K} = \delta_{\pi} + \delta_{K}$  and  $0 < \eta < 1$  is the elasticity parameter. By comparing eq. (A.3) and eq. (A.1) one can easily deduce:

$$\eta^2 = 1 - 4|T_{12}|^2 \ . \tag{A.4}$$

Analogously, for  $T_{aa}$  we have:

$$T_{aa;l}^{I}(s) = \frac{(\eta_l^{I}(s) e^{2i\delta_{a;l}^{I}(s)} - 1)}{2i} , \qquad (A.5)$$

where l and I label the angular momentum and isospin respectively. Extracting the real and imaginary parts via

$$R_{aa;l}^{I} = \frac{\eta_{l}^{I} \sin(2\delta_{a;l}^{I})}{2},$$

$$I_{aa;l}^{I} = \frac{1 - \eta_{l}^{I} \cos(2\delta_{a;l}^{I})}{2}$$
(A.6)

leads to the very important bounds

$$|R_{aa;l}^I| \le \frac{1}{2} , \qquad 0 \le I_{aa;l}^I \le 1 .$$
 (A.7)

Unitarity also requires  $|T_{12;l}^I| < 1/2$  .

Now we relate these partial wave amplitudes to the invariant amplitudes. The invariant amplitude for  $\pi_i(p_1) + \pi_j(p_2) \to \pi_k(p_3) + \pi_l(p_4)$  is decomposed as:

$$\delta_{ij}\delta_{kl}A(s,t,u) + \delta_{ik}\delta_{jl}A(t,s,u) + \delta_{il}\delta_{jk}A(u,t,s) , \qquad (A.8)$$

where s, t and u are the usual Mandelstam variables. Note that the phase of eq. (A.8) corresponds to simply taking the matrix element of the Lagrangian density of a fourpoint contact interaction. Projecting out amplitudes of definite isospin yields:

$$T_{11}^0(s,t,u) = 3A(s,t,u) + A(t,s,u) + A(u,t,s)$$
,

$$T_{11}^{1}(s,t,u) = A(t,s,u) - A(u,t,s) ,$$
  

$$T_{11}^{2}(s,t,u) = A(t,s,u) + A(u,t,s) .$$
(A.9)

The needed I=0  $\pi\pi\to K\overline{K}$  amplitude can be obtained as:

$$T_{12}^{0}(s,t,u) = -\sqrt{6}A(\pi^{0}(p_{1})\pi^{0}(p_{2}), K^{+}(p_{3})K^{-}(p_{4}))$$
 (A.10)

We then define the partial wave isospin amplitudes according to the following formula:

$$T_{ab;l}^{I}(s) \equiv \frac{1}{2} \sqrt{\rho_a \rho_b} \int_{-1}^{1} d\cos\theta P_l(\cos\theta) T_{ab}^{I}(s,t,u) , \qquad (A.11)$$

where  $\theta$  is the scattering angle and

$$\rho_a = \frac{1}{S \ 16\pi} \sqrt{\frac{s - 4m_\pi^2}{s}} \ \theta(s - 4m_a^2) \ . \tag{A.12}$$

S is a symmetry factor which is 2 for identical particles ( $\pi\pi$  case) and 1 for distinguishable particles ( $K\overline{K}$  case).

## A.2 Unregularized amplitudes

### A.2.1 Amplitudes for the $\pi\pi \to \pi\pi$ channel

The current algebra contribution to A(s, t, u) is

$$A_{ca}(s,t,u) = 2\frac{(s-m_{\pi}^2)}{F_{\pi}^2} . \tag{A.13}$$

The amplitude for the vectors can be expressed in the following form

$$A_{\rho}(s,t,u) = -\frac{g_{\rho\pi\pi}^2}{2m_{\rho}^2} \left[ \frac{t(u-s)}{m_{\rho}^2 - t} + \frac{u(t-s)}{m_{\rho}^2 - u} \right] , \qquad (A.14)$$

where  $g_{\rho\pi\pi}$  is the coupling of the vector to two pions.

For the scalar particle we deduce

$$A_{f_0}(s,t,u) = \frac{\gamma_0^2}{2} \frac{(s-2m_\pi^2)^2}{m_{f_0}^2 - s} . \tag{A.15}$$

To calculate the tensor exchange diagram we need the spin 2 propagator [44]

$$\frac{i}{q^2 - m_{f_2}^2} \left[ \frac{1}{2} \left( \theta_{\mu_1 \nu_1} \theta_{\mu_2 \nu_2} + \theta_{\mu_1 \nu_2} \theta_{\mu_2 \nu_1} \right) - \frac{1}{3} \theta_{\mu_1 \mu_2} \theta_{\nu_1 \nu_2} \right] , \qquad (A.16)$$

where

$$\theta_{\mu\nu} = -g_{\mu\nu} + \frac{q_{\mu}q_{\nu}}{m_{f_2}^2} \ . \tag{A.17}$$

A straightforward computation then yields the  $f_2$  contribution to the  $\pi\pi$  scattering amplitude:

$$A_{f_2}(s,t,u) = \frac{\gamma_2^2}{2(m_{f_2}^2 - s)} \left( -\frac{16}{3} m_{\pi}^4 + \frac{10}{3} m_{\pi}^2 s - \frac{1}{3} s^2 + \frac{1}{2} (t^2 + u^2) - \frac{2}{3} \frac{m_{\pi}^2 s^2}{m_{f_2}^2} - \frac{s^3}{6 m_{f_2}^2} + \frac{s^4}{6 m_{f_2}^4} \right). \tag{A.18}$$

## **A.2.2** Amplitudes for $\pi^0 \pi^0 \to K^+ K^-$

Current algebra amplitude:

$$A_{ca}(\pi^0\pi^0, K^+K^-) = \frac{s}{2F_{\pi}^2}.$$
 (A.19)

Vector meson contribution:

$$A_{Vector}(\pi^{0}\pi^{0}, K^{+}K^{-}) = \frac{g_{K^{*}K\pi}^{2}}{8m_{K^{*}}^{2}} \left[ \frac{t(s-u)}{m_{K^{*}}^{2} - t} + \frac{u(s-t)}{m_{K^{*}}^{2} - u} + (m_{k}^{2} - m_{\pi}^{2})^{2} \left( \frac{1}{m_{K^{*}}^{2} - t} + \frac{1}{m_{K^{*}}^{2} - u} \right) \right]. \quad (A.20)$$

Direct-channel contribution for the scalar:

$$A_{f_0}(\pi^0\pi^0, K^+K^-) = \frac{1}{4}\gamma_{f_0\pi\pi}\gamma_{f_0K\overline{K}}\frac{(s-2m_\pi^2)(s-2m_k^2)}{m_{f_0}^2 - s}.$$
 (A.21)

Cross-channel contribution for the scalar:

$$A_{K_0^*}(\pi^0\pi^0, K^+K^-) = \frac{\gamma_{K_0^*K\pi}^2}{8} \left[ \frac{(m_K^2 + m_\pi^2 - t)^2}{m_{K_0^*}^2 - t} + \frac{(m_K^2 + m_\pi^2 - u)^2}{m_{K_0^*}^2 - u} \right] . (A.22)$$

Direct channel tensor contribution:

$$A_{f_2}(\pi^0\pi^0, K^+K^-) = \frac{\gamma_{2\pi\pi}\gamma_{2K\overline{K}}}{2(m_{f_2}^2 - s)} \left[ \left( \frac{s^2}{4m_{f_2}^2} + \frac{t}{2} - \frac{(m_{\pi}^2 + m_K^2)}{2} \right)^2 + \left( \frac{s^2}{4m_{f_2}^2} + \frac{u}{2} - \frac{(m_{\pi}^2 + m_K^2)}{2} \right)^2 - \frac{2}{3} \left( \frac{s^2}{4m_{f_2}^2} - \frac{s}{2} + m_{\pi}^2 \right) \left( \frac{s^2}{4m_{f_2}^2} - \frac{s}{2} + m_K^2 \right) \right]. \quad (A.23)$$

Cross-channel tensor contribution:

$$A_{K_{2}^{*}}(\pi^{0}\pi^{0}, K^{+}K^{-}) = \frac{\gamma_{2K\pi}^{2}}{16(m_{K_{2}^{*}}^{2} - t)} \left\{ \left[ (2m_{\pi}^{2} - s) - \frac{1}{2m_{K_{2}^{*}}^{2}} (m_{\pi}^{2} - m_{K}^{2} + t)^{2} \right] \right.$$

$$\times \left. \left[ (2m_{K}^{2} - s) - \frac{1}{2m_{K_{2}^{*}}^{2}} (m_{K}^{2} - m_{\pi}^{2} + t)^{2} \right] \right.$$

$$+ \left. \left[ (u - m_{\pi}^{2} - m_{K}^{2}) + \frac{1}{2m_{K_{2}^{*}}^{2}} (t^{2} - (m_{K}^{2} - m_{\pi}^{2})^{2}) \right]^{2} \right.$$

$$- \left. \frac{2}{3} \left[ (t - m_{\pi}^{2} - m_{K}^{2}) - \frac{1}{2m_{K_{2}^{*}}^{2}} (t^{2} - (m_{K}^{2} - m_{\pi}^{2})^{2}) \right]^{2} \right\}$$

$$+ \left. (t \longleftrightarrow u) \right. \tag{A.24}$$

# Appendix B

# Part II Appendix

#### **B.1** Classical Potential

Here we will show how to compute the relevant matrix elements associated with the classical potential.

For any fixed value of  $k' \neq 0$  the heavy meson light cloud spin  $(\boldsymbol{J}_{\text{light}})$  takes the values  $j_l = k' \mp \frac{1}{2}$  since  $\boldsymbol{K}' = \boldsymbol{J}_{\text{light}} + \boldsymbol{I}_{\text{light}}$ , where  $\boldsymbol{I}_{\text{light}}$  is the heavy meson isospin. Hence the classical potential will be, in general, a  $2 \times 2$  matrix schematically represented as

$$V(k' \neq 0) = \begin{pmatrix} \langle H_{\mu_1 \cdots \mu_{k'-1}} | V | H_{\mu_1 \cdots \mu_{k'-1}} \rangle & \langle H_{\mu_1 \cdots \mu_{k'-1}} | V | H_{\mu_1 \cdots \mu_{k'}} \rangle \\ \langle H_{\mu_1 \cdots \mu_{k'}} & | V | H_{\mu_1 \cdots \mu_{k'-1}} \rangle & \langle H_{\mu_1 \cdots \mu_{k'}} & | V | H_{\mu_1 \cdots \mu_{k'}} \rangle \end{pmatrix} . \tag{B.1}$$

Here  $|H_{\mu_1\cdots\mu_{k'-1}}\rangle$  corresponds to the  $j_l=k'-\frac{1}{2}$  state while  $|H_{\mu_1\cdots\mu_{k'}}\rangle$  corresponds to  $j_l=k'+\frac{1}{2}$ . In order to compute the potential there is no need to distinguish even parity heavy mesons  $\mathcal{H}$  from odd parity ones H. The diagonal matrix elements are obtained by substituting the appropriate rest frame ansatz (6.39) into the general potential term as:

+ 
$$M d_n \int d^3x \operatorname{Tr} \left[ H^{\mu_1 \cdots \mu_n} \gamma^{\alpha} \gamma_5 p_{\alpha} \bar{H}_{\mu_1 \cdots \mu_n} \right]$$

$$= d_n \frac{F'(0)}{2} (-1)^n \int d\Omega \, \psi_{i_1 \cdots i_n, dl}^* \left( k', k'_3, r \right) \boldsymbol{\sigma}_{ll'} \cdot \boldsymbol{\tau}_{dd'} \psi_{i_1 \cdots i_n, d'l'} \left( k', k'_3, r \right) , \, (B.2)$$

where  $j_l = n + \frac{1}{2}$  and  $n = k' \mp 1$  for the two diagonal matrix elements. The operator which mesures the total light cloud spin  $j_l$  is

$$\left(J_{\text{light}}^{a}\right)_{i_{1}j_{1},\dots,i_{n}j_{n};ll'} = \frac{\sigma_{ll'}^{a}}{2} \otimes \delta_{i_{1}j_{1}} \otimes \dots \otimes \delta_{i_{n}j_{n}} + \delta_{ll'} \otimes \left(-i\epsilon_{ai_{1}j_{1}}\right) \otimes \delta_{i_{2}j_{2}} \otimes \dots \otimes \delta_{i_{n}j_{n}} + \dots + \delta_{ll'} \otimes \delta_{i_{1}j_{1}} \otimes \dots \otimes \delta_{i_{n-1}j_{n-1}} \otimes \left(-i\epsilon_{ai_{n}j_{n}}\right) .$$
(B.3)

where  $\epsilon_{aij}$  is the totally antisymmetric tensor. The isospin operator is

$$I_{\text{light}} = \frac{\tau}{2}$$
 (B.4)

We can write Eq. (B.3) compactly in the following way

$$J_{\text{light}} = s + \hat{l} ,$$
 (B.5)

where  $\mathbf{s} \equiv \frac{\boldsymbol{\sigma}}{2}$ . Due to the total symmetrization of the vectorial indices we have  $\hat{l} = n$ . We want to stress that  $\mathbf{s}$  and  $\hat{\boldsymbol{l}}$  do not necessarily agree with  $\boldsymbol{S}_{\text{light}}$  and  $\boldsymbol{\ell}$ . Indeed for  $\Phi_{ld}$  associated with  $\mathcal{H}$  in Eq. (6.16),  $\hat{l} = 0$  and  $\boldsymbol{J}_{\text{light}} = \mathbf{s} = \boldsymbol{S}_{light} + \boldsymbol{\ell}$  while for associated  $\Phi_{i,ld}$  with  $\mathcal{H}_{\mu}$ ,  $\hat{l} = 1$ . Now we have, for fixed  $n = j_l - \frac{1}{2}$ , the following useful result:

$$\int d\Omega \, \psi^* \boldsymbol{s} \psi = \frac{\int d\Omega \psi^* \, (\boldsymbol{s} \cdot \boldsymbol{J}_{\text{light}}) \, \psi}{j_l(j_l + 1)} \int d\Omega \, \psi^* \boldsymbol{J}_{\text{light}} \psi = \frac{1}{2 \, j_l} \int d\Omega \, \psi^* \boldsymbol{J}_{\text{light}} \psi . \tag{B.6}$$

By using Eq. (B.6) we can write Eq. (B.2) as

$$(-1)^{n} d_{n} \frac{F'(0)}{j_{l}} \int d\Omega \, \psi^{*}(k', k'_{3}, r) \, \boldsymbol{J}_{\text{light}} \cdot \boldsymbol{I}_{\text{light}} \psi (k', k'_{3}, r)$$

$$= (-1)^{n} d_{n} \frac{F'(0)}{2j_{l}} \left[ k'(k'+1) - j_{l}(j_{l}+1) - \frac{3}{4} \right] . \tag{B.7}$$

For  $j_l = k' \mp \frac{1}{2}$  we get the diagonal matrix elements for both, the H type as well as the  $\mathcal{H}$  type fields

$$(-1)^{k'-1} \frac{F'(0)}{2} \cdot \begin{cases} d_{k'-1}, & j_l = k' - \frac{1}{2}, \\ d_{k'} \left(\frac{2k'+3}{2k'+1}\right), & j_l = k' + \frac{1}{2}, \end{cases}$$
(B.8)

where we used  $n = j_l - 1/2$ .

For the non–diagonal matrix elements we consider the contribution to the potential due to the following f type term:

$$-M f_n \int d^3x \operatorname{Tr} \left[ H^{\mu_1 \cdots \mu_n} p^{\mu} \gamma_5 \bar{H}_{\mu_1 \cdots \mu_n \mu} \right]$$

$$= i f_n \frac{F'(0)}{2} \int d\Omega \, \psi_{i_1 \cdots i_n, dl}^* \left( k', k'_3, r \right) \tau_{dd'}^i \psi_{i_1 \cdots i_n i, d'l} \left( k', k'_3, r \right) . \tag{B.9}$$

This corresponds to the transition between  $j_l = n + \frac{1}{2}$  and  $j_l = n + \frac{3}{2}$  states. Now we notice that by construction any wave function  $\psi$  must satisfy the condition

$$(P^{3/2})_{ii_1:ll'} \psi_{i_1 i_2 \cdots i_n, dl'} = \psi_{ii_2 \cdots i_n, dl} ,$$
 (B.10)

where  $P^{3/2}$  is the spin 3/2 projection operator

$$\left(P^{3/2}\right)_{ik;ll'} = \frac{2}{3} \left(\delta_{ik}\delta_{ll'} - \frac{i}{2}\epsilon_{jik}\sigma_{ll'}^{j}\right) .$$
(B.11)

The condition (B.10) yields the following identity

$$\int d\Omega \, \psi_{i_{1} \cdots i_{n}, dl}^{*} \left( k', k'_{3}, r \right) \tau_{dd'}^{i} \psi_{i_{1} \cdots i_{n}i, d'l} \left( k', k'_{3}, r \right) = 
\int d\Omega \, \psi_{i_{1} \cdots i_{n}, dl}^{*} \left( k', k'_{3}, r \right) \tau_{dd'}^{j} \left( P^{3/2} \right)_{jk:ll'} \psi_{i_{1} \cdots i_{n}k, d'l'} \left( k', k'_{3}, r \right) .$$
(B.12)

Using the fact that  $P^{3/2}\tau$  commutes with K', we get

$$(P^{3/2})_{jk;ll'} \tau^k_{dd'} \psi_{i_1 \cdots i_n, d'l'} (k', k'_3, r) = N \psi_{i_1 \cdots i_n j, dl} (k', k'_3, r) ,$$
 (B.13)

where N is a normalization constant. It is evaluated as

$$|N|^2 = \int d\Omega \, \psi_{i_1 \cdots i_n, dl}^* \left( k', k_3', r \right) \tau_{dd'}^c \left( P^{3/2} \right)_{ck; ll'} \tau_{d'd''}^k \psi_{i_1 \cdots i_n, d''l'} \left( k', k_3', r \right) = \frac{8}{3} . \quad (B.14)$$

The non-diagonal matrix element is, up to a phase factor in Eq. (B.9)

$$if_n F'(0)\sqrt{\frac{2}{3}}$$
,  $\forall k' \neq 0$ . (B.15)

For k' = 0 we have only one diagonal element with  $j_l = \frac{1}{2}$ . The second line of Eq. (B.8) provides

$$V(k'=0) = -\frac{3}{2}F'(0)d_0.$$
(B.16)

## **B.2** Collective Lagrangian

Here the relevant matrix elements associated with the collective coordinate Lagrangian are computed. We will restrict k' to be nonzero since there is no contribution for k' = 0 to the collective Lagrangian.

The kinetic Lagrangian for H type and  $\mathcal{H}$  type fields is:

$$\mathcal{L}_{kin} = +i \, M V^{\mu} \sum_{n} \text{Tr} \left[ H^{\mu_1 \cdots \mu_n} D_{\mu} \bar{H}_{\mu_1 \cdots \mu_n} \right] - i \, M V^{\mu} \sum_{n} \text{Tr} \left[ \mathcal{H}^{\mu_1 \cdots \mu_n} D_{\mu} \bar{\mathcal{H}}_{\mu_1 \cdots \mu_n} \right] . \tag{B.17}$$

In the following we will not distinguish between the H and  $\mathcal{H}$  types of field. We need to consider the collective coordinate Lagrangian for a given k' classical bound channel in the heavy meson rest frame. For  $k' \neq 0$  the bound state wave–function can schematically be represented as

$$|Bound\ State; k'\rangle = \alpha |H_{\mu_1 \cdots \mu_{k'-1}}\rangle + \beta |H_{\mu_1 \cdots \mu_{k'}}\rangle,$$
 (B.18)

where  $|\alpha|^2 + |\beta|^2 = 1$ .

The collective coordinate Lagrangian ( $\delta L_{\text{coll}}$ ), induced by the heavy meson kinetic term, is obtained by generalizing Eqs. (4.24) and (6.28) to the higher excited heavy meson fields, introducing the collective coordinate A(t) rotation via

$$\bar{H}_{i_1\cdots i_n}(\boldsymbol{x},t) = A(t)\bar{H}_{i_1\cdots i_nc}(\boldsymbol{x}) , \qquad (B.19)$$

where the  $\bar{H}_{i_1\cdots i_n c}(\boldsymbol{x})$  classical ansatz is given in Eq. (6.39). The contribution for fixed  $k' \neq 0$  is:

$$\delta L_{\text{coll}} = -\Omega^{q} \left[ |\alpha|^{2} \int d\Omega \, \psi_{i_{1} \cdots i_{k'-1}, dl}^{*} (k', k'_{3}, r) \frac{\tau_{dd'}^{q}}{2} \psi_{i_{1} \cdots i_{k'-1}, d'l} (k', k'_{3}, r) \right. \\
+ |\beta|^{2} \int d\Omega \, \psi_{i_{1} \cdots i_{k'}, dl}^{*} (k', k'_{3}, r) \frac{\tau_{dd'}^{q}}{2} \psi_{i_{1} \cdots i_{k'}, d'l} (k', k'_{3}, r) \right] \\
\equiv -|\alpha|^{2} \int d\Omega \, \psi^{*} (k', k'_{3}, j_{l} = k' - 1/2) \, \mathbf{\Omega} \cdot \mathbf{I}_{\text{light}} \psi (k', k'_{3}, j_{l} = k' - 1/2)$$

$$-|\beta|^2 \int d\Omega \psi^* (k', k'_3, j_l = k' + 1/2) \mathbf{\Omega} \cdot \mathbf{I}_{light} \psi (k', k'_3, j_l = k' + 1/2) ,$$
(B.20)

where the over all minus sign in Eq. (B.20) is required, as explained in section 6.4. According to the Wigner-Eckart theorem:

$$\int d\Omega \, \psi^* \boldsymbol{I}_{\text{light}} \psi = \frac{\left[k'(k'+1) - j_l(j_l+1) + \frac{3}{4}\right]}{2 \, k'(k'+1)} \int d\Omega \, \psi^* \boldsymbol{K}' \psi , \qquad (B.21)$$

we thus obtain the following heavy meson contribution to the collective coordinate Lagrangian for  $k' \neq 0$ 

$$\delta L_{\text{coll}} = -\chi(k') \, \mathbf{\Omega} \cdot \mathbf{K}' \,. \tag{B.22}$$

The quantity  $\chi(k')$  is given by

$$\chi(k') = \frac{1}{2k'(k'+1)} \left[ \frac{1}{2} \pm \left( k' + \frac{1}{2} \right) \cos 2\theta \right] , \qquad (B.23)$$

where  $|\alpha|^2 - |\beta|^2 = \pm \cos 2\theta$  was used. In Eq. (B.23) the  $\pm$  sign corresponds to the two possible eigenvalues in the potential matrix for given  $k' \neq 0$ .

## Bibliography

- [1] H. Fritsch and M. Gell-Mann. Current algebra: Quarks and what else?, in Proc. XVI Int. Conf. on High Energy Physics, ed J.D. Jackson and A. Roberts (National Accelerator Laboratory, Batavia, Ill.) (1972).
- [2] W.J. Marciano and H. Pagels. Quantum chromodynamics, Phys. Rep. 36 C, 137 (1978).
- [3] D.J. Gross and F. Wilczek. *Ultraviolet behavior of nonabelian gauge theories*, Phys. Rev. Lett. **30**,1343 (1973).
- [4] D.J. Gross and F. Wilczek. Asymptotically free gauge theories I., Phys. Rev. D8,3633 (1973) (1973).
- [5] H.D. Politzer. Reliable Perturbative results for strong interactions?Phys. Rev. Lett. 30, 1346 (1973).
- [6] E. Witten, Nucl. Phys. B160 57 (1979); S. Coleman, Aspects of Symmetry, Cambridge University Press (1985). G. 't Hooft, Nucl. Phys. B72 461 (1974).
- [7] S. Weinberg, Physica 96A, 327 (1979). J. Gasser and H. Leutwyler,
  Ann. of Phys. 158 142 (1984); J. Gasser and H. Leutwyler, Nucl. Phys.
  B250 465 (1985); Ulf-G. Meißner, Rept. Prog. Phys. 56, 903 (1993).

- [8] F. Sannino and J. Schechter, Phys. Rev. D 52, 96 (1995).
- [9] F. Sannino, Proceedings of the Montreal, Rochester, Syracuse, Toronto Meeting, May 8-9, 1995, University of Rochester, N.Y., pag.133.
- [10] M. Harada, F. Sannino and J. Schechter, Phys. Rev. D 54, 1991 (1996).
- [11] G. Veneziano, Nuovo Cim. 57A 190 (1968). M.B. Green, J.H. Schwarz and E. Witten, Superstring Theory Vol 1 Cambridge University Press (1987).
- [12] S. Coleman and E. Witten, Phys. Rev. Lett. 45, 100 (1980); G.
   Veneziano, Phys. Lett. B 95, 90 (1980); A. Salomone, J. Schechter and
   T. Tudron, Phys. Rev. D 24, 492 (1981).
- [13] J. R. Taylor, Scattering Theory (Krieger, Boca Raton, FL, 1987).
- [14] C. Callan, S. Coleman, J. Wess and B. Zumino, Phys. Rev. 177, 22, 409 (1969).
- [15] Ö. Kaymakcalan and J. Schechter, Phys. Rev. D **31**, 1109 (1985).
- [16] M. Bando, T. Kugo and K. Yamawaki, Phys. Rep. 164, 217 (1988).
- [17] J. Schechter, A. Subbaraman, and H. Weigel, Phys. Rev. D 48, 339 (1993).
- [18] M. Harada and J. Schechter, Phys. Rev. D 54, 1991, (1996).
- [19] M. Harada, F. Sannino, J. Schechter, H. Weigel, Phys. Lett. B 384, 5, 1996.
- [20] G. D'Ambrosio, M. Miragliuolo, F. Sannino, Z. Phys. C 59, 451 (1993).

- [21] F. Buccella, O. Pisanti, F. Sannino, Z. Phys. C 66, 135 (1995).
- [22] S. Weinberg, Phys. Rev. Lett. 17, 616 (1966).
- [23] S.M. Roy, Phys. Lett. 36, 353 (1971); J.-L. Basdevant, C.D. Froggatt and J.L. Petersen, Nucl. Phys. B72, 413 (1974); J.-L. Basdevant, P. Chapelle, C. Lopez and M. Sigelle, *ibid.* B98, 285 (1975); C.D. Froggatt and J.L. Petersen, *ibid.* B129, 89 (1977).
- [24] G. Ecker, J. Gasser, H. Leutwyler, A. Pich and E. De Rafael, Phys. Lett. B 223, 425 (1989).
- [25] K. Kawarabayashi and M. Suzuki, Phys. Rev. Lett. 16, 255 (1966);Riazuddin and Fayyazudding, Phys. Rev. 147, 107 (1994).
- [26] S. Weinberg, Phys. Rev. 177, 2604, 1969; S. Weinberg, Phys. Rev. Lett. 65, 1177, (1990).
- [27] J. Donoghue, C. Ramirez and G. Valencia, Phys. Rev. D 39, 1947
  (1989); G. Ecker, J. Gasser, A. Pich and E. de Rafael, Nucl. Phys.
  B221, 311 (1989); N. Kaiser, in Effective Field Theories of the Standard Model, Proceedings of the Workshop, Dobogoko, Hungary, 1991, edited by Ulf-G. Meißner, (World Scientific, Singapore, 1992) pag. 41.
- [28] E.A. Alekseeva et al., Soc. Phys. JETP **55**, 591 (1982).
- [29] G. Grayer et al., Nucl. Phys. **B75**, 189 (1974).
- [30] J. Gasser and Ulf-G. Meißner, Phys. Lett. B 258, 219 (1991).
- [31] R.L. Jaffe, Phys. Rev. D 15, 281 (1977)
- [32] N.A. Törnqvist, Z. Phys. C 68, 647 (1995).

[33] N.A. Törnqvist and M. Roos, Phys. Rev. Lett. 76, 1575 (1996); N.A.Törnqvist and M. Roos, idem. 77, 23333 (1996).

- [34] N. Isgur and J. Speth, Phys. Rev. Lett. 77, 2332 (1996);N.A. Törnqvist and M. Roos, *ibid*, 2333 and references therein.
- [35] N.A. Törnqvist, The Scalar  $q\bar{q}$  Nonet and Confirmation of the Broad  $\sigma(\approx 500)$  Meson, Report No. HU-SEFT R 1996-18, hep-ph/9608464.
- [36] G.E. Brown and M. Rho, Phys. Rept. **269**, 333, (1996).
- [37] Review of Particle Properties, L. Montanet et al., Phys. Rev. D 50 1173 (1994).
- [38] Review of Particle Properties, L. Montanet *et al.*, Phys. Rev. D **54** 1 (1996). There are no substantial differences with respect the previous edition of the PDG, except for the inclusion of the  $\sigma$  particle which appears as  $f_0(400-1200)$ .
- [39] F. Sannino, Phys. Lett. B **322** (1994) 259.
- [40] L.I. Schiff, Quantum Mechanics 2nd ed. (McGraw-Hill, New York, 1955), pag. 109.
- [41] G. Janssen, B.C. Pearce, K. Holinde and J. Speth, Phys. Rev. D 52, 2690 (1995); D. Lohse, J.W. Durso, K. Holinde and J. Speth, Nucl. Phys. A516 (1990) 513.
- [42] D. Morgan and M. Pennington, Phys. Rev. D 48, 1185 (1993).
- [43] J. Weinstein and N. Isgur, Phys. Rev. D 41, 2236 (1990).
- [44] G. Wentzel, Quantum Theory of Fields, (Interscience, New York, 1949).

- [45] D. Cohen et al., Phys. Rev. D 22, 2595 (1980).
- [46] E.P. Wigner, Phys. Rev. **98**, 145 (1955).
- [47] A. Di Giacomo, Lezioni di Fisica Teorica, (ETS, Pisa, 1992).
- [48] R. Blankenbecler and R. Sugar, Phys. Rev. **142**, 1051 (1966).
- [49] A.A. Bolokhov, A.N. Manashov, M.V. Polyakov and V.V. Vereshagin, Phys. Rev. D 48, 3090 (1993); V.A. Andrianov and A.N. Manashov, Mod. Phys. Lett. A 8, 2199 (1993).
- [50] V.V. Vereshagin, Phys. Rev. D 55, 5349, 1997.
- [51] D. Atkinson, M. Harada and A.I. Sanda, Phys. Rev. D 46, 3884 (1992).
- [52] V. Elias, M. Tong and M.D. Scadron, Phys. Rev. D 40, 3670 (1989).
- [53] R. Delbourgo and M.D. Scadron, Mod. Phys. Lett. A 10, 251 (1995).
- [54] N. Isgur and J. Speth, Phys. Rev. Lett. **77**, 2332 (1996)
- [55] M. Harada, F. Sannino and J. Schechter, Phys. Rev. Lett. 78, 1603, 1997.
- [56] S. Ishida, T. Ishida, M. Ishida, K. Takamatsu, T. Tsuru. Report Number NUP-A-97-17, (Jun 1997). 10pp. S. Ishida, T. Ishida,
  M. Ishida, K. Takamatsu, T. Tsuru, Report Numbers: hepph-9705437,
  Feb 1997. 9pp. S. Ishida, M. Ishida, H. Takahashi, T. Ishida,
  K. Takamatsu, T. Tsuru . KEK-PREPRINT-95-183, Dec 1995. 22pp,
  Prog. Theor. Phys. 95, 745, 1996

[57] GAMS Collaboration (D. Alde et al.). KEK-PREPRINT-96-174, Feb1997. 11pp, Phys. Lett. B397, 350,1997

- [58] Other relevant papers on ππ scattering: N.N. Achasov and G.N. Shestakov, Phys. Rev. D 49, 5779 (1994); R. Kaminski, L. Lesniak and J.P. Maillet, *ibid.* 50, 3145 (1994); C.D. Roberts, R.T. Cahill, M.E. Sevior and N. Iannella, *ibid.* 49, 125 (1994); A. Dobado and J.R. Pelaez, Report N. LBL-38645, Apr. 1996, hep-ph/9604416.
- [59] C.G. Callan and I. Klebanov, Nucl. Phys. B262, 365 (1985);
  C.G. Callan, K. Hornbostel and I. Klebanov, Phys. Lett. B 202, 296 (1988); I. Klebanov, in Hadrons and hadronic matter, Proc. NATO advanced study institute, Cargese, 1989, eds. D. Vautherin, J. Negele and F. Lenz (Plenum, New York, 1989) p. 223.
- [60] J. Blaizot, M. Rho and N.N. Scoccola, Phys. Lett. B209, 27 (1988);
  N.N. Scoccola, H. Nadeau, M.A. Nowak and M. Rho, Phys. Lett. B201, 425 (2988);
  D. Kaplan and I. Klebanov, Nucl. Phys. B335, 45 (1990);
  Y. Kondo, S. Saito and T. Otofuji, Phys. Lett. B256, 316 (1991);
  M. Rho, D.O. Riska and N.N. Scoccola, Z. Phys. A341, 341 (1992);
  H. Weigel, R. Alkofer and H. Reinhardt, Nucl. Phys. A576, 477 (1994).
- [61] E. Eichten and F. Feinberg, Phys. Rev. D23, 2724 (1981);
  M.B. Voloshin and M.A. Shifman, Yad. Fiz. 45, 463 (1987) [Sov. J. Nucl. Phys. 45, 292 (1987)]; N. Isgur and M.B. Wise, Phys. Lett. B232, 113 (1989); ibid. 237, 527 (1990); H. Georgi, Phys. Lett. B230, 447 (1990); A relevant review is M.B. Wise, Lectures given at the CCAST Symposium on Particle Physics at the Fermi Scale, in

- Proceedings edited by Y. Pang, J. Qiu and Z. Qiu, Gordon and Breach 1995, hep-ph/9306277.
- [62] Z. Guralnik, M. Luke and A.V. Manohar, Nucl. Phys. B390, 474
  (1993); E. Jenkins, A.V. Manohar and M. Wise, Nucl. Phys. B396, 27, 38 (1993); E. Jenkins and A.V. Manohar, Phys. Lett. B294, 273 (1992).
- [63] M. Rho, in Baryons as Skyrme solitons, ed. G. Holzwarth (World Scientific, Singapore, 1994); D.P. Min, Y. Oh, B.-Y. Park and M. Rho, Seoul report no. SNUTP-92-78, hep-ph/9209275 (unpublished);
  H.K. Lee, M.A. Nowak, M. Rho and I. Zahed, Ann. Phys. 227, 175 (1993); M.A. Nowak, M. Rho and I. Zahed, Phys. Lett. B303, 13 (1993); Y. Oh, B.-Y. Park and D.P. Min, Phys. Rev. D49, 4649 (1994);
  Y. Oh, B.-Y. Park and D.P. Min, Phys. Rev. D50, 3350 (1994);
  D.P. Min, Y. Oh, B.-Y. Park and M. Rho, Int. J. Mod. Phys. E4, 47 (1995); Y. Oh and B.-Y. Park, Phys. Rev. D51, 5016 (1995); Y. Oh and B.-Y. Park, Report No. TUM/T39-97-05, SNUTP-97-023, hep-ph/9703219 (unpublished).
- [64] K.S. Gupta, M.A. Momen, J. Schechter and A. Subbaraman, Phys. Rev. D47, R4835 (1993); A. Momen, J. Schechter and A. Subbaraman, Phys. Rev. D49, 5970 (1994).
- [65] J. Schechter and A. Subbaraman, Phys. Rev. **D51**, 2331 (1995).
- [66] J. Schechter, A. Subbaraman, S. Vaidya and H. Weigel, Nucl. Phys. A590, 655 (1995); E. Nucl. Phys. A598, 583 (1996).
- [67] Y. Oh and B.-Y. Park, Phys. Rev. **D53**, 1605 (1996).

[68] P. Jain, R. Johnson, N.W. Park, J. Schechter and H. Weigel, Phys. Rev. **D40**, 855 (1989).

- [69] R. Johnson, N.W. Park, J. Schechter, V. Soni and H. Weigel, Phys. Rev. **D42**, 2998 (1990).
- [70] N.W. Park and H. Weigel, Phys. Lett. A268, 155 (1991); Nucl. Phys. A541, 453 (1992).
- [71] M. Harada, A. Qamar, F. Sannino, J. Schechter and H. Weigel, Phys. Lett. B390, 329 (1997).
- [72] C.K. Chow and M.B. Wise, Phys. Rev. **D50**, 2135 (1994).
- [73] For example, see S. Capstick and N. Isgur, Phys. Rev. **D34**, 2809 (1986).
- [74] J. G. Körner, Proceedings of the 7<sup>th</sup> Int. Conf. on the Structure of Baryons, Santa Fe 1995, p. 221.
- [75] Particle Data Group, R.M. Barnett et al., Phys. Rev. **D54**, 1 (1996).
- [76] Notation as in J. Schechter and A. Subbaraman, Phys. Rev. D48, 332 (1993). See also R. Casalbuoni, A. Deandrea, N. Di Bartolomeo,
  R. Gatto, F. Feruglio and G. Nardulli, Phys. Lett. B292, 371 (1992).
- [77] G.S. Adkins, C.R. Nappi and E. Witten, Nucl. Phys. **B228**, 552 (1983).
- [78] A.F. Falk and M. Luke, Phys. Lett. **B292**, 119 (1992); see alsoA.F. Falk, Nucl. Phys. **B378**, 79 (1992).
- [79] R. Casalbuoni, A. Deandrea, N. Di Bartolomeo, R. Gatto, F. Feruglio, and G. Nardulli, Phys. Rep. 281, 145 (1997).

[80] T.H.R. Skyrme, Proc. R. Soc. A260, 127 (1961); A.P. Balachandran,
V.P. Nair, S.G. Rajeev and A. Stern, Phys. Rev. Lett. 49, 1124 (1982);
Phys. Rev. D27, 1153 (1983); A.P. Balachandran, A. Barducci,
F. Lizzi, V. Rodgers and A. Stern, Nucl. Phys. B256, 525 (1985). For reviews see: A.P. Balachandran, G. Marmo, B.S. Skagerstam and
A. Stern, Classical Topology and Quantum States, World Scientific
Publishing, 1991. G. Holzwarth and B. Schwesinger, Rep. Prog. Phys.
49, 825 (1986); I. Zahed and G.E. Brown, Phys. Rep. 142, 481 (1986);
Ulf-G. Meißner, Phys. Rep. 161, 213 (1988); B. Schwesinger, H. Weigel,
G. Holzwarth and A. Hayashi, Phys. Rep. 173, 173 (1989).

- [81] H. Weigel, Int. J. Mod. Phys. **A11**, 2419 (1996).
- [82] M. Karliner and M. P. Mattis, Phys. Rev. **D34**, 1991 (1986).
- [83] N. N. Scoccola, Phys. Lett. **B236**, 245 (1990).
- [84] B. Schwesinger, Nucl. Phys. **A537**, 253 (1992).
- [85] Ulf-G. Meißner, N. Kaiser, H. Weigel, and J. Schechter, Phys. Rev. D39 (1989) 1956.
- [86] Ö. Kaymakcalan, S. Rajeev, and J. Schechter, Phys. Rev. D30 (1984) 594.
- [87] P. Jain, R. Johnson, Ulf-G. Meißner, N. W. Park, and J. Schechter, Phys. Rev. **D37** (1988) 3252.
- [88] P. Jain, A. Momen, and J. Schechter, Intl. J. Mod. Phys A10 (1995) 2467.

[89] F. Meier and H. Walliser, Quantum corrections to baryon properties in chiral soliton models, Siegen University preprint, February 1996, hep-ph/9602359.

- [90] M. Harada, A. Qamar, F. Sannino, J. Schechter and H. Weigel, Hyperfine Splitting of Low-Lying Heavy Baryons, Report Numbers:SU-4240-658, UNITU-THEP-3/1997, March 1997, hep-ph/9703234. Accepted for publication in Nucl. Phys. A.
- [91] M. Harada, F. Sannino, J. Schechter and H. Weigel, Generalization of the Bound State Model, Report Numbers:SU-4240-659, April 1997, hep-ph/9704358. Accepted for publication in Phys. Rev. D.
- [92] G. Brandenburg et al., Phys. Rev. Lett. **78** (1997) 2304.